

## PUBLISHER

On Behalf of Textile and Apparel Research  
Application Center

Faruk BOZDOĞAN

## EDITOR IN CHIEF

Arif Taner ÖZGÜNEY  
arif.taner.ozguney@ege.edu.tr

## ASSOCIATE EDITORS

Mehmet KÜÇÜK  
mehmet.kucuk@ege.edu.tr  
Pelin SEÇİM KARAKAYA  
pelinsecim@mail.ege.edu.tr

## EDITORIAL BOARD

Ahmet ÇAY  
Esen ÖZDOĞAN  
Gözde ERTEKİN  
Nilgün ÖZDİL

## SCIENTIFIC ADVISORY BOARD

Andrej DEMŠAR  
Arzu MARMARALI  
Bojana VONČINA  
Bülent ÖZİPEK  
E. Perrin AKÇAKOCA KUMBASAR  
Ender BULGUN  
Hüseyin KADOĞLU  
Mirela BLAGA  
Oktay PAMUK  
Ozan AVİNÇ  
Peter J. HAUSER  
Recep EREN  
Rıza ATAV  
Savvas G. VASSILIADIS  
Turan ATILGAN

## ABSTRACTING / INDEXING

Science Citation Index Expanded (SCIE)  
Scopus  
WOS  
EBSCO  
TR Dizin  
Ulakbim

## TYPESETTING AND PRINTING

META Basım Matbaacılık Hizmetleri  
+90 232 343 64 54 / E-mail: metabasim@gmail.com  
Printed Date: December, 2019

**Evaluating the Effect of Water-Repellent Finishing on  
Thermal Insulation Properties of Rowing Shirts Using a  
Thermal Manikin**

Derya TAMA, André CATARINO, Maria José ABREU ..... 279

**Experimental Investigation of the Performance of a Feedback  
Tension Control System Designed for Warping Machines**

Recep EREN, Merve İHTİYAR, Özge ÇELİK..... 289

**Sewing Machine Selection Using Linear Physical Programming**

Mehmet Ali ILGIN ..... 300

**Development of 3-D Hemispherical Biaxial Weft-Knitted  
Thermoset Composites**

Özgür DEMİRCAN, Tatsuya KOSUI, Shinsuke ASHİBE,  
Asami NAKAI ..... 305

**A Comparative Thermal Analysis of Fire-off Treated Cotton,  
PET and Co/PET Fabrics**

Raziye ATAKAN, Gülay ÖZCAN ..... 311

**Performance and Characterization of Aloe Vera Microcapsules on  
Silk/Lyocell Blended Fabric**

Mariyam ADNAN, Jeyakodi MOSES J..... 317

**Experimental and numerical study of sewing seams of automobile  
seat covers under unidirectional and multiaxial loading**

Natalia KOVALOVA, Petr KULHYVÝ, Josef VOSÁHLO,  
Antonin HAVELKA ..... 322

**Colorimetric changes of thermochromic ink printed on smart  
textile materials exposed to different heat transfer methods**

Stefan ĐURĐEVIĆ, Dragoljub NOVAKOVIĆ, Savka ADAMOVIĆ,  
Nemanja KAŠIKOVIĆ, Neda MİLİĆ, Branko ŠTRBAC,  
Miodrag HADŽIŠTEVIĆ..... 336

**Supplier Selection Under Fuzzy Environment**

Çağdaş GÜNDÜZ, Gonca Şimşek GÜNDÜZ ..... 344

## CONTACT

Ege Üniversitesi Tekstil ve Konfeksiyon Araştırma-Uygulama Merkezi  
35100 Bornova – İzmir, TÜRKİYE  
Tel: +90 232 311 38 89-83

www.dergipark.gov.tr/tekstilvekonfeksiyon  
E-mail: tekstilkonfeksiyon@mail.ege.edu.tr





# Evaluating the Effect of Water-Repellent Finishing on Thermal Insulation Properties of Rowing Shirts Using a Thermal Manikin

Derya Tama<sup>1,2</sup>, André Catarino<sup>1</sup> and Maria José Abreu<sup>1</sup>

<sup>1</sup>University of Minho, 2C2T-Center for Textile Science and Technology, Campus de Azurem, Guimarães, Portugal

<sup>2</sup>EgeUniversity, Faculty of Engineering, Department of Textile Engineering, 35100 Bornova, Izmir, Turkey

**Corresponding Author:** Derya Tama, derya.tama@ege.edu.tr

## ABSTRACT

The activity of rowing is majorly performed outside, namely on rivers or lakes, and the probability of getting the t-shirt wet due to splash or rain is high. In order to evaluate the impact of water repellent finishing on the thermal insulation, several rowing shirts made with different structures and raw material were tested and compared by means of a thermal manikin, before and after finishing. The shirts were treated with a 5% of a fluorocarbon-based product water repellent finishing. The heat loss values of rowing shirts were measured by using a thermal manikin and the effective clothing insulation values were calculated. Moreover, the effect of garment design on thermal insulation was investigated by comparing shirts with more than one knitted structure with single knitting structures shirts. Considering the results for the heat loss values, after WRF, the heat flux of rowing shirts was lower. Shirt B and shirt B-1 had higher effective thermal insulation value after WRF, where the other shirts had lower thermal insulation values. Moreover, not only the water repellent finishing, but also the structure of garment is also important in terms of heat loss and thermal insulation.

## ARTICLE HISTORY

Received: 04.10.2018

Accepted: 30.10.2019

## KEYWORDS

rowing shirts, thermal comfort, thermal manikin, heat loss, total thermal insulation, effective clothing insulation

## ABBREVIATIONS

$I_T$	The total thermal clothing insulation
$I_{cle}$	The effective thermal clothing insulation
$I_a$	Thermal insulation of the boundary air layer
$f_i$	Relationship between the surface area of the segment $i$ of the manikin ( $A_i$ )
$A$	The total surface area of the manikin
$t_o$	The operative temperature [ $^{\circ}C$ ]
$t_{si}$	Skin surface temperature of the body segment of the manikin
$\dot{Q}_{si}$	Sensible heat flux of the manikin obtained by area
CST	Constant skin temperature
WRF	Water Repellent Finishing

## 1. INTRODUCTION

Nowadays, clothing comfort is one of the most important aspects for consumers, designers and manufacturers. Slater (1985) defined comfort as "a pleasant state of physiological, psychological, neurophysiological and physical harmony between a human being and the environment" [1-3].

Moreover, the term comfort is defined as either "the absence of unpleasantness or discomfort;" or "a neutral state compared to the more active state of pleasure." Therefore, the clothing comfort is classified into four basic groups: psychological, sensory, ergonomic and thermo-physiological comfort. Psychological comfort is mainly related to the fashion, colors and design features and acceptability in society which help people to feel confident. The sensory comfort is related with the sensations when a

**To cite this article:** Tama D, Catarino A, Abreu MJ. 2019. Evaluating the effect of water-repellent finishing on thermal insulation properties of rowing shirts using a thermal manikin, *Tekstil ve Konfeksiyon*, 29 (4), 279-288.

---

fabric comes into contact with the skin e.g. cold, warm, soft or stiff. The ergonomic comfort is related with the shapes, forms and ease of body movement of the wearer. The thermo-physiological comfort, which is the most researched element for improving comfort in clothing, is about the transmission of heat and moisture through fabric [4].

Different variables contribute for thermal comfort perception of a human being, such as air temperature and movement (speed, humidity, activity level, the environment mean radiant temperature), among others, resulting in a complex interaction between man and the environment. Thermal comfort relates body heat production and loss, and thermal manikins are a suitable mean for evaluating the thermal interface of the human body and the surrounding environment [5].

The thermal insulation of clothing has great significance in the thermoregulation process, which keeps body temperature within safe internal temperature boundaries. Clothing thermal insulation depend on factors such as specific design, dimensions and fabric characteristics, namely the air gap between skin and clothing [6]. The former is usually quantified by means of thermal manikins due to their experimental simplicity and repeatability procedures, and precision [7]. The thermal manikins now exist for more than 60 years [8] and provide a good estimate of the total dry heat loss from the body and the distribution of heat flow over the body surface. When in a standard environment, these measures can be used to describe the thermal characteristics of clothing [9].

Rowing is a competitive sport initiated in 1716 on the River Thames and depends on the speed of the shell [10]. Rowing is a highly repetitive action [11] and a periodic movement involving several phases such as catch, drive, finish and recovery [12]. In Northern Europe and Scandinavia, rowing is also a leisure sport practiced in riggers where oarlocks are on the side of the boat [13]. Since nowadays, many clubs developed an interest in the leisure-rowing scene and clothing for the rowing sport has become a subject for research and development.

In long distance rowing tours, one of the cardiac output has to be directed to the skin for heat exchange. The temperature regulation affects the performance of athletes and also may limit the maximum performance in hot climates. When the core temperature reaches 40°C, cellular damage occurs rapidly, initiating a cascade of events that may lead to organ failure and possible fatality [14]. After the exercise, the high amount of heat produced during rowing needs to be unloaded. This puts an additional burden to the already stressed central nervous system and can lead in some case to collapse, loss of consciousness and, if untreated, to fatality [13].

Rowing is an outdoor sport, being water the place where it is practiced, namely lakes and rivers. To protect the athletes, features like water-repellent and windproof are of paramount importance in rowing shirts. However, an exaggerated insulation and low absorbency may lead to a

significant increase of skin temperature, leading to higher moisture accumulation between skin and clothing. In order to overcome this, sports clothing should comply with some requisites: they need to be breathable, well fit, maintain the athlete in fresh condition by allowing an adequate heat change between the body and the environment [15]. As a result, sportswear should be able to protect the wearer from external elements such as wind, sun, rain and snow, but also be capable of maintaining the heat balance between excess heat produced by the wearer due to increased metabolic rate. Subsequently, the wear comfort of sportswear is an important property for a sportsperson. If, for example, an active person wears a clothing system with poor breathability, heart rate and body temperatures will increase more rapidly compared to wearing breathable sportswear [5].

Therefore, in order to prevent the high heat loss in thermoregulation using a high amount of energy due to the splashed water and the wind [16], a water-repellent finish can be applied to the rowing shirts. Moreover, water repellent finishing is an important factor to prevent health issues due to contaminated water. Awareness of environmental protection has increased during last decades and regarding to rowing sport, protecting the rower from all environmental impacts, namely contaminated water, which can result in skin problems [9], became one of the goals of manufacturers. Also, due to the possible exposure to splash water and rain, the body of the rower can easily get wet. When the shirt of the rower is getting wet, his body cools down. To avoid this, the shirt could be prepared with a water-repellent finish. If a water-repellent finish is applied, it is crucial that it will not deteriorate the breathability [5].

There are several repellents, which are currently used in water repellent finishing such as paraffin, stearic acid-melamine, silicone and fluorocarbons. The paraffin repellents, which are one of the earliest water repellents, increase the adhesion of the finish to polar fibre surfaces by forming polar-non-polar junctions. The paraffin repellents are available at relatively low costs and they generate uniform waterproof effects. However, there are also disadvantages including an increase of flammability and the lack of durability to laundering and dry cleaning. Furthermore, they have low air and vapour permeability, which limits the use of paraffin-based repellents [18].

The other class of water-repellent materials are the compounds formed by reacting stearic acid and formaldehyde with melamine constitute. There are some disadvantages of stearic acid-melamine repellents such as a tendency to exhibit finish mark-off, decreased fabric tear strength and abrasion resistance, changes in shade of dyed fabric, and release of formaldehyde [18]. Due to the high water, oil and soil repellence of finished fabrics [19], fluorocarbons are the most used water repellent finishes. Moreover, fluorocarbon is appropriate to apply on fabrics based on synthetic fibres and their mixtures with cellulosic fibre [17].

The main purpose of this study was to analyse the influence of water repellent finishing on thermal insulation properties of rowing shirts, which were manufactured in different materials and knitting structures. Some previous researches [5, 9, 20] were presented before such as the initial studies of this type of product, as parts of the conducted project. The optimal combination of base fabric constructions were discussed [20] as the part of the same project.

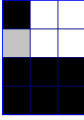
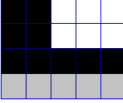
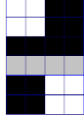
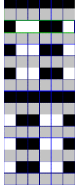
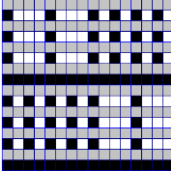
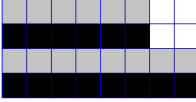
## 1. MATERIAL AND METHOD

### 2.1 Rowing shirts

The Shirt B and Shirt D produced by the collaborating company for outdoor rowing were tested in the present research. Since the former shirts had three combined

knitting structures each, shirts with single structures were manufactured and named as Shirt B-1, B-2 and B-3 of Shirt B and as Shirt D-1, D-2 and D-3 of Shirt D in order to also observe the influence of garment design on thermal insulation. In addition, a 100% Cotton shirt, which is a well-known product and usually used during rowing practice, was involved in the study to compare its behaviour with the tested rowing shirts. The compositions, knitted structures and the shirt codes are given in Table 1. All the shirts were produced in the same conditions, using seamless knitting machines.

**Table 1.** The compositions, knitting structures and the codes of shirts

Code	Composition	Knitting Structure	The Stitch Diagram*	Fabric Thickness	Machine Gauge
Shirt A	100% Cotton	Single jersey		1,096	E24
Shirt B	Composition of structures in different areas used in shirt B-1, B-2 and B-3		-		E26
Shirt B-1	60% Polyamide (black)	False Rib 1		1,317	E26
Shirt B-2	35% Polyester (grey) 5% Elastane (transparent)	False Rib 2		1,606	E26
Shirt B-3		Single Jersey Jacquard 1		1,1	E26
Shirt D	Composition of structures in different areas used in shirt D-1, D-2 and D-3		-		E26
Shirt D-1	60% Polyamide (black)	Single Jersey Jacquard 2		0,956	E26
Shirt D-2	35% Polypropylene (grey) 5% Elastane (transparent)	Single Jersey Jacquard 3		0,993	E26
Shirt D-3		False Rib 3		1,248	E26

\*Colour codes: Knit loops: Light grey and black; White: float loop; Light grey: polyester yarn or polypropylene yarn; black: polyamide yarn.

The 100% cotton long sleeve basic shirt, which was coded as A, can be seen in Figure 1. The shirt was designed with conventionally sewed side seams and round-necked.



Figure 1. 100% cotton long sleeve basic shirt

The shirt B, which was a turtleneck raglan sleeve tight-fitting shirt, was a combination of shirts B-1, B-2 and B-3, located on particular regions of the garment (Figure 2). Structure B-1 was mostly located on upper and lower arms, as well as on the pelvis while structure B-2 was used on the shoulders, collar and the centre of the chest covering the body parts, where the lungs are located. Furthermore, structure B-3 was positioned as a vertical stripe of about 5

cm on the back as well as near the armpits and on both sides of the shirt.

Shirt D was a rounded-neck raglan sleeve tight-fitting shirt produced by combining shirts D-1, D-2 and D-3 (Figure 3). Structure D-1 covered the most parts of the chest as well as blade bones, lower back, upper and lower arms. Structure D-2 was located on the centre chest, armpits and as two stripes one above and the other one below of each sleeve. Structure D-3 was used on the back of the shirt and located at the shoulders and the top sides of the upper arms as well as at both sides of the pelvis.

## 2.2 Water-Repellent Finishing

All shirts were treated with 5% of a fluorocarbon-based product: Imofob FMU. The finishing was selected and applied by the collaborating company regarding to the market expectations and their knowledge. Moreover, not only the water-repellent finishing but also the fabric constructions and garment design were evaluated in this study. Therefore, the treatment was done by the chemicals that collaborating company recommended.

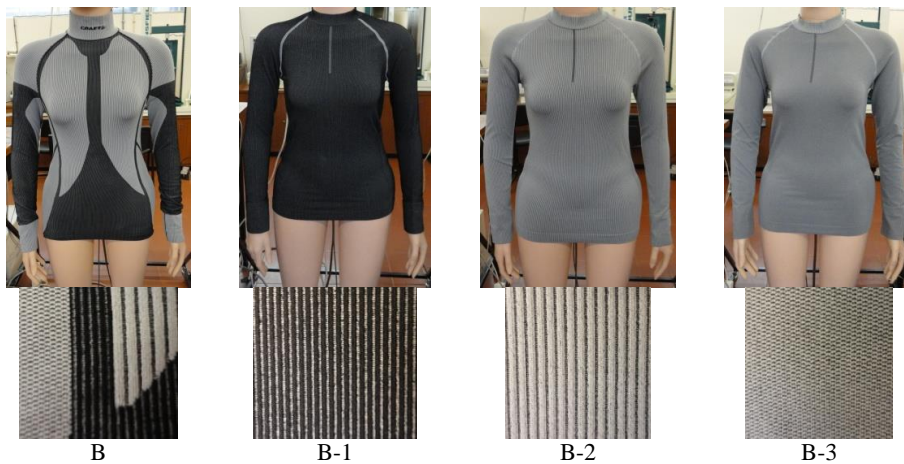


Figure 2. The type B shirts and views of the knitted structures

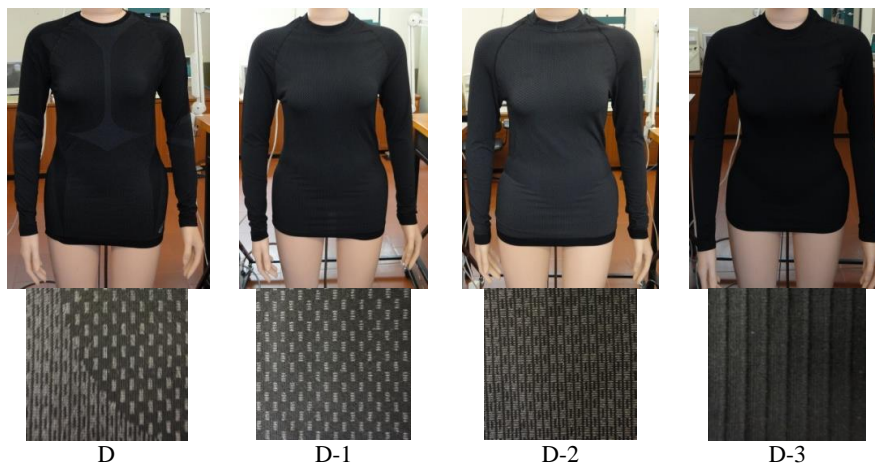


Figure 3. The type D shirts and views of the knitted structures

The characteristics of Imofob FMU are favourable for the usage on sports shirts, namely on rowing, because Fluorocarbon provides fibre surfaces with the lowest surface energies compared to other repellent finishes in use. It's a product for water-repellent articles based on synthetic fibres and their mixtures with cellulosic fibres [17].

The special properties of this product are good water and oil repellent characteristics, soft touch (even on printed items with pigments) and fastness in washing and dry cleaning. Furthermore, the product is suitable for applications with spray or in drum machines (on the fabricated article) [5].

### 2.3 Test Equipment

In order to observe heat loss, a female model thermal manikin (PT-Teknik, Denmark) (Figure 4), which has similar size and configurations with an adult woman, was used in this study. The thermal manikin is installed in the research laboratory of the (2C2T- Centre for Textile Science and Technology) of the University of Minho in Portugal. It only senses dry heat transfer and is divided in 20 thermally independent sections. The tests were conducted by placing the thermal manikin inside a climatic chamber which is able to achieve temperatures around 15 °C to 35 °C and relative humidity around 35% to 85%. Throughout the period of analysis, the thermal manikin was placed around 0.1m above the floor with hanging arms and legs.



Figure 4. Thermal manikin

### 2.4 Experimental Procedure

The tests were carried out according to “ISO 9920:2007: Ergonomics of the thermal environment - Estimation of thermal insulation and water vapour resistance of a clothing ensemble” standard [21]. The trials were performed with constant skin temperature mode and the skin temperature of

thermal manikin was set to 33 ±0,2°C regarding to ISO 9920. The thermal manikin was dressed with the rowing shirts and for the measurement of heat loss, the manikin was kept in a stationary standing position, with its legs hanging straight and the arms hanging straight at its sides. The tests were performed at constant ambient temperature of 23±1,5°C and relative humidity of 60±5%. The test time of each measurement was 60 minutes. The mean skin temperature, the heat flux of the manikin, and the room physical parameters were continuously monitored on computers. At the end of each measurement, the heat loss was obtained and recorded to the computer. Afterwards, the total thermal clothing insulation ( $I_T$ ) and the effective thermal clothing insulation  $I_{cle}$  were calculated according to the obtained data.

In order to calculate  $I_T$  and  $I_{cle}$ , the methods existing in literature were investigated. There are three thermal insulation calculation methods in literature; the serial, the global and the parallel methods. Due to the operation of thermal manikin was set with the constant skin temperature (CST) in this study, the global method was chosen with respect to the research conducted by Oliveira et al. (7) In their research, the thermal insulation of clothing was compared according to the three thermal insulation calculation methods and different manikin regulation modes in the body parts. Oliveira et al. obtained that, when the CST regulation mode is used, the general formula for defining the whole body resistance, i.e., the global method turns into a summation of local resistances according to a typical parallel model [7]. Moreover, in another research, Oliveira et al. found out that the serial and global methods always had statistically significant difference, while the global and parallel methods had not significant difference [22]. In this research, the insulation from skin surface to the environment,  $I_{T,}$ , was determined by using the global method under static conditions. In this method, the sum of all heat losses weighted areas and skin temperatures of each body segment is calculated before  $I_T$  is obtained, thus assuming the manikin has having only one segment. The general equation for defining the whole body resistance is:

$$I_T = \frac{\sum (f_i \times t_{si}) - t_0}{\sum (f_i \times \dot{Q}_{si})} \quad (1)$$

The  $I_{cle}$ , consisting of the difference between  $I_T$  and  $I_a$  (thermal insulation of the boundary air layer) is calculated by equation 2, considering  $I_a$  is measured by operating the manikin nude.

$$I_{cle} = I_T - I_a \quad (2)$$

Where:

$f_i$  = relationship between the surface area of the segment  $i$  of the manikin ( $A_i$ ) and the total surface area of the manikin  $A$  ( $f_i=A_i/A$ ).

$t_0$  = the operative temperature (°C)

$$f_i = re(^{\circ}C)$$

$\bar{Q}_{si}$  = sensible heat flux of the manikin obtained by area.

## 2.5 Statistical Analysis

In this study, statistical analysis was performed by using last version of SPSS statistical analysis package software. Independent-samples t-tests were conducted to compare heat loss and  $I_{cle}$  values for tests conducted with the specimens before and after WRF. *Post hoc* least significant difference tests were also carried out by using Bonferroni correction.

## 2. RESULTS AND DISCUSSION

### 3.1 Heat loss

The heat loss values for all rowing shirts were presented and comparisons were done graphically and statistically between the obtained data. Figure 5, 6 and 7 shows the heat loss from nine manikin body segments, which were related with upper garment conducted before and after WRF.

When the heat loss from the skin to the environment is higher, the temperature will decrease and the freshness feeling will be more intense [23, 24]. While the material absorbs and conducts the heat well, the sensation of being a “coolest” garment emerges. Thus, heat loss is closely related to thermal insulation, where they are inversely proportional parameters.

**Shirt A**

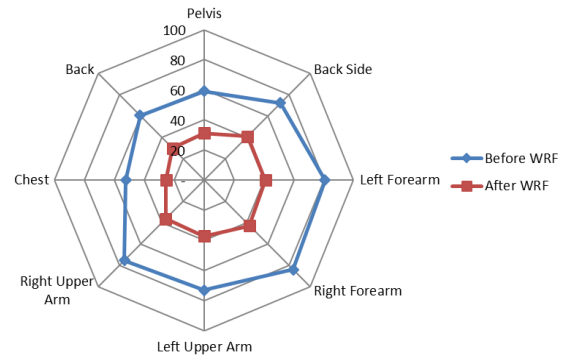


**Figure 5.** Heat loss values in  $W/m^2$  from the body segments of shirt A

As it can be seen in Figure 5, the heat loss change was around 50% after water repellent finishing treatment. Shirt A was produced from 100% cotton fabric. Water repellent finishing treatment changes the features of cotton from hydrophilic to hydrophobic. Therefore, it can be said that, water repellent finishing had considerable influence on thermal insulation properties of rowing shirts that produced from 100% cotton fabrics, in positive way for outdoor sports if one considers cold environment.

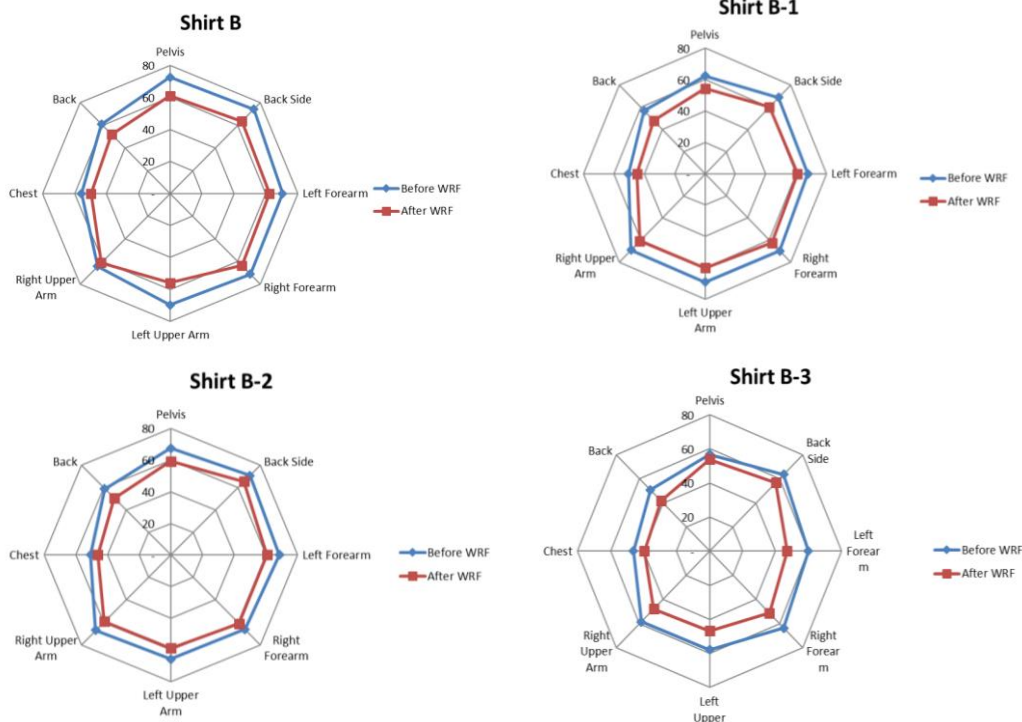


**Figure 6.** Heat loss values in  $W/m^2$  from the body segments of shirts B, B-1, B-2 and B-3

Figure 6 shows the heat loss values for shirts B, B-1, B-2 and B-3. It can be said that, the heat loss values decreased after water repellent finishing treatment for each shirt. The heat loss changes for shirts B, B-1, B-2 and B-3 were 13%, 12%, 10% and 16%, respectively.

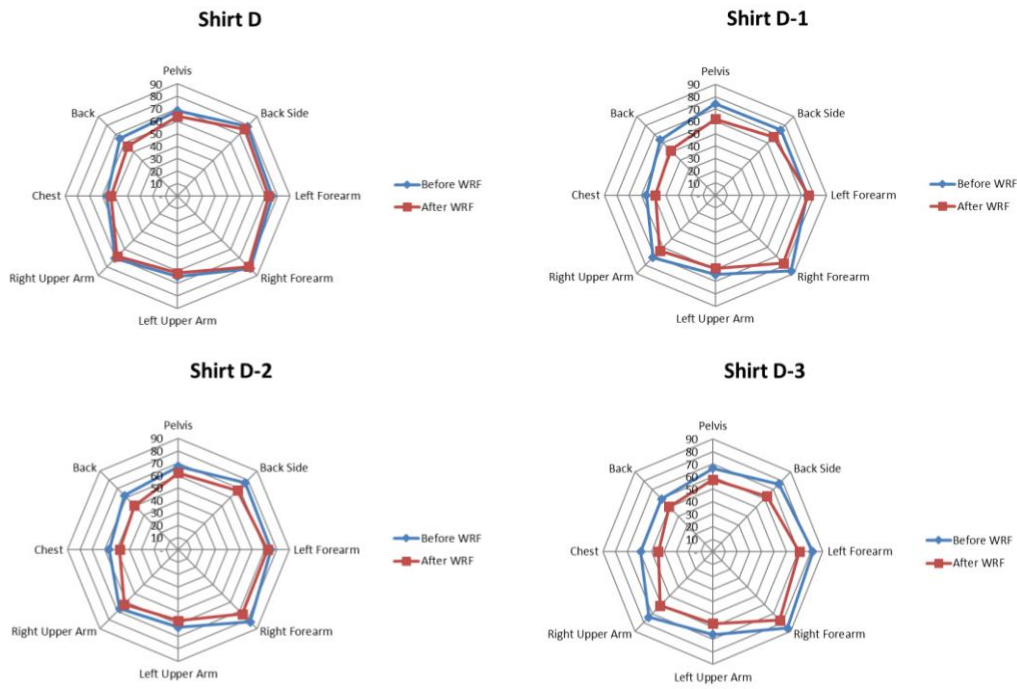


**Figure 7.** Heat loss values in  $W/m^2$  from the body segments of shirts D, D-1, D-2 and D-3

Figure 7 demonstrates the heat loss values for shirts D, D-1, D-2 and D-3. With respect to the graphs, it can be seen that, for each shirt the heat loss values decreased after water repellent finishing treatment as other specimens. The heat loss changes for shirts D, D-1, D-2 and D-3 were 4%, 11%, 11% and 16%, respectively.

**Table 2.** The T-Test results for heat loss values ( $W/m^2$ )

		N	Mean	Std. Deviation	t	df	p
Shirt A	Before WRF	30.00	80.88	0.80	258.02	37.50	0.000
	After WRF	30.00	40.52	0.31			
Shirt B	Before WRF	30.00	81.32	1.37	54.16	31.31	0.000
	After WRF	30.00	67.48	0.27			
Shirt B-1	Before WRF	30.00	78.93	0.50	124.63	35.58	0.000
	After WRF	30.00	66.87	0.17			
Shirt B-2	Before WRF	30.00	78.19	1.61	42.27	32.35	0.000
	After WRF	30.00	65.39	0.39			
Shirt B-3	Before WRF	30.00	72.77	1.14	70.85	35.48	0.000
	After WRF	30.00	57.16	0.38			
Shirt D	Before WRF	30.00	86.72	1.15	60.22	32.09	0.000
	After WRF	30.00	73.69	0.27			
Shirt D-1	Before WRF	30.00	85.08	1.20	50.58	31.84	0.000
	After WRF	30.00	73.69	0.27			
Shirt D-2	Before WRF	30.00	83.99	0.79	87.25	35.89	0.000
	After WRF	30.00	70.75	0.27			
Shirt D-3	Before WRF	30.00	83.99	0.79	100.89	33.74	0.000
	After WRF	30.00	68.94	0.23			

Table 2 shows the t-test results of average heat loss values for each shirt. With respect to the obtained data, it was clear that, there was a significant difference in average heat loss scores for all shirts between the tests conducted before and after WRF.

### 3.2 Clothing insulation

The total thermal insulation and effective thermal insulation values were calculated regarding to global method and the minimum, maximum, mean and standard deviation values are given in Table 3.

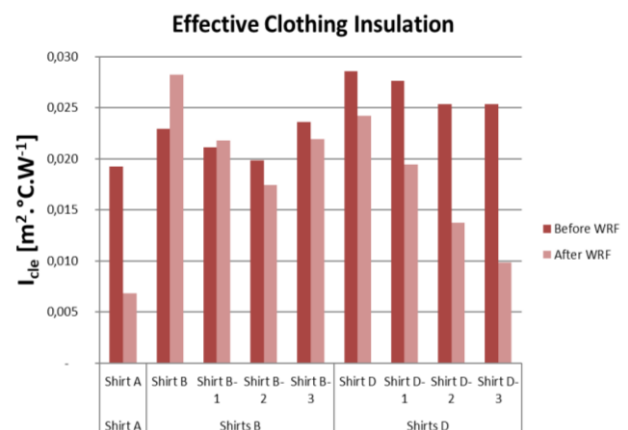
**Table 3.** Total thermal insulation and effective thermal insulation values of all shirts.

		$I_T$ [ $m^2.K.W^{-1}$ ]				$I_{cle}$ [ $m^2.K.W^{-1}$ ]			
		Min.	Max.	Mean	Std. Deviation	Min.	Max.	Mean	Std. Deviation
Shirt A	Before WRF	0.124	0.129	0.127	0.001	0.016	0.022	0.019	0.002
	After WRF	0.117	0.120	0.118	0.001	0.006	0.008	0.007	0.001
Shirt B	Before WRF	0.125	0.133	0.129	0.002	0.017	0.026	0.023	0.003
	After WRF	0.138	0.140	0.139	0.001	0.027	0.029	0.028	0.000
Shirt B-1	Before WRF	0.125	0.128	0.127	0.001	0.018	0.025	0.021	0.002
	After WRF	0.132	0.133	0.133	0.000	0.021	0.023	0.022	0.001
Shirt B-2	Before WRF	0.121	0.130	0.125	0.003	0.016	0.022	0.020	0.002
	After WRF	0.127	0.130	0.128	0.001	0.017	0.018	0.017	0.000
Shirt B-3	Before WRF	0.122	0.131	0.129	0.002	0.018	0.028	0.024	0.003
	After WRF	0.131	0.135	0.133	0.001	0.021	0.023	0.022	0.000
Shirt D	Before WRF	0.131	0.139	0.136	0.002	0.024	0.032	0.029	0.002
	After WRF	0.137	0.140	0.139	0.001	0.023	0.025	0.024	0.001
Shirt D-1	Before WRF	0.130	0.137	0.135	0.002	0.025	0.031	0.028	0.002
	After WRF	0.134	0.135	0.134	0.000	0.019	0.021	0.019	0.001
Shirt D-2	Before WRF	0.127	0.138	0.133	0.003	0.019	0.031	0.025	0.003
	After WRF	0.128	0.129	0.129	0.000	0.012	0.015	0.014	0.001
Shirt D-3	Before WRF	0.130	0.135	0.133	0.001	0.019	0.031	0.025	0.003
	After WRF	0.123	0.126	0.125	0.000	0.009	0.012	0.010	0.001

The effective clothing insulation values were calculated and comparisons were done both graphically as well as statistically. Figure 8 shows the average values of the effective clothing insulation of all shirts obtained before and after WRF. The heat loss value of shirt A decreased after WRF treatment (Figure 5), however, the effective clothing insulation value of shirt A also decreased after WRF treatment. This result can be related to the air gap between the manikin's body and the shirt. Shirt A was a loose fitting 100% cotton shirt and did not fit very tight to the thermal manikin and there was a higher air gap for shirt A than the other shirts. Therefore, it can be concluded that, the 180% decrease on effective clothing insulation might be caused by this air gap. Moreover, since the thermal manikin only senses dry heat transfer and all tests were conducted in dry state, the negative effect of poor moisture transportation and release of cotton fabric on thermal insulation is not considered.

Since the testing conditions were  $23 \pm 1,5^\circ C$  constant ambient temperature and  $60 \pm 5\%$  relative humidity, which can be consider as a warm environment, lower thermal insulation will provide more heat flux and better thermoregulation. In this scope, it can be considered as more appropriate if the thermal insulation is the same or lower after WRF. The increase in effective clothing insulation of shirt B-1 was not statistically significant ( $p=0,158$ ), where the increase in effective clothing insulation of shirt B was statistically significant ( $p=0,000$ ).

The decreases in effective clothing insulation of shirt B-2, B-3, D, D-1 D-2 and D-3 were 14%, 8%, 18%, 42%, 84% and 157%, respectively. Table 4 shows the t-test results of effective clothing insulation values of shirts regarding to water repellent finishing state.

**Figure 8.** Average values of effective clothing insulation of all shirts

As it can be seen in Table 4, in shirt B-1, there was no significant difference in effective clothing insulation scores between the test results obtained before WRF ( $M=0,02$ ,  $SD=0,002$ ) and after WRF ( $M=0,02$ ,  $SD=0,001$ );  $t(32,93)=-1,44$ ,  $p=0,158$ . For shirts A, B, B-2, B-3, D, D-1, D-2 and D-3, it was observed that there was a significant difference in average effective clothing insulation scores between the

test results obtained before and after WRF. In order to determine the difference within groups and to perform pairwise comparisons, repeated measures ANOVA was used. According to the effective clothing insulation values obtained from the tests before WRF, there was a significant difference between all shirts ( $p=0,00$ ). With regards to the test results obtained from the tests conducted after WRF, there was a significant difference between all shirts ( $p=0,03$ ). Taking into consideration the pairwise tests, there were no significant differences between shirt B and shirt B-2 ( $p=0,717$ ), shirt B and shirt B-3 ( $p=0,313$ ) and shirt D and shirt D-1 ( $p=0,099$ ).

Regarding to Figure 8 and statistical treatment, shirt B presented higher effective clothing insulation properties, in which the water repellent finishing treatment had an unexpected behaviour. Moreover, the change in effective clothing insulation of shirt B-1 was not statistically significant (Table 4) and this showed that, B-1 seemed to be the only structure that was not influenced from water repellent finishing treatment and it can be concluded the finishing does not affect the thermal comfort properties of shirt B-1.

### 3. CONCLUSION

In the present study, evaluating the effect of water repellent finishing on thermal insulation properties of rowing shirts by using a thermal manikin was aimed. Regarding to the recommendations of the collaborating company, two rowing shirts were chosen, which have three combined knitting structures each. The shirts with these different knitting structures were manufactured as single structures and in addition, one 100% Cotton shirt was included to the study. The thermal manikin tests were conducted with all

shirts and later the shirts were treated with a water-repellent finishing (5% of a fluorocarbon-based product). After WRF, the thermal manikin tests were repeated in same conditions.

Regarding to the obtained data there was a statistically significant difference in average heat loss scores for all shirts between the tests conducted before and after WRF.

100% Cotton shirt had 180% decrease in effective clothing insulation and this might be caused the lack of the negative effect of poor moisture transportation and release of cotton fabric on thermal insulation. In warmer temperatures, lower thermal insulation provides heat flux and as a conclusion, better thermoregulation. As obtained by the conducted ANOVA tests, shirt B and shirt B-1 had higher effective thermal insulation value after WRF, where the difference was statistically significant ( $p=0,000$ ) for shirt B and the difference was not statistically significant ( $p=0,158$ ) for shirt B-1. Regarding to literature, the thermal conductivity of cotton fibre is 11,85 (W/(m K)) while for polyester it is 9,25 (W/(m K)), for polyamide it is 8,38 (W/(m K)), and for polypropylene it is 11,18 (W/(m K)) [25]. Comparing shirts group B with D, shirts group D had greater thermal insulation values although they have polypropylene in their combination instead of polyester. As exists in literature [26], this proves that, the fabric construction such as the channels on the fabric surface or the fibres placed intensely inside surface of the fabric as well as the fabric thickness have significant effect on thermal insulation value in combined materials. The shirts D, D-1 D-2 and D-3, which had 35% Polypropylene distinctly than the shirts B, B-1, B-2 and B-3, had higher difference in effective thermal insulation.

**Table 4.** The T-Test results for effective clothing insulation values for test series 1 and test series 2

		N	Mean	Std. Deviation	t	df	p
Shirt A	Before WRF	30.00	0.02	0.002	40.49	37.96	0.000
	After WRF	30.00	0.01	0.001			
Shirt B	Before WRF	30.00	0.02	0.003	-11.02	30.36	0.000
	After WRF	30.00	0.03	0.000			
<b>Shirt B-1</b>	<b>Before WRF</b>	<b>30.00</b>	<b>0.02</b>	<b>0.002</b>	<b>-1.44</b>	<b>32.93</b>	<b>0.158</b>
	<b>After WRF</b>	<b>30.00</b>	<b>0.02</b>	<b>0.001</b>			
Shirt B-2	Before WRF	30.00	0.02	0.002	7.66	31.69	0.000
	After WRF	30.00	0.02	0.000			
Shirt B-3	Before WRF	30.00	0.02	0.003	3.45	30.87	0.020
	After WRF	30.00	0.02	0.000			
Shirt D	Before WRF	30.00	0.03	0.002	11.11	33.47	0.000
	After WRF	30.00	0.02	0.001			
Shirt D-1	Before WRF	30.00	0.028	0.002	27.49	38.03	0.000
	After WRF	30.00	0.019	0.001			
Shirt D-2	Before WRF	30.00	0.025	0.003	3.391	29.00	0.002
	After WRF	30.00	0.01	0.001			
Shirt D-3	Before WRF	30.00	0.03	0.003	26.26	32.13	0.000
	After WRF	30.00	0.01	0.001			

The combined shirts had different effective clothing insulation values than the single structured shirts and it can be concluded that the garment design has an effect on thermal insulation of shirts. It can be suggested that, before designing process, the single structures should be tested and the results should be considered together with human body thermal and sweating responses during designing fabric-body part combination.

This study proves that, the thermal insulation of rowing shirts change according to the water repellent finishing treatment. Moreover, as it has been discussed in the previous researches [20], not only the water repellent finishing, but also the structure of garment is also important in terms of heat loss and thermal insulation.

Further studies will be conducted by new eco-friendly water repellent finishing products. Moreover, in order to

investigate the behaviour of climatic change on thermal insulation of rowing shirts, the thermal manikin tests will be conducted in different air temperature and humidity. In addition, the locked power mode of thermal manikin, which simulates the metabolism during exercise, will be used instead of constant skin temperature mode and the tests will be conducted again in the same climatic conditions.

### Acknowledgement

This work was supported by FEDER funds through the Competitiveness Operational Program - COMPETE and by national funds through FCT – Foundation for Science and Technology within the scope of the project POCI-01-0145-FEDER-007136. We would like to thank Elisabeth Martin and Silke Küblbeck for their kind support.

### REFERENCES

- Choudhury AKR, Majumdar PK, Datta C. 2011. *Improving comfort in clothing, Chapter 1: Factors affecting comfort: human physiology and the role of clothing*. The Textile Institute, England: Woodhead Publishing Limited, 459p.
- Das A, Alagirusamy R. 2010. *Science in clothing comfort*. The Textile Institute, England: Woodhead Publishing Limited, 173p.
- Li Y, Wong ASW. 2006. *Clothing biosensory engineering, Chapter 1: Introduction to clothing biosensory engineering*. The Textile Institute, England: Woodhead Publishing Limited, 381p.
- Abreu MJ. 2008. Validation of the thermal comfort behaviour of active wear through thermal manikin measurements. Proceedings of Futurotextiles 08 - 2nd International Scientific Conference Textiles of the Future, Kortrijk, Belgium.
- Abreu MJ, Catarino A, Cardoso C, Kueblbeck S. 2012. Influence of water-repellent finishing on outer water sportswear regarding thermal insulation. The Fiber Society 2012 Spring Conference, 23-25 May 2012, St. Gallen, Switzerland, pp. 40-42.
- Abreu MJ, Braga I, Duarte F. 2010. Simulating human physiological response with a thermal manikin testing different non active medical devices. *Journal Materials Science Forum, Editora Transtec*, 636-637, 36-40.
- Oliveira AVM, Branco VJ, Gaspar AR, Quintela DA. 2008. Measuring thermal insulation of clothing with different manikin control methods, comparative analysis of the calculation methods. 7th International Thermal Manikin and Modelling Meeting, Retrieved from: [https://www.adai.pt/7i3m/Documentos\\_online/papers/11.oliveira\\_portugal.pdf](https://www.adai.pt/7i3m/Documentos_online/papers/11.oliveira_portugal.pdf)
- Holmer I. 2004. Thermal manikin history and applications. *European Journal of Applied Physiology*, 92, 614-618.
- Abreu MJ, Catarino A, Cardoso C, Martin E. 2011. Effects of sportswear design on thermal comfort, AUTEX 2011 Conference, 8-10th June, Mulhouse, France, 50-55.
- Secher NH. 1993. Physiological and Biomechanical Aspects of Rowing. *Sports Medicine*, 15: 24. <https://doi.org/10.2165/00007256-199315010-00004>.
- McGregor A. 2015. Injury prevention and performance –are they mutually exclusive? What does science tell us?. *BMC Sports Science, Medicine and Rehabilitation*, 7 (Suppl 1):O7, doi: 10.1186/2052-1847-7-S1-O7
- Abreu MJ, Catarino AP, Haussermann N. 2016. Comfort effects of weft-knitted structures on rowing shirts using ir thermography, the fiber society, 2016 Spring Conference, Textile Innovations - Opportunities and Challenges.
- Secher NS, Volianitis S. 2009. *Handbook of sports medicine and science*. Rowing, John Wiley & Sons. Malaysia.
- Wang F, Song W. 2017. An investigation of thermophysiological responses of human while using four personal cooling strategies during heatwaves. *Journal of Thermal Biology*, 70, 37-44.
- Abreu I, Ribeiro P, Abreu MJ. 2017. The issue of thermal comfort of medical clothing in the operating room. *DYNA* 84(200), 234-239.
- Shishoo R. 2005. *Textiles in sport*. Cambridge: Woodhead Publishing Ltd.
- Horrocks A, Anand S. 2000. *Handbook of Technical Textiles*. Woodhead Publishing. England.
- Schindler WD, Hauser PJ. 2004, Chemical finishing of textiles. Woodhead Publishing in Textiles, England.76-83.
- Rastogi D, Breja K, Goyal N, Jassal M, Agrawal AK. 2013. Comparative analysis of selected fluorocarbon-based oil and water-repellent finishes on textiles. *Research Journal of Textile and Apparel*, 17, 20-28.
- Abreu MJ, Catarino A, Tama D. 2018. Evaluating the effect of fabric type on thermal insulation properties of sports clothing. *IOP Conference Series: Materials Science and Engineering*, Volume 460.
- ISO 9920:2007: Ergonomics of the thermal environment - Estimation of thermal insulation and water vapour resistance of a clothing ensemble.
- Oliveira AVM, Gaspar AR, Quintela DA. 2008. Measurements of clothing insulation with a thermal manikin operating under the thermal comfort regulation mode: comparative analysis of the calculation methods. *European Journal of Applied Physiology*. Vol. 104, 679-688.
- Hensel H. 1973. Neural processes in thermoregulation. *Physiological Reviews*, 53, 948-1017
- Das A, Alagirusamy R. 2011. *Improving comfort in clothing, Chapter 9: Improving tactile comfort in fabrics and clothing*, The Textile Institute. Woodhead Publishing Limited, England, 459p.
- Morton WE, Hearle JWS. 2008. *Physical properties of textile fibres*, Woodhead Publishing Limited. England.
- Bhatia D, Malhotra U. 2016. Thermophysiological wear comfort of clothing: An overview. *Journal of Textile Science and Engineering*, 6, 250. pp. 1-8.

# Experimental Investigation of the Performance of a Feedback Tension Control System Designed for Warping Machines

Recep Eren, Merve İhtiyar, Özge Çelik

Bursa Uludag University, Faculty of Engineering, Textile Engineering Department, Gorukle Campus 16059 Nilüfer, Bursa, Turkey

**Corresponding Author:** Recep Eren, erecep@uludag.edu.tr

## ABSTRACT

This paper presents a research work which investigates experimentally the performance of a tension control system realized by a controlled disc brake. An experimental set-up was established by using a creel with step motor-controlled disc brake, laser distance sensor, yarn tension sensor and a 2-unit winding machine. A software was developed in C programming language to read yarn tension and bobbin diameter data and then to control the disc brake by step motor drive. Experimental investigation was carried out with three different cotton yarn counts and unwinding speeds. It was shown that yarn tension changed from full to empty bobbin at a significant amount depending mainly on yarn number and unwinding speed. The feedback tension control system based on adjusting level of braking responded well to short, medium and long term tension variations and enabled unwinding tension control mostly within  $\pm 1$  cN deviation from the adjusted value.

## ARTICLE HISTORY

Received: 10.04.2019

Accepted: 22.10.2019

## KEYWORDS

warping, tension control, creel, tension measurement, weaving preparation

## 1. INTRODUCTION

Warping is an important preparation process before weaving and directly affects the efficiency of weaving process and quality of woven fabrics. Sectional warping is most widely used warping method among the others and warping tension is a critical parameter for a good quality warp preparation especially with increasing warping speeds. As it is well known, yarn tension shows a significant increase with decreasing bobbin diameter especially at last one third part of full bobbin diameter during unwinding. This tension change becomes more severe and deteriorates the warping quality at increasing warping speeds. Warp is wound on a conical drum in sections side by side in sectional warping machine until the total number of warp yarn is wound. Any tension change between sections causes winding of warp sections at different diameters and therefore different lengths. During transfer of the warp from conical drum to warp beam

(i.e., during beaming process), sections of different diameters are wound at different tension and this will produce irregular dyed sections in woven fabrics.

At increasing warping speeds, tension-controlled creels are required to keep the warping tension at the adjusted value irrespective of bobbin diameter for a good quality warp preparation. Tension to yarn can be given by two methods. First method has long been used in textile machines and processes and applies tension to yarns by friction. Friction is applied to yarns either by drawing yarns between two metal plates (additive) or by wrapping around certain number of cylindrical rods (multiplying type) [1]. These mechanical elements are called yarn brakes or yarn tensioners. In many yarn brakes, a combination of additive and multiplying methods is used. Weigh or spring force is employed to adjust tension in additive type yarn tensioners and wrapping angle is adjusted to apply the desired yarn tension in multiplying type of tensioners. Second method

**To cite this article:** Eren R, İhtiyar M, Çelik Ö. 2019. Experimental investigation of the performance of a feedback tension control system designed for warping machines. *Tekstil ve Konfeksiyon* 29(4), 289-299.

---

for applying tension to a yarn is to adjust the yarn feeding speed. As yarn is drawn at certain speed in warping, its tension is determined by yarn feeding speed from a bobbin in the creel. Most of the tension-controlled creels employ yarn brakes or tensioners using the first method. Individual yarn tension-controlled creel uses the second tensioning method where tension of each individual warp yarn is measured and yarn feeding speed is adjusted by a feedback tension control system to keep yarn tension at the adjusted value during warping process irrespective of bobbin diameter. There are as many feedback tension control systems as the number of bobbins in the creel. As there are as many tension sensors and yarn feeding motors as number of bobbins in the creel, it is more expensive tension control method. But it minimizes tension differences between warp yarns in a section and provides more precise tension control. Individual tension control system is available in commercially [2].

When the literature is reviewed, there are mainly patents explaining warp tension control in warping creels and its effect on warping quality. There are also some researches related to yarn tension in warping creels and its effect on warping quality and warp properties. Fernando and Kuruppu analyzed theoretically warp yarn tension change in warping creel during unwinding from conical bobbins [3]. They expressed mathematical relationships for different regions of the creel and calculated yarn tension for 20 and 40 tex warp yarns at 200 and 400 m/min speeds. Mathematical calculations showed that yarn tension changed significantly at different regions of warping creel from unwinding to warping drum. Yarn tension at yarn guide in unwinding region was calculated by the mathematical expression recommended by Isakov [4]. After evaluating the results, they recommended to use a tension controlled warping creel for a good quality and homogeneous warp preparation. Dorgham investigated experimentally the effect of warping speed and warp tension on warp yarn properties like breaking strength and breaking elongation [5]. Warps were prepared from polyester filaments with three yarn numbers (70, 150, 300 denier) and each with three applied tensions (0.15, 0.22, 0.29 cN/dtex) at 200, 400, 600 m/min warping speeds. Tensile strength and elongation at break were measured. The results of measurements showed optimum tensile strength at warping speed of 400m/min under a tension of 0.22 cN/dtex. In addition, the optimum elongation percentage was obtained at warping speed of 200 m/min, under a tension of 0.22 cN/dtex for 70 denier yarns. For 150 and 300 denier yarns, the optimum tensile strength and elongation percentage were measured at warping speed of 600 m/min under a tension of 0.29 cN/dtex [5]. Beerli and Guntli explained an apparatus and a method to control yarn tension in the creel of a sectional warping machine. The creel had a central drive motor for adjusting amount of braking in yarn brakes. Section warp tension was measured in the measuring roller unit just before the winding on cone drum and compared with the desired value. Depending on

the difference between them, yarn brakes of all units were adjusted by motor drive centrally to keep tension of warp sections constant [6]. Zeller et al explained a process for the operation of a bobbin creel. In addition to warp sheet tension measurement in each warp section, they measured tension of each individual warp end by a separate tension sensor. They also used an individual step motor drive for yarn brake of each bobbin. Yarn tension sensors were positioned at the front of creel in rows of 8 sensors. Before yarn brakes, yarn tensioners of rod and crepe type were used for pre-tensioning. Yarn tensioners were also able to be controlled by electric motors centrally or individually like yarn brakes. Yarn tensioners also prevented entanglements due to high yarn twist. According to invention in the patent, yarn tension of each individual warp was measured and the measured tension was compared with the desired tension. Pressure of yarn brake was adjusted by the step motor of each unit. In this way, irrespective of yarn length and bobbin position in the creel always the same yarn tension was obtained. Warp tension was also measured in sections and when there was a deviation between the set and the measured values, yarn brakes of all bobbins were adjusted. It was recommended in the patent that yarn tension would be measured at a position as close to winding unit as possible, for example between leasing reed and measuring rollers. Conventional controlled additive type of yarn brakes were used in the creel [7]. Kleiner and Jakop explained a method and a device for regulating and controlling warp yarn tension in warping creels. Brake unit or tensioning element of each bobbin was controlled by a separate motor. Apart from disc or rod type of brakes, a yarn wheel driven by a separate motor was used as a yarn tensioning element in which yarn was wrapped certain number of revolutions around the wheel and then taken to the winding unit after passing over a tension measurement sensor. A separate tension sensor was used for each warp yarn in the creel. In this way, as many feedback tension control systems as the number bobbins in the creel were formed and yarn tension was controlled and regulated during normal running in this way. The same control algorithms were not found sufficient for the start and stop periods of a warping machine. A different control method was explained in the patent based on winding speed of warp to drum for the start and stop periods. Based on winding speed change, acceleration of yarn, yarn tension, drive motor inertia and frictional forces affecting the motor were determined and total motor torque required during start and stop periods of a warping machine were calculated. By adjusting motor current during start and stop periods, yarn tension deviations from the set value were minimized. Individual yarn tension control also minimized tension differences between warp yarns of different lengths [8]. Baba explained a tension control method for warping machines in which he combined yarn speed control and breaking force adjustment. He conducted experiments at 800 m/min unwinding speed with Ne 40/1 cotton yarn and measured bobbin diameter together with yarn tension. He did not mention any other parameter regarding his measurements. He showed that yarn tension decreased up to

certain diameter starting from full bobbin and then after a minimum it turned to increase. Towards the empty bobbin, yarn tension showed a very sharp increase. He also showed a linear increase in yarn tension with yarn winding speed between 500 and 800 m/min corresponding around to 5.5 gr tension change. Baba explained a tension control approach based on adjusting yarn braking force at bobbin diameters relatively larger. As yarn tension showed increase above the adjusted value even after yarn brake is put out of action, he decreased winding speed to keep yarn tension constant during winding [9].

Although there are patents in the literature related to tension control systems in warping creels, no published research has been found in the literature investigating theoretically or experimentally the performance and limitations of tension control systems in warping creels. This paper presents an experimental research explaining the performance and limitations of a creel tension control system using controlled disc brakes.

## 2. MATERIAL AND METHOD

A research stand was developed by using a single unit creel and a bobbin winding unit as shown in Figure 1.

A tensiometer of 200 cN measuring interval was included in the research stand to measure yarn tension. Disc type of yarn brake was employed in the system and spring pressure was adjusted by a stepper motor in the disc brake to regulate yarn tension. Second stepper motor was included in the system to drive continuously the bottom disc. Motion is transmitted to the pressure spring via a worm and worm wheel and a screw mechanism. Bobbin diameter was measured by a laser sensor. Two stepper motors, the tension and laser sensors were interfaced to a PC and a software was developed in C programming language to collect data from tension and laser diameter sensors and to implement feedback tension control algorithms.

Figure 2 shows in more detail the pressure application mechanism in disc brake. The upper end of the spring is driven downwards by the nut of screw mechanism in which the thread pitch is 0.8 mm. Force induced in the spring due to compression affects as normal force to the upper plate of the disc brake. The motion is transmitted from the stepper motor to the screwed shaft via 1:16 gear ratio. Step motor used was able to run at maximum 300 rpm. Hence a spring pressure application speed of 0.25 mm/s was possible.

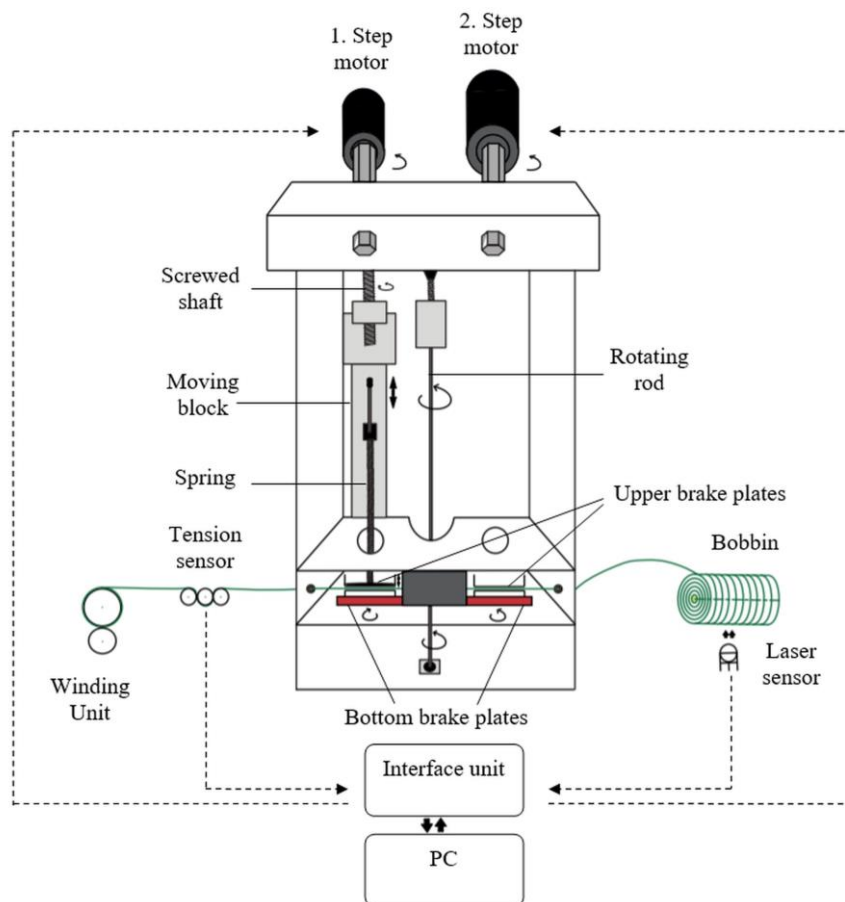
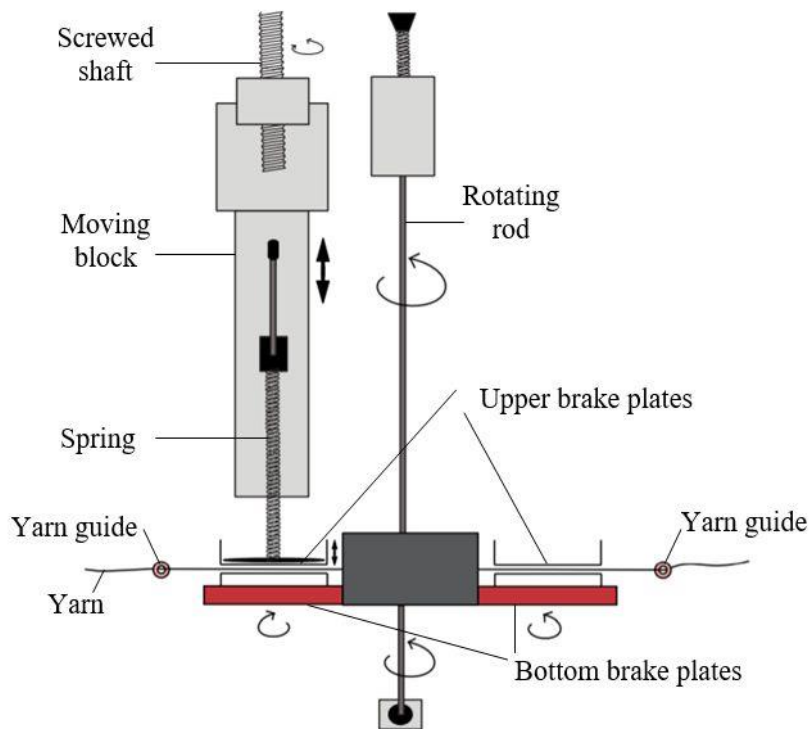


Figure 1. Experimental research stand



**Figure 2.** Pressure application mechanism in disc brake unit

To be able to develop and implement the feedback tension control system, yarn tension during unwinding needs to be analyzed. Figure 3 shows an example of typical yarn tension change during unwinding. As seen from the tension curve, yarn tension during unwinding fluctuates around its average value very significantly. There will always be tension fluctuations as in Figure 3 as the point of unwinding on bobbin surface shifts forward and backward during unwinding. Period of tension fluctuation is dependent on unwinding speed and bobbin and winding parameters. Therefore, it is difficult to determine a yarn length corresponding to one period of yarn tension change. On the other hand, one period of tension change corresponding to around 1.25 meters of yarn in one type of bobbin takes 125 msec for 600 m/min unwinding speeds. This period will be even shorter at speeds above 600 m/min. In warping machines, warp yarn is drawn from up to 800-1000 bobbins in sections. In this case, there will be a shift in tension curves due to different unwinding points on the different bobbins and total tension will be measured as the sum of all yarn tensions in a warp section. Therefore, total yarn tension change is expected to be different from single yarn tension change in both magnitude and shape and is not easy to predict. For this purpose, it will be a better strategy to apply a digital filter to the measured tension signal and obtain a stable tension value representing the average of tension change for automatic tension control purpose.

Experiments were carried out with 3 different cotton yarn counts. Yarn, winding and unwinding parameters used in the experimental work are presented in Table 1. Feedback tension control was applied at 330, 660 and 880 m/min unwinding speeds with Ne 40/1, 20/1 and 10/1 cotton yarns

from 200 mm full bobbin to 60 mm empty bobbin. Initially, all the bobbins were unwound at the specified speeds in Table 1 to determine warp tension variation from full to empty bobbin when braking was kept constant. Then, feedback tension control algorithms were implemented to keep yarn tension constant within the defined limits from full to empty bobbin. In implementing feedback tension control algorithms, initial average yarn tension was calculated over 25 tension values measured at 1.5 msec intervals and then 10-values moving average tension was determined and compared with the desired yarn tension. A  $\pm 0.5$  cN deviation in tension was allowed. When the moving average yarn tension reached above the desired one more than 0.5 cN, the stepper motor was driven in such a way as to decrease spring compression and release braking. In the case of the moving average tension decreasing more than 0.5 cN compared to the desired yarn tension, the stepper motor was driven in opposite direction to increase the spring compression and therefore braking effect. Stepper motor of braking unit was not driven when the moving average tension stayed within  $\pm 0.5$  cN of the desired tension. Stepper motor speed was not changed depending on the amount of deviation in tension; it was always driven at 2000 pulses/sec speed (around 300 rpm). Moving average approach was adopted in applying digital filtering to yarn tension data. For this purpose, yarn tension was measured at 1.5 msec intervals and 25 of them were initially averaged. The yarn length over which the initial average yarn tension was calculated corresponds to 0.5 meter of yarn at 800 m/min unwinding speed. Moving average tension was then calculated by using last initially averaged 10 and 50 tension values. When a last initially averaged tension is added as the first tension value, 10<sup>th</sup> or

50<sup>th</sup> tension value is removed and all the other initially averaged tension values are shifted one position further and new moving average tension is calculated. Figure 4 shows initially averaged yarn tension (grey) and 10- and 50-values moving averaged tension (black) curves from full to empty bobbin for Ne10/1 cotton yarn unwound at 880 m/min speed. Comparison of Figure 4.a and 4.b shows clearly a better filtered tension curve with 50-values moving average. In this research, 10-values moving average was used in forming feedback tension control system as it can be more responsive to even relatively shorter period average tension changes.

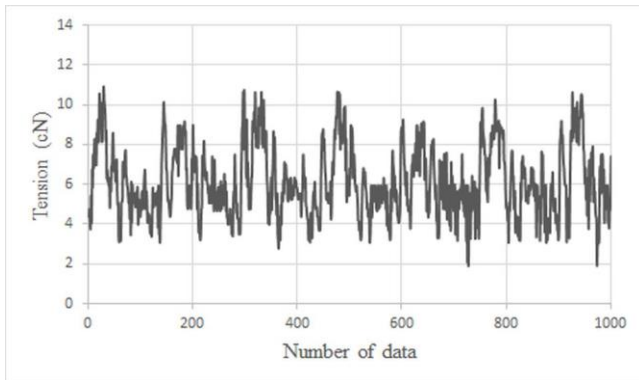
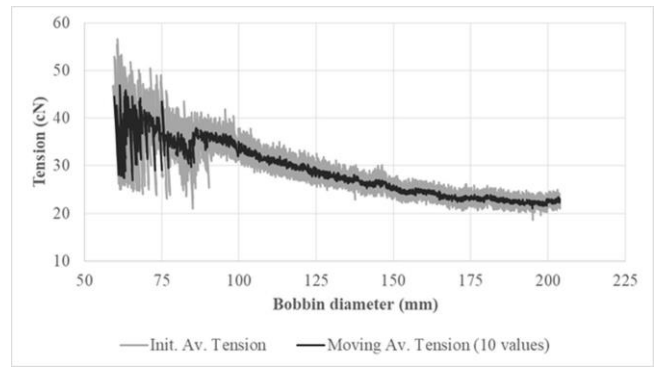
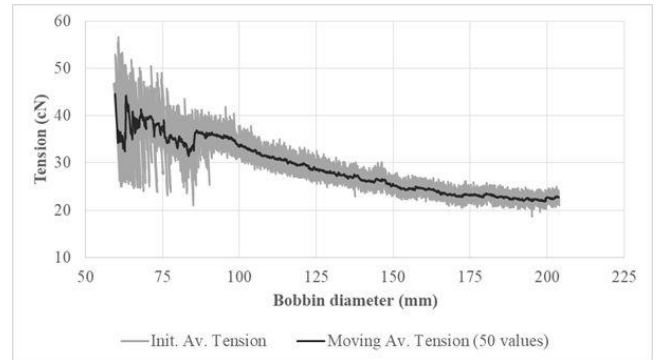


Figure 3. Yarn tension change during unwinding [10]



a. 10-values moving average curve



b. 50-values moving average curve

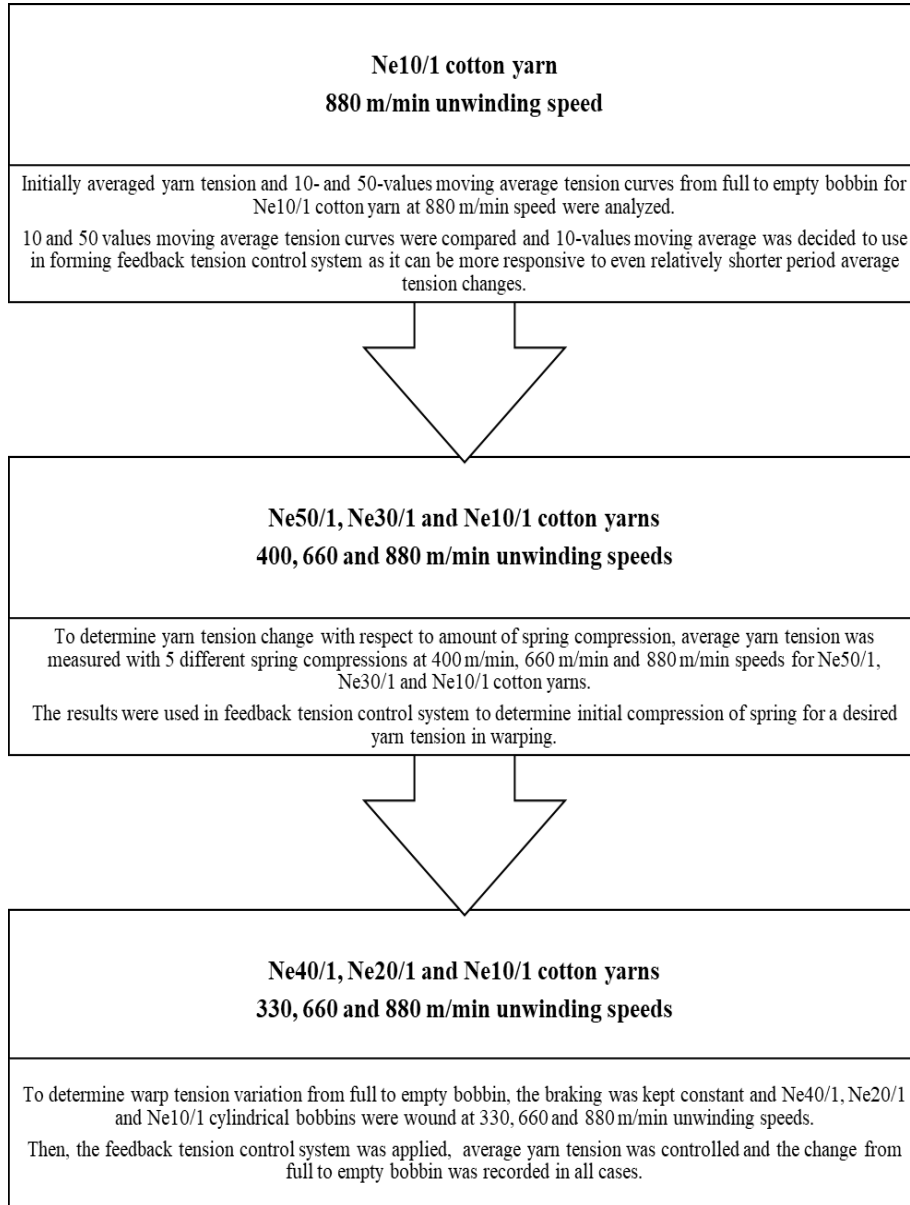
Figure 4. Initial averaged and moving averaged tension curves for Ne 10/1 cotton yarn unwound at 880 m/min speed

Table 1. Yarn, winding and unwinding parameters used in the experimental work

Yarn type, Winding type, Bobbin shape	Yarn count	Unwinding speed (m/min)	Full bobbin diameter (mm)	Empty bobbin diameter (mm)
Cotton,	Ne 10/1	330	200	60
		660	200	60
		880	200	60
Random winding, Cylindrical	Ne 20/1	330	200	60
		660	200	60
		880	200	60
	Ne 40/1	330	200	60
		660	200	60
		880	200	60

The method of the experimental study can be summarized as in Table 2.

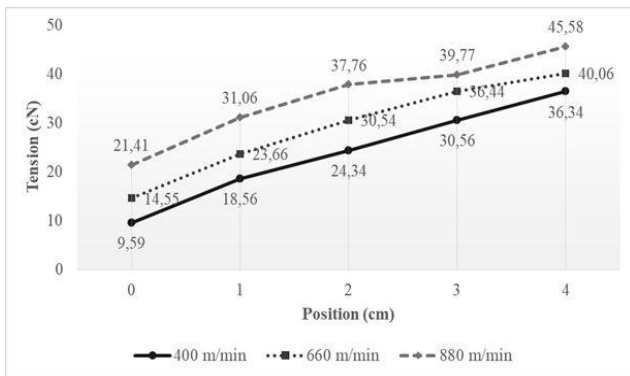
**Table 2.** Summary of the experimental work



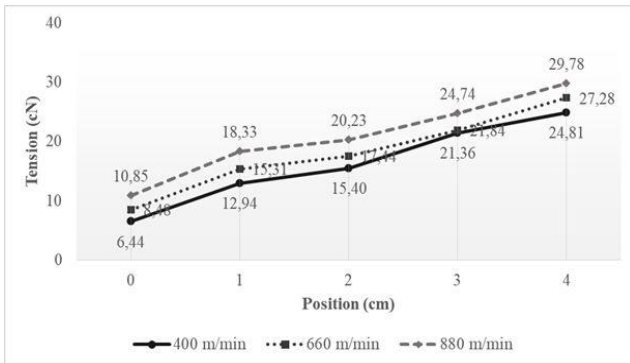
### 3. RESULTS AND DISCUSSION

Before implementing feedback tension control algorithms, experiments were conducted to determine yarn tension change with respect to amount of spring compression. Between 0 and 40 mm, yarn tension was measured with 6000 successive readings of 1.5 msec intervals and average tension was calculated in 5 different spring compressions at 400, 660 and 880 m/min speeds for Ne50/1, 30/1 and 10/1 yarn counts. Figure 5.a, 5.b and 5.c show yarn tension change with respect to the amount of spring compression for Ne10/1, 30/1 and 50/1, respectively. As seen from all figures, the average yarn tension increases almost linearly with the amount of compression. Slope of tension curves for

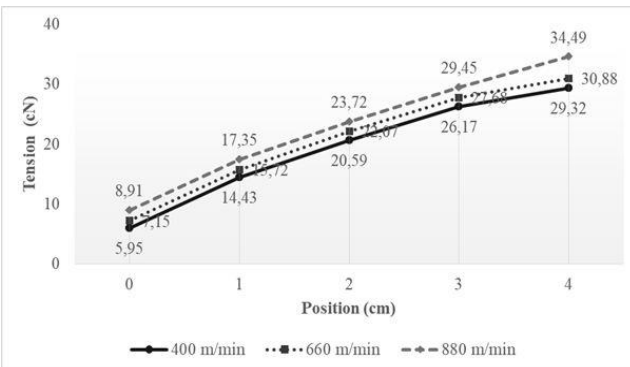
different speeds is very close to each other which indicate very close amount of tension change with increasing spring compression irrespective of yarn unwinding speed. These results will be used in feedback tension control system to determine initial compression of spring for a desired yarn tension in warping.



a. For Ne10/1 cotton yarn



b. For Ne30/1 cotton yarn

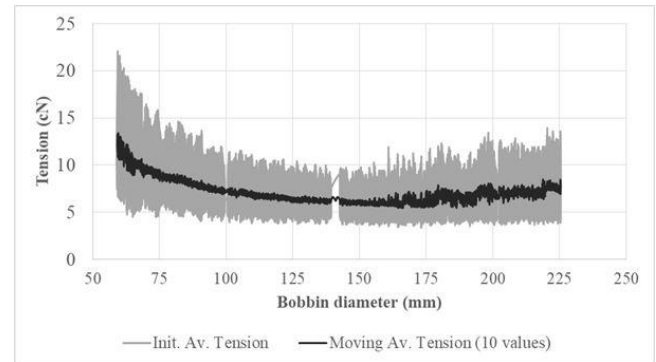


c. For Ne50/1 cotton yarn

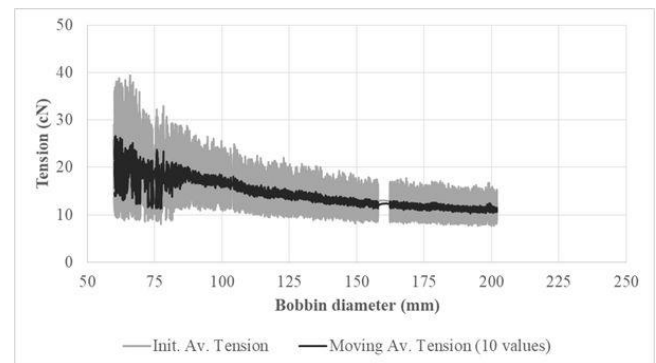
**Figure 5.** Yarn tension change with respect to amount of spring compression

Figure 6.a, 6.b and 6.c show initial average (grey) and moving average (black) tension changes with respect to bobbin diameter for Ne10/1 cotton yarn at unwinding speeds of 330, 660 and 880 m/min, respectively. At 330 m/min speed (Figure 6.a), there is around 8 cN deviation in yarn tension from full to empty bobbin. Also, medium and relatively short-term tension variations are observed between 170 and 200 mm bobbin diameters. Relatively short term, medium term and long term (from full to empty bobbin) tension variations are significant from practical point of view and require a feedback tension control system. In the case of unwinding speeds of 660 and 880 m/min speeds, yarn tension increases with few cN fluctuations (black curve) from full bobbin to 90 and 80 mm diameters for 660 and 880 m/min speeds, respectively. From these diameters up to empty bobbin, there are large

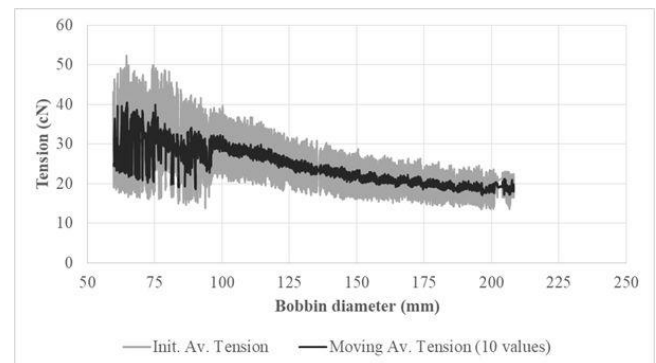
amount of tension fluctuations due to shift from to single to double balloon formation. Around 15 cN tension increases from full to empty bobbin at 660 m/min and 20 cN at 880 m/min speeds can be seen from Figure 6.b and 6.c. Also, short and medium term tension fluctuations of 10-15 cN level occur towards the end of bobbins at both 660 and 880 m/min speeds. Tension change and variations at this level can be very dangerous for both warping quality and efficiency and require control of tension.



a. For 330 m/min unwinding speed



b. For 660 m/min unwinding speed

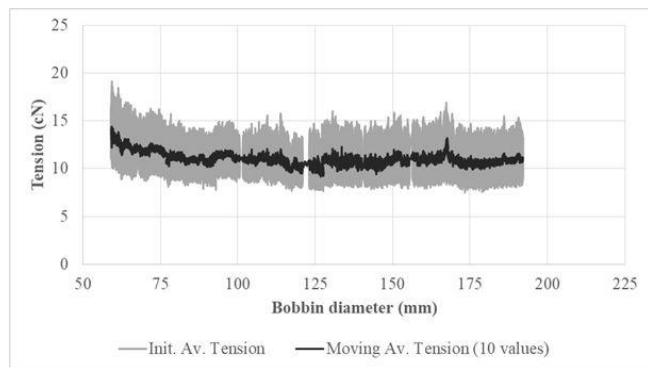


c. For 880 m/min unwinding speed

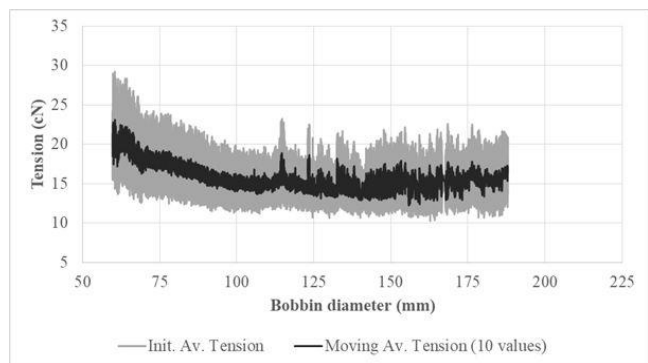
**Figure 6.** Change of initial average (grey) and 10-values moving average (black) tensions with respect to bobbin diameter for Ne 10/1 cotton yarn

Figure 7.a, 7.b and 7.c show yarn tension change during unwinding from full to empty bobbin at 330, 660 and 880 m/min speeds, respectively for Ne20/1 cotton yarn. At all unwinding speeds, yarn tension increases around 5 cN at 330 m/min, 9 cN at 660 m/min and 12 cN at 880 m/min

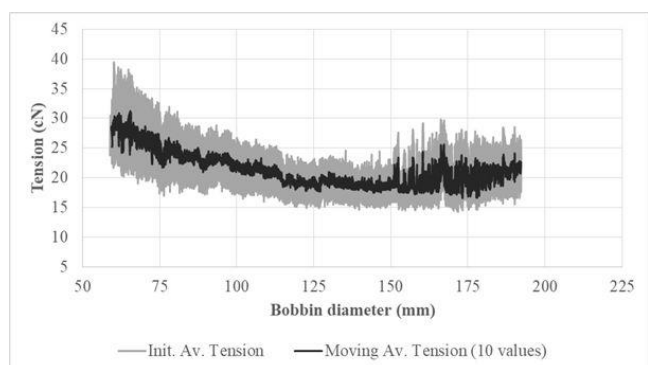
speeds from full to empty bobbin. In some bobbin diameters, yarn tension shows short and medium term fluctuations amounting up to 5 cN. Amount of short, medium and long term (from full to empty bobbin) tension fluctuations is at unacceptable levels from practical point of view and harms the quality of warping. Short and medium term tension fluctuations are thought to be due to lower quality bobbin winding.



a. For 330 m/min unwinding speed



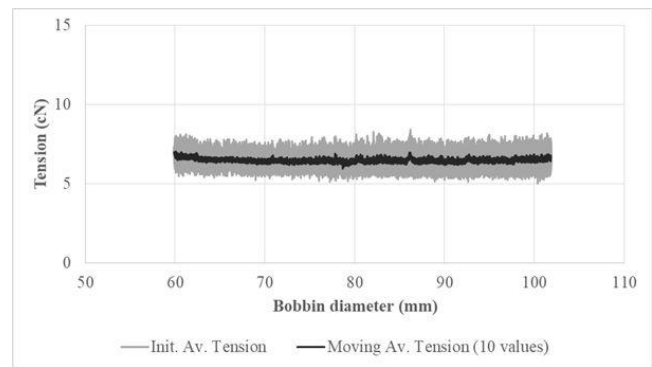
b. For 660 m/min unwinding speed



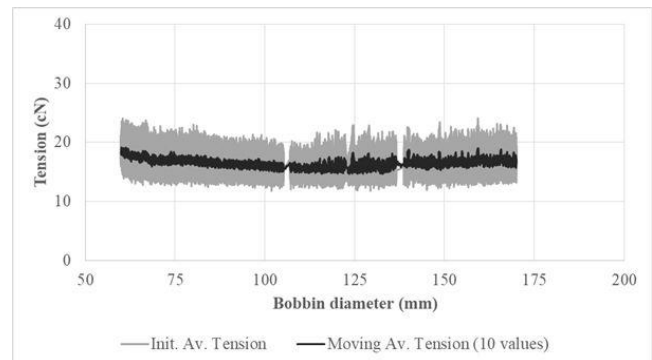
c. For 880 m/min unwinding speed

**Figure 7.** Change of initial average (grey) and 10-values moving average (black) tensions with respect to bobbin diameter for Ne 20/1 cotton yarn

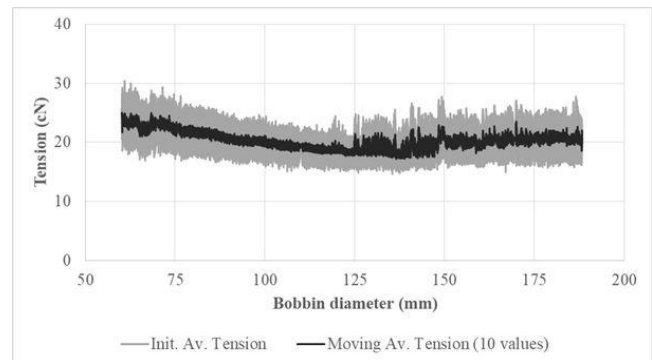
In the case of Ne40/1 cotton yarn, practically no significant tension change occurs at 330 m/min unwinding speed (Figure 8.a). But, around 4 cN tension change at 660 m/min speed and 7 cN tension change at 880 m/min can be observed from Figure 8.b and Figure 8.c. Also, some tension fluctuations of short and medium term arise at 660 and 880 m/min unwinding speeds.



a. For 330 m/min unwinding speed



b. For 660 m/min unwinding speed



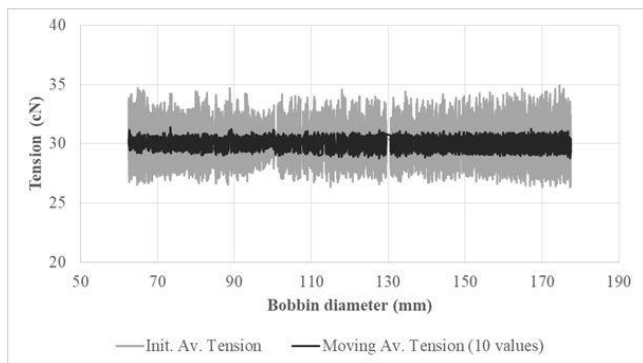
c. For 880 m/min unwinding speed

**Figure 8.** Change of initial average (grey) and 10-values moving average (black) tensions with respect to bobbin diameter for Ne 40/1 cotton yarn

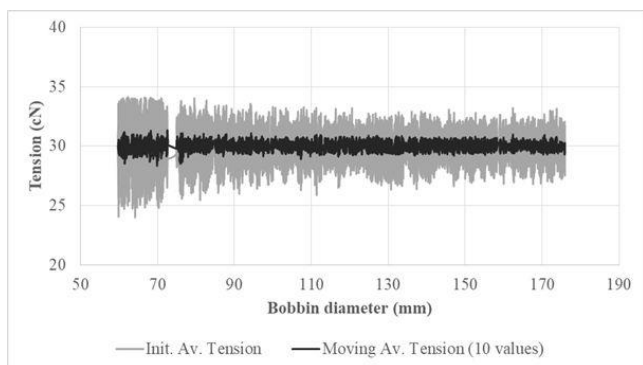
The yarn tension change curves of Ne10/1, 20/1 and 40/1 yarns show that there are significant deviations from the initially adjusted yarn tension during unwinding at even lower speeds like 330 m/min. At speeds like 660 and 880 m/min tension changes during unwinding are very significant and at harmful level for both quality and efficiency of warping process. These results show the importance of using a feedback tension control system in warping creels.

Feedback tension control system was applied in a single unit creel by using Ne 40/1, 20/1 and 10/1 cylindrical bobbins at 330, 660 and 880 m/min unwinding speeds and yarn tension change from full to empty bobbin was recorded in all cases. Feedback control system algorithms were applied as explained in "Material and Method" part.

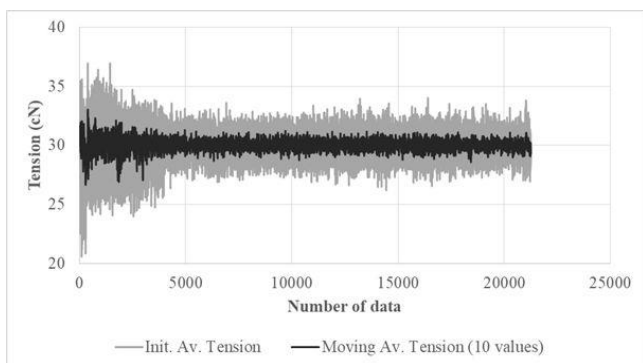
Figure 9.a, 9.b and 9.c show tension change from full to empty bobbin for Ne10/1 cotton yarn at 330, 660 and 880 m/min speeds with feedback control algorithms applied. Yarn tension change turned to horizontal with a small fluctuation remaining within  $\pm 1$  cN at 330 and 660 m/min speeds (Figure 9.a and 9.b). At 880 m/min speed, yarn tension showed the same change as in 330 and 660 m/min speeds except the region corresponding last 90 mm bobbin diameter. In this region, yarn tension could be controlled with mostly  $\pm 2$  cN fluctuation. This fluctuation is thought to be due to the higher tension fluctuations occurring without tension control presented in Figure 6.c.



a. For 330 m/min unwinding speed



b. For 660 m/min unwinding speed

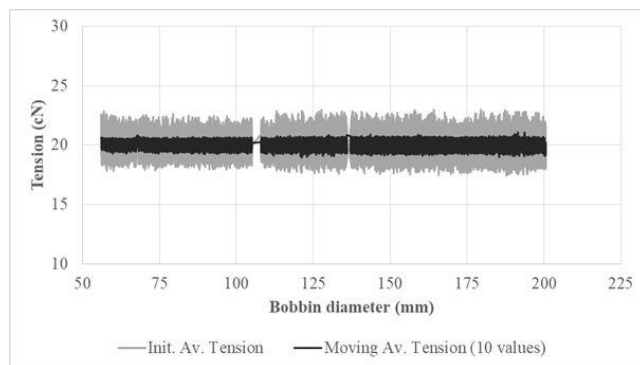


c. For 880 m/min unwinding speed

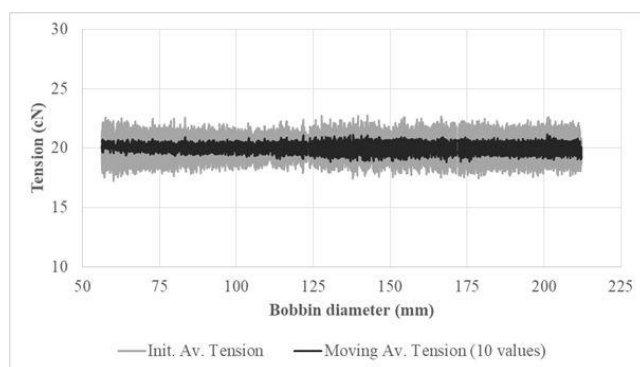
**Figure 9.** Change of initial average (grey) and 10-values moving average (black) tensions with respect to bobbin diameter for Ne 10/1 cotton yarn after applying feedback control algorithms

Figure 10 and Figure 11 show tension change from full to empty bobbin for Ne 20/1 and 40/1 cotton yarn respectively at 330, 660 and 880 m/min speeds with feedback control algorithms applied. As seen from all tension curves in

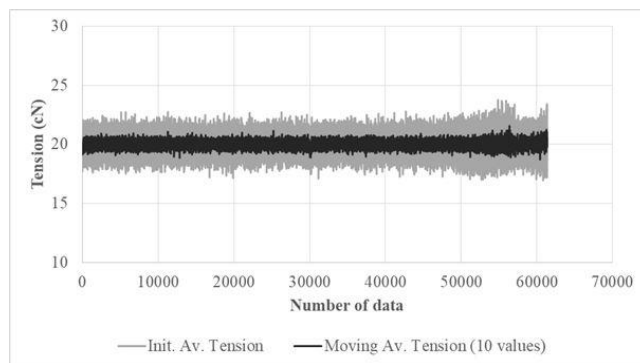
Figure 10 and Figure 11, yarn tension control was carried out at worst within  $\pm 1$  cN with both yarn counts. In many cases, control system performance was even better than  $\pm 1$  cN.



a. For 330 m/min unwinding speed



b. For 660 m/min unwinding speed

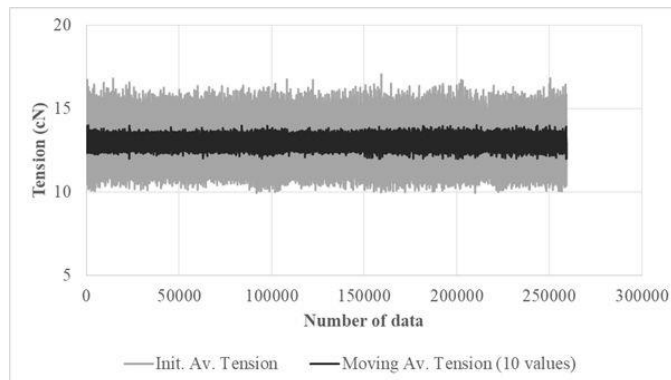


c. For 880 m/min unwinding speed

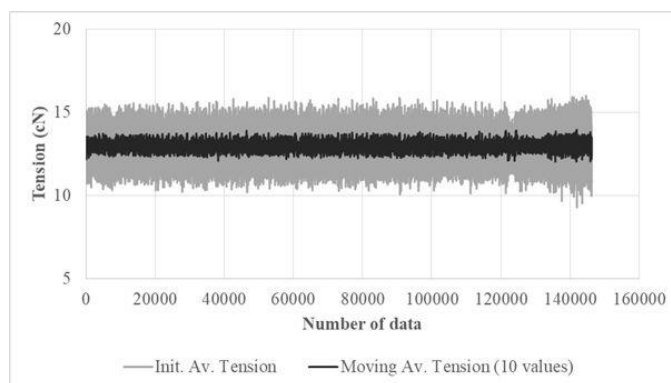
**Figure 10.** Change of initial average (grey) and 10-values moving average (black) tensions with respect to bobbin diameter for Ne 20/1 cotton yarn after applying feedback control algorithms

It should be noted here that yarn tension was measured at the exit of yarn brake and yarn contacted to only the yarn guide and yarn brake in this study. Therefore, some pressure was applied to yarn brake to obtain the desired tension even for thin yarn of Ne 40/1. As there are certain number of contact points in creels and winding unit, yarn tension is increased due to frictional forces in contact points and there may not be any need for brake application in thin yarns to reach to the desired yarn tension for warping. At high speeds like over 500 m/min, practically significant

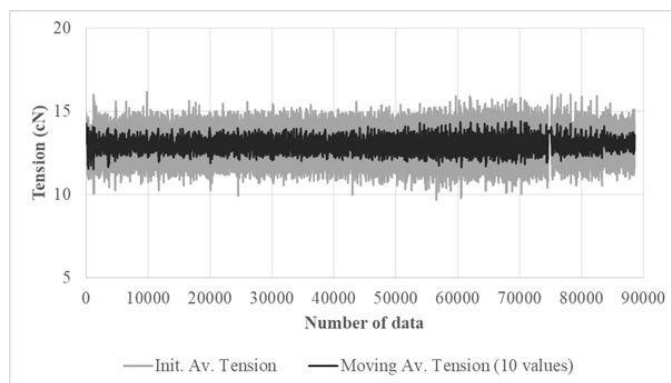
tension variations can occur even with yarns requiring tension control application. This limits the application of feedback tension control system in warping machines with disc brakes.



a. For 330 m/min unwinding speed



b. For 660 m/min unwinding speed



c. For 880 m/min unwinding speed

**Figure 11.** Change of initial average (grey) and 10-values moving average (black) tensions with respect to bobbin diameter for Ne40/1 cotton yarn after applying feedback control algorithms

#### 4. CONCLUSION

An experimental set up was developed to analyze yarn tension variations during unwinding from bobbins for warping process. Short, medium and long term yarn tension variations were observed at the significant level during unwinding of especially thicker yarns at higher speeds.

Depending on winding quality, relatively short or medium level tension variations were also recorded. At relatively high speeds for warping like 600 and 800 m/min, a significant yarn tension fluctuation occurred with thick yarns towards the empty bobbin (i.e., Ne 10/1) due to the shift from single to double balloon formation. Experimental results obtained with cotton yarns indicate the necessity for tension control in warping process at even moderate speeds like 300-400 m/min for good quality of warp preparation.

A controlled disc brake was included in the single unit creel to form a feedback tension control system. Amount of brake was adjusted by increasing or decreasing the spring compression using a stepper motor. Stepper motor speed was not sufficient for quick response during stop period of warping machine. Therefore, it was focused mainly on controlling medium and long term tension variations. Feedback control algorithms were applied to Ne 40/1, 20/1 and 10/1 cotton yarns at 330, 660 and 880 m/min speeds. It was shown that feedback tension control system successfully kept yarn tension at the adjusted value within  $\pm 1$  cN from full to empty bobbin for most of the experiments. Control system performance showed some deviations like  $\pm 2$  cN in experiments conducted with Ne 10/1 cotton yarn at 880 m/min unwinding speed in about last one third of full bobbin. Compared to tension fluctuations without feedback control, it can still be assessed as a good performance. In warp preparation with thicker yarns at high speeds, control system performance can be further improved by reducing unwinding speed towards empty bobbin.

In controlled brakes, control action is generated by decreasing braking with an increase in unwinding tension. There are many contact points on the yarn path between bobbin in the creel and winding head like cone drum. Friction in these contact points adds tension to the yarn and no brake application can be required for thin yarns at high speeds. In this case, tension increase during unwinding may not be compensated. This puts limitation to the use of controlled disc brakes for relatively thin yarns at high speeds. For yarns other than thin ones, sufficient amount of initial braking might be required from disc brake to compensate for yarn tension increase from full to empty bobbin.

Tension control system studied in this research does not include stop and start period of warping machines. As warping machines are suddenly stopped by applying a very strong brake yarn, tension of unwound yarns shows also a sudden decrease. Start period of a warping machine is much longer than stop period. Start and stop periods require application of the predetermined tension control algorithms to minimize tension variations for a short time interval and therefore necessitate a further study to develop the predetermined tension control algorithms. Research is in progress and will be the subject of another publication.

---

## ACKNOWLEDGEMENT

Main component of experimental set-up was developed in the project (Project Number: 215M372) supported by The Scientific and Technological Research Council of Turkey

(TÜBİTAK). We would like to express our sincere thanks to TÜBİTAK for supporting this project. Also, we would like to thank to Devsan Makina Tekstil San. Tic. Ltd. Şti. for manufacturing step motor drive unit of yarn brake.

## REFERENCES

1. Eren R. 2009. *Dokuma Hazırlık Teknolojisi*. Bursa: MKM Yayınları.
2. Karl Mayer. 2019, March 20. Yarn tensioners/ yarn stop motions. Retrieved from <https://www.karlmayer.com/en/products/warp-preparation/creels/yarn-tensioners-yarn-stop-motions/>.
3. Fernando E, Kuruppu RU. 2015. Tension Variation in sectional warping, Part I: Mathematical modeling of yarn tension in a creel. *International Journal of Engineering and Advanced Technolog* 4(3), 158-164.
4. Isakov NP. 1961. Yarn tension in a balloon. *Tech. of Textile Industry U.S.S.R.* 2, 92-98.
5. Dorgham ME. 2013. Warping parameters influence on warp yarns properties: Part I: Warping speed and warp yarn tension. *Journal of Textile Science and Engineering* 3(132), doi:10.4172/2165-8064.1000132.
6. Beerli M, Guntli E. 1989. Apparatus for regulating the warp section tension during warping. US4819310A. Place:US Patent.
7. Zeller HP, Bollen M, Spari A, Hane S. 2003. Process for the operation of a bobbin creel and bobbin creel for a winding system. US6513748B2. Place:US Patent.
8. Kleiner, A., Jakob, A. 2010. Method and device for operating a creel designed for a winding system and corresponding creel. US7770271B2. Place:US Patent.
9. Baba Y. 1991. Tension controller for warping machine and warping method. US5027484A. Place:US Patent.
10. Çelik Ö. 2018. Bobin sağımında iplik gerginliğine etki eden faktörlerin deneysel araştırılması (Doctoral dissertation). Bursa Uludag University Graduate School of Natural and App. Science Textile Engineering Department, Bursa.



# Sewing Machine Selection Using Linear Physical Programming

Mehmet Ali Ilgın

Manisa Celal Bayar University, Department of Industrial Engineering, Manisa, Turkey

**Corresponding Author:** Mehmet Ali Ilgın, mehmetali.ilgin@cbu.edu.tr

## ABSTRACT

Sewing is a critical operation in garment production process. Therefore, alternative sewing machines must carefully be evaluated prior to procurement. Multiple criteria decision making (MCDM) techniques can effectively be used in sewing machine evaluation process since multiple evaluation criteria including speed and price must be considered. However, physically meaningless subjective weights are assigned to evaluation criteria in most MCDM techniques. Linear Physical Programming (LPP) is a MCDM methodology that eliminates this subjective weight assignment process by allowing decision makers to express their preferences in a physically meaningful way. In this study, a sewing machine selection problem faced by a textile company is solved using LPP.

## ARTICLE HISTORY

Received: 13.08.2018

Accepted: 15.10.2019

## KEYWORDS

multiple criteria decision making, linear physical programming, sewing, machine selection, textile company

## 1. INTRODUCTION

Sewing is one of the most critical operations in garment production [1, 2]. Industrial sewing operations are usually carried out by using industrial sewing machines. There are many industrial sewing machine alternatives since various companies produce many different types of industrial sewing machines. Hence a textile company must evaluate those alternatives by considering multiple criteria including price, speed, weight and power consumption.

Multi-criteria decision making techniques were commonly used in industrial sewing machine evaluation due to the above-mentioned multi-criteria nature of the problem. Ertuğrul and Öztaş, 2015 applied MOORA (multi-objective optimization on the basis of ratio analysis) and TOPSIS (Technique for Order Preference by Similarity to Ideal Solution) multi criteria decision making techniques to a sewing machine selection problem [3]. The rankings proposed by those two techniques were compared. Ulutaş, 2017 employed EDAS (Evaluation based on Distance from Average Solution) for the evaluation of alternative sewing machines for a textile company [4].

The weights for the evaluation criteria were assigned subjectively in both of the above-cited studies. In this study, the subjective weight assignment process is eliminated by using linear physical programming (LPP). In LPP, the decision maker expresses his/her preferences for each criterion in a flexible and natural way. Then a weight algorithm is used to determine the criteria weights based on the preferences of the decision maker.

The rest of the paper is organized as follows. Section 2 provides brief information on LPP. The details on the application of LPP to a sewing machine selection problem faced by a company are presented in section 3. Finally, conclusions and future research directions are presented in section 4.

## 2. LINEAR PHYSICAL PROGRAMMING

Linear Physical Programming (LPP) was proposed by Messac et al., 1996 as an alternative to traditional optimization techniques [5]. LPP lets the decision maker define a multi objective decision making problem in a natural and flexible way. The decision maker can use one of

**To cite this article:** Ilgın MA. 2019. Sewing machine selection using linear physical programming. *Tekstil ve Konfeksiyon* 29 (4), 300-304.

the following four LPP classes for each criterion in the problem formulation [6, 7]: 1S (smaller is better), 2S (larger is better), 3S (value is better) and 4S (range is better). Figure 1 presents the LPP classes. The horizontal axis in this figure represents the preference ranges. These ranges can be presented for Class 2S as follows:

- Unacceptable range :  $c_k \leq s_{k5}^-$
- Highly undesirable range :  $s_{k5}^- \leq c_k \leq s_{k4}^-$
- Undesirable range :  $s_{k4}^- \leq c_k \leq s_{k3}^-$
- Tolerable range :  $s_{k3}^- \leq c_k \leq s_{k2}^-$
- Desirable range :  $s_{k2}^- \leq c_k \leq s_{k1}^-$
- Ideal range :  $c_k \geq s_{k1}^-$

The quantities  $s_{k1}^-$  through  $s_{k5}^-$  are specified by the decision maker for the  $k^{\text{th}}$  generic criterion. Let us assume that the decision maker specifies the values of  $s_{k1}^-$  through  $s_{k5}^-$  as 300, 250, 200, 150, 100, respectively. If the criterion value of an alternative is 280, it would locate in the

desirable range. If the criterion value is 180, it would be in the undesirable range [8].

The class function  $f_k$  is presented on the vertical axis. Criteria values are mapped into non-dimensional, strictly positive real numbers using this function. In other words, the class function creates a common scale with dimensionless values for each criterion. Considering Class 2S as an example, we can see that the value of the class function is very small if the criterion value is in the desirable range. If the criterion value is in the highly undesirable range, the value of the class function becomes too large.

The application steps of LPP can be presented as follows:

1. Appropriate class functions are determined for the criteria.
2. The limits for the desirability ranges are determined.
3. The following LPP weight algorithm [5] is employed for the calculation of the incremental weights:

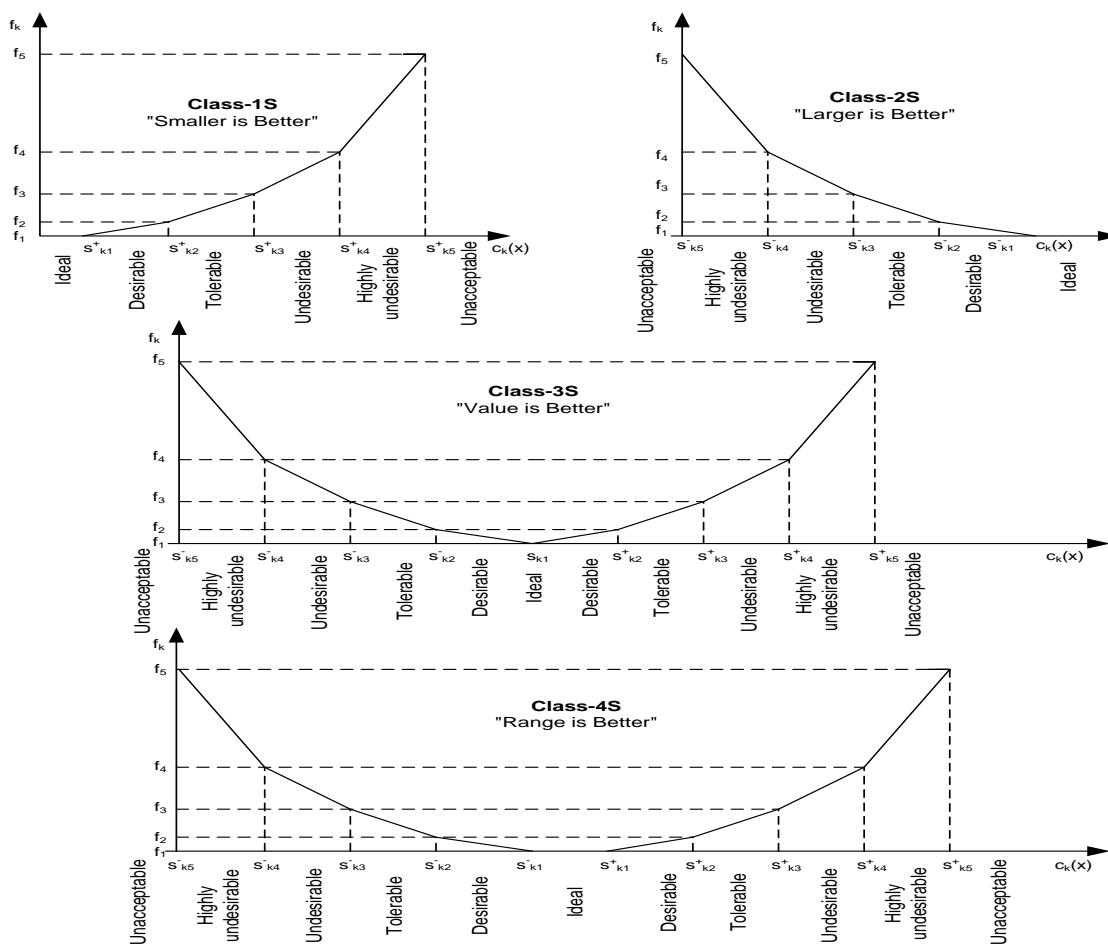


Figure 1. Classes in LPP

3.1. Initialize:

$\beta = 1.1, w_{k1}^+ = 0, w_{k1}^- = 0, \tilde{f}^2 =$  small positive number (say, 0.01),  $k=0; j=1, NC$ : number of criteria.

3.2. Set  $k = k + 1$

3.3. Set  $j = j + 1$

Evaluate, in sequence,

$$\tilde{f}^j, \tilde{s}_{kj}^+, \tilde{s}_{kj}^-, w_{kj}^+, w_{kj}^-, \tilde{w}_{\min}$$

If  $\tilde{w}_{\min}$  is less than a small positive number (say, 0.01), then increase  $\beta$ , and go to 3.2.

3.4. If  $j \geq 5$ , go to 3.3.

3.5. If  $k \neq NC$ , go to 3.2.

where  $k$  represents criterion,  $j$  represents range,  $\beta$  is a parameter of convexity (see [5]),  $f_k$  is the class function for the criterion  $k$ ,  $\tilde{f}^j$  represents the change in  $f_k$  that occurs as one travels across the range  $j$ ,  $\tilde{s}_{kj}^-$  and  $\tilde{s}_{kj}^+$  represent the widths of the  $j^{\text{th}}$  ranges on the negative and positive sides of criterion  $k$ ,  $w_{kj}^-$  and  $w_{kj}^+$  are negative and positive weights, respectively, for the range  $j$  of criterion  $k$  and  $\tilde{w}_{\min}$  is the minimum of  $w_{kj}^-$  and  $w_{kj}^+$ .

In class function, the slope increments between different desirability ranges are represented with positive and negative weights [7]. The following equations can be used for the calculation of those weights:

$$w_{kj}^+ = \frac{\tilde{f}^j}{\tilde{s}_{kj}^+} \quad (1)$$

$$w_{kj}^- = \frac{\tilde{f}^j}{\tilde{s}_{kj}^-} \quad (2)$$

In those equations,  $\tilde{f}^j$ ,  $\tilde{s}_{kj}^+$  and  $\tilde{s}_{kj}^-$  are calculated as follows:

$$\tilde{f}^j = \beta(NC - 1)\tilde{f}^{j-1} \quad (3)$$

$$\tilde{s}_{kj}^+ = s_{kj}^+ - s_{k(j-1)}^+ \quad (4)$$

$$\tilde{s}_{kj}^- = s_{kj}^- - s_{k(j-1)}^- \quad (5)$$

4. A total score ( $T$ ) for each alternative is calculated by taking the weighted sum of deviations:

$$\min T = \sum_{d_{ij}^-, d_{ij}^+} \sum_{k=1}^{NC} \sum_{j=2}^5 (w_{kj}^- \cdot d_{ij}^- + w_{kj}^+ \cdot d_{ij}^+) \quad (6)$$

where  $d_{ij}^-$  and  $d_{ij}^+$  represent the deviations from the corresponding target values for the  $k^{\text{th}}$  criterion value of the alternative of interest. Alternatives are ranked using total scores. The best alternative is the one with the lowest total score value.

LPP-based solution methodologies were developed in order to solve various problems in different domains including production planning [9], reverse logistics [10] and robot selection [11]. The interested reader is referred to a comprehensive review by Ilgin and Gupta, 2012 for more information on LPP applications [6].

### 3. INDUSTRIAL SEWING MACHINE SELECTION USING LPP

This section presents the application of LPP to a sewing machine selection problem faced by a textile company. The

company tries to determine the most suitable single-needle lockstitch industrial sewing machine. The following five evaluation criteria were determined by interviewing the managers of the company:

- **Price:** Average market price in dollars (\$) was used. Price must be minimized in order to minimize the total cost of investment.
- **Power Consumption:** The company prefers industrial sewing machines with low power consumption in order to minimize its energy costs. The unit for power consumption is Volt-Amperes (VA).
- **Weight:** The weight of machine head in kilogram (kg) was considered as a criterion. The weight should be as low as possible for ease of transportation.
- **Maximum Speed:** Maximum speed in stitches per minute (spm) was considered as a criterion. Maximum speed of the machine should be as high as possible.
- **After-sale Support:** The quality of the after-sale support services offered by a sewing machine manufacturer is a vital criterion. This criterion is evaluated using a 10-point scale (10 being the highest after-sale support and 1 being the lowest after-sale support).

Table 1 presents the criteria values for the eight alternative industrial sewing machines (ISM) considered in this study. Target values for each criterion were presented in Table 2. Those values were determined by interviewing the managers of the company. The three criteria (Price, Power Consumption and Weight) were modeled as Class 1S while the other two criteria (Maximum Speed and After-sale Support) were modeled as Class 2S.

C++ programming language was used to code the LPP weight algorithm and the criteria weights presented in Table 3 were obtained using this algorithm. A screenshot from this algorithm is presented in Figure 2.

An LPP model for each ISM was constructed using Lingo (v17) mathematical programming software. Deviations from the target values for each ISM were determined using this model. As an example, deviations for ISM 1 are presented in Table 4. For instance, consider the first criterion (*price* -  $f_1$ ). The deviation for  $j=2$  can be determined in two steps. First, the value of the criterion (i.e., 1495, see the bolded number in Table 1) is subtracted from the target value (i.e., 1250; see the bolded number in Table 2). Then the absolute value (i.e., 245, see the bolded number in Table 4) of this difference is taken.

The total score for each ISM (see Table 5) was determined by solving the associated LPP model. For instance, the total score for ISM 1 is calculated by using the deviations from Table 4 and the criteria weights from Table 3:

$$\text{Total\_Score}_{\text{ISM1}} = 245*0.04 + 100*0.2 + 50*0.138462 + 7*2 + 2*2.4 + 500*0.01 + 5*1 = 65.5231$$

A ranking of alternative ISMs is also presented in Table 5. ISM 1 with the lowest total score is the best ISM based on the preferences of the decision makers.

Table 1. Characteristics of alternative ISMs

Machines	Price (\$)	Power Consumption (VA)	Weight (kg)	Maximum Speed (spm)	After-sale Support
ISM 1	1495	400	37	5000	8
ISM 2	1800	415	46	5000	8
ISM 3	2150	520	40.5	5000	6
ISM 4	1300	250	36	4000	6
ISM 5	2049	320	30	5000	6
ISM 6	1825	450	34.5	5000	8
ISM 7	2079	390	28	5500	6
ISM 8	1850	320	38	5000	6

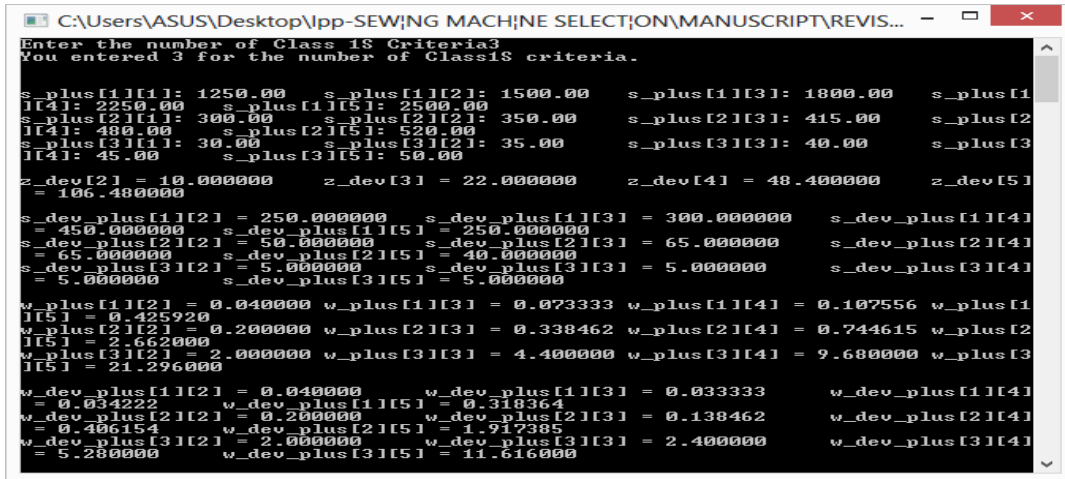


Figure 2. A screenshot from the weight algorithm

Table 2. Target values for the evaluation criteria

Criterion 1 (k=1): Price				Criterion 2 (k=2): Power Consumption			
Class 1S				Class 1S			
Preference	Preference Range	Limit	Limit Value	Preference	Preference Range	Limit	Limit Value
I	$\leq s_{11}$	$s_{11}$	1250	I	$\leq s_{21}$	$s_{21}$	300
D	$(s_{11}, s_{12})$	$s_{12}$	1500	D	$(s_{21}, s_{22})$	$s_{22}$	350
T	$(s_{12}, s_{13})$	$s_{13}$	1800	T	$(s_{22}, s_{23})$	$s_{23}$	415
UD	$(s_{13}, s_{14})$	$s_{14}$	2250	UD	$(s_{23}, s_{24})$	$s_{24}$	480
HU	$(s_{14}, s_{15})$	$s_{15}$	2500	HU	$(s_{24}, s_{25})$	$s_{25}$	520
UA	$\geq s_{15}$			UA	$\geq s_{25}$		
Criterion (k=3): Weight				Criterion 4 (k=4): Maximum Speed			
Class 1S				Class 2S			
Preference	Preference Range	Limit	Limit Value	Preference	Preference Range	Limit	Limit Value
I	$\leq s_{31}$	$s_{31}$	30	I	$\geq s_{41}$	$s_{41}$	5500
D	$(s_{31}, s_{32})$	$s_{32}$	35	D	$(s_{41}, s_{42})$	$s_{42}$	5000
T	$(s_{32}, s_{33})$	$s_{33}$	40	T	$(s_{42}, s_{43})$	$s_{43}$	4500
UD	$(s_{33}, s_{34})$	$s_{34}$	45	UD	$(s_{43}, s_{44})$	$s_{44}$	4000
HU	$(s_{34}, s_{35})$	$s_{35}$	50	HU	$(s_{44}, s_{45})$	$s_{45}$	3000
UA	$\geq s_{35}$			UA	$\leq s_{45}$		
Criterion 5 (k=5): After-sale Support				I: Ideal D: Desirable T: Tolerable UD: Undesirable HU: Highly Undesirable UA: Unacceptable			
Class 2S							
Preference	Preference Range	Limit	Limit Value				
I	$\geq s_{51}$	$s_{51}$	9				
D	$(s_{51}, s_{52})$	$s_{52}$	7				
T	$(s_{52}, s_{53})$	$s_{53}$	5				
UD	$(s_{53}, s_{54})$	$s_{54}$	3				
HU	$(s_{54}, s_{55})$	$s_{55}$	1				
UA	$\leq s_{55}$						

**Table 3.** Weights for each criterion

Criteria	$w_{k2}^+$	$w_{k3}^+$	$w_{k4}^+$	$w_{k5}^+$	$w_{k2}^-$	$w_{k3}^-$	$w_{k4}^-$	$w_{k5}^-$
Price ( $k=1$ )	0.04	0.033333	0.034222	0.318364	-	-	-	-
Power Consumption ( $k=2$ )	0.2	0.138462	0.406154	1.917385	-	-	-	-
Weight ( $k=3$ )	2	2.4	5.28	11.616	-	-	-	-
Max. Speed ( $k=4$ )	-	-	-	-	0.01	0.017400	0.010138	0.013889
After-sale Support ( $k=5$ )	-	-	-	-	5	1.85	2.5345	3.472265

**Table 4.** Deviations for ISM 1

Criteria	$j=2$	$j=3$	$j=4$	$j=5$
Price ( $k=1$ )	245	0	0	0
Power Consumption ( $k=2$ )	100	50	0	0
Weight ( $k=3$ )	7	2	0	0
Max. Speed ( $k=4$ )	500	0	0	0
After-sale Support ( $k=5$ )	1	0	0	0

**Table 5.** Total scores and ranks of alternative ISMs

Alternatives	Total Score	Rank
ISM 1	65.5231	1
ISM 2	175.6959	7
ISM 3	315.2143	8
ISM 4	70.719	2
ISM 5	84.63109	3
ISM 6	111.7504	6
ISM 7	102.3962	5
ISM 8	86.42765	4

#### 4. CONCLUSION

The use of the most suitable sewing machine has an utmost importance in the profitability and effectiveness of sewing operations. In this study, LPP was employed in order to solve the sewing machine selection problem faced by a textile company. A ranking of eight alternative industrial sewing machines was obtained based on the preferences of company managers. ISM 1 is proposed as the best sewing machine since it has the lowest total score.

Although LPP allows the decision maker to express his/her preferences using physically meaningful values it cannot consider the uncertainty and vagueness associated with decision maker's preferences. That is why development of a sewing machine selection approach based on fuzzy linear physical programming can be an interesting future research topic.

#### REFERENCES

1. Silva LF, Lima M, Carvalho H, Rocha AM, Ferreira FN, Monteiro JL, Couto C. 2003. Actuation, monitoring and closed-loop control of sewing machine presser foot. *Transactions of the Institute of Measurement and Control* 25 (5), 419-432.
2. Syduzzaman M, Golder AS, 2015. Apparel analysis for layout planning in sewing section. *International Journal of Current Engineering and Technology* 5 (3), 1736-1742.
3. Ertuğrul I, Öztaş T. 2015. The application of sewing machine selection with the multi-objective optimization on the basis of ratio analysis method (moora) in apparel sector. *Tekstil ve Konfeksiyon* 25 (1), 80-85.
4. Ulutaş A. 2017. Sewing machine selection for a textile workshop by using edas method. *Journal of Business Research-Türk* 9 (2), 169-183.
5. Messac A, Gupta S, Akbulut B. 1996. Linear physical programming: a new approach to multiple objective optimization. *Transactions on Operational Research* 8 (2), 39-59.
6. Ilgin MA, Gupta SM, 2012. Physical programming: A review of the state of the art". *Studies in Informatics and Control* 21 (4), 349-366.
7. Messac A. 2015. Optimization in practice with matlab: for engineering students and professionals. Cambridge University Press, New York.
8. Ilgin MA, Gupta SM. 2012. Remanufacturing modeling and analysis. *CRC Press*, Boca Raton.
9. Gulsun B, Tuzkaya G, Tuzkaya UR, Onut S. 2009. An aggregate production planning strategy selection methodology based on linear physical programming. *International Journal of Industrial Engineering* 16 (2), 135-146.
10. Pochampally KK, Gupta SM. 2012. Use of linear physical programming and bayesian updating for design issues in reverse logistics. *International Journal of Production Research* 50 (5), 1349-1359.
11. Ilgin MA. 2017. Integrating linear physical programming and fuzzy logic for robot selection. *International Journal of Robotics Applications and Technologies* 5 (2), 1-17.



# Development of 3-D Hemispherical Biaxial Weft-Knitted Thermoset Composites

Özgür Demircan<sup>1</sup>, Tatsuya Kosui<sup>2</sup>, Shinsuke Ashibe<sup>2</sup>, Asami Nakai<sup>3</sup>

<sup>1</sup>Metallurgical and Materials Engineering Department, Faculty of Engineering, Ondokuz Mayıs University, Samsun, Turkey

<sup>2</sup>R&D New Technology Applications, Shima Seiki Mfg. Ltd., Wakayama, Japan

<sup>3</sup>Department of Mechanical and Systems Engineering, Faculty of Engineering, Gifu University, Gifu City, Japan

**Corresponding Author:** Özgür Demircan, ozgur.demircan@omu.edu.tr

## ABSTRACT

The present work concentrates on the development of 3-D hemispherical biaxial weft-knitted (BWK) thermoset composites. The objective is to improve the quality of the 3-D composites with BWK preform. Two kinds of the 3-D hemispherical BWK composites with the flat surfaced and 3-D dome shaped biaxial weft-knitted preforms were produced by hand lay-up method. The quantitative analysis of wrinkles was done by measuring the locking angles between the fiber bundles in the composites. Small numbers of wrinkle heights (1 height/1 cm) were observed on the flange surface of the 3-D hemispherical BWK composite with the dome shaped preform compared to the 3-D hemispherical BWK composite with the flat surfaced preform (10 heights/1 cm).

## ARTICLE HISTORY

Received: 31.01.2019

Accepted: 15.10.2019

## KEYWORDS

biaxial weft-knitting, 3-D thermoset composites, locking angle, wrinkle of surface

## 1. INTRODUCTION

The architecture of the fiber reinforcement affects strongly the form ability of the composites. A material with good form ability will require low forming pressure and will demonstrate the lesser instability. Knitted fabrics have high drapeability and complex geometrical parts can be manufactured by knitting technology.

Until now a lot of researches were done on the development of hemispherical 3-D composites [1-6]. The drapeability of dry textile fabrics for stampable thermoplastic preforms was investigated by Rozant et al. [7]. They studied the mechanical behaviour and drapeability of some woven and knitted fabrics. The preliminary studies on single point incremental forming for composite materials were reported by Fiorotto et al. [8]. They formed aluminum and composite by single point incremental forming technique and conducted a compression test in order to compare the mechanical properties of materials. The experimental device for the preforming step of the RTM process was

reported by Soulat et al. [9]. They developed tetrahedral and square punches and analyzed the evolution of preform of woven process, such as wrinkles and bucklings. They showed that preforming quality can be affected from the punch geometry, the number and the position of blank holders and values of pressure punch strokes and speeds. Vanclooester et al. [10] optimized deep drawing of multi-layered fabric composites and found out thicker preforms reduce the wrinkles of composites.

Because, the fabrication method of the biaxial weft-knitted fabrics was comparatively very new compare to the traditional knitting fabrics, it was very necessary to fabricate the 3-D composites with the BWK fabric. Additionally, there was found no research about the 3-D hemispherical BWK thermoset composites, which was produced with the dome shaped BWK preform. Also, we found no study about the 3-D dome shaped BWK preform, which was produced by the knitting machine. In this study, we would like to show the shapeability of the biaxial weft-knitted composites. The present work concentrates on the

**To cite this article:** Demircan Ö, Kosui T, Ashibe S, Nakai A. 2019. Development of 3-D Hemispherical Biaxial Weft-Knitted Thermoset Composites. *Tekstil ve Konfeksiyon* 29(4), 305-310.

development of the 3-D hemispherical biaxial weft-knitted thermoset composites.

## 2. MATERIAL AND METHOD

### 2.1 Material

330 tex and 44 tex aramid yarns (Kevlar 29, Toray Dupon Co. Ltd., Japan) were used as reinforcement and stitch yarns (Table 1). The wale density (wale/cm) was 2 end/cm, course density (course/cm) was 10 end/cm and machine gauge (needles/inch) was 18 needles/inch. Vinyl ester resin (Ripoxy R-806, Showa High Polymer Co. Ltd., Japan) was used as matrix. The curing agent (methyl ethyl ketone peroxide (PERMEK® N)) was obtained from NOF Corporation, Japan. Thin and flexible polypropylene (PP) film (Futamura Kogac Ltd., Japan) was used during fabrication of the composite panels. The biaxial plain weft-

knitted fabrics were produced on a flat bed knitting machine (Shima Seiki Mfg., Ltd., Japan). The schematic drawing of the BWK fabric is shown in Figure 1. The biaxial weft-knitted fabric structures had same plain knitted loop architecture. The flat surfaced and dome shaped BWK structures are shown in Figure 2a, b. There was ellipse shapes on the surface of the dome shaped biaxial weft-knitted fabric. The ellipse shapes were given by a special knitting technique (short row knitting) during fabrication of the BWK fabric (Figure 2c, d). In knitting, a short row is a row that is not fully knitted; the work is turned before reaching the end of the row. Just before the work is turned, the yarn is generally passed around the next unknitted stitch. When dome shaped biaxial weft-knitted specimen was produced on the machine, it had a flat surface. The dome shape was given by hand in a second process (Figure 3). The flat surfaced and dome shaped BWK materials were prepared by Shima Seiki Mfg. Ltd., Japan.

Table 1. Parameters of the BWK fabric

Sample name	Biaxial (warp and weft) yarns	Stitch yarn	Density of warp yarn in fabric (end/cm)	Density of weft yarn in fabric (end/cm)
Biaxial weft-knitted, aramid	AR 330 Tex	AR 44Tex	2	10

AR: Aramid

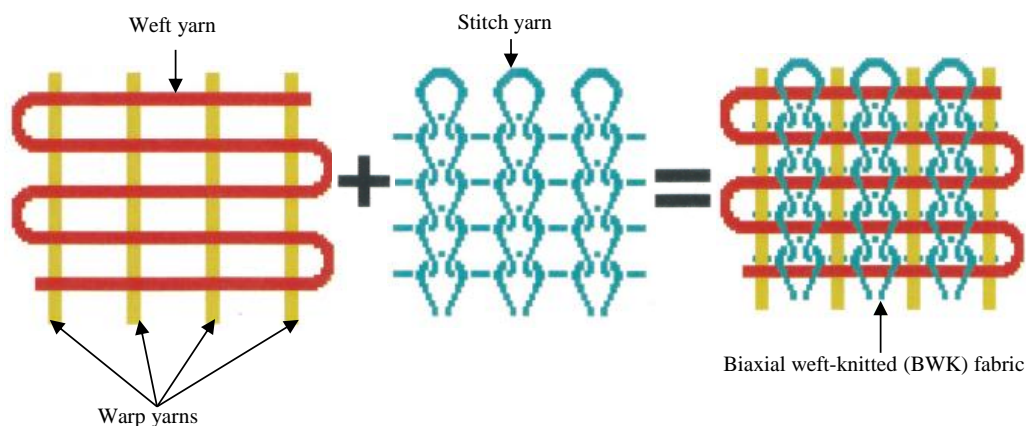
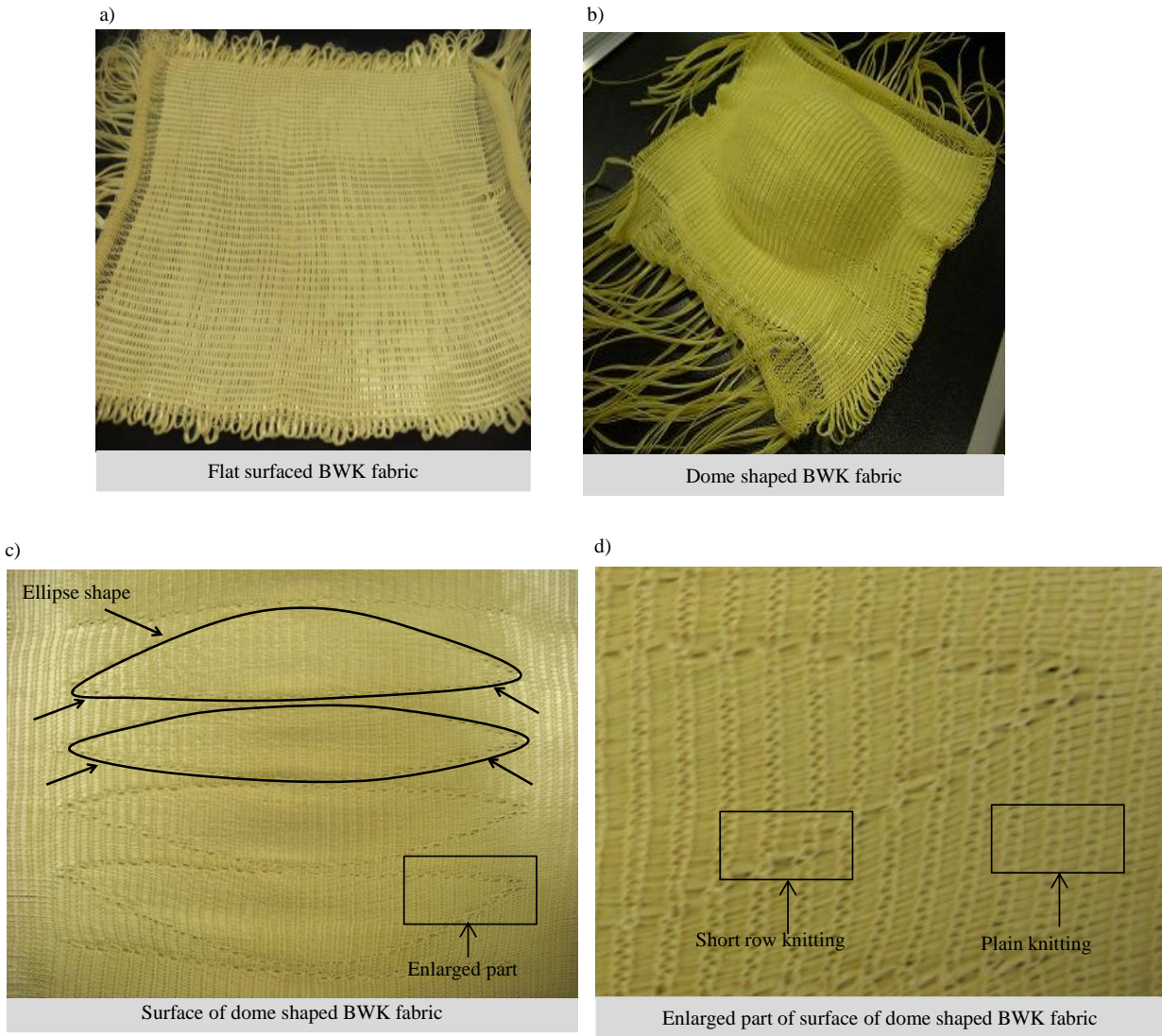


Figure 1. Schematic drawing of biaxial weft-knitted (BWK) preform

### 2.2 Method

In order to fabricate the 3-D composites, at first, the one layer BWK fabrics were impregnated with resin on a flat space of a table; the bottom and top surfaces of the resin impregnated BWK fabrics were covered with a film. After a few seconds, they were put into the PU molds. Polyurethane (PU) foam was used for the lower and upper molds. A special (thin and flexible) polypropylene (PP) film, Futamura Kogac Ltd., Japan, with 0.03 mm thickness was used during impregnation of the resin into the BWK

fabric. Two kinds of the one ply composite panels were fabricated by hand lay-up lamination method: (i) 3-D hemispherical BWK composite with flat surfaced fabric, (ii) 3-D hemispherical BWK composite with dome shaped fabric. The average thickness and the fiber volume fraction of the 3-D composite panels were about 2.0 mm and 35% respectively.



**Figure 2.** Biaxial weft-knitted (BWK) preforms a) flat surfaced, b) dome shaped, c) ellipse shapes on the surface of dome shaped BWK, d) enlarged part of the ellipse shape (short row knitting and plain knitting)

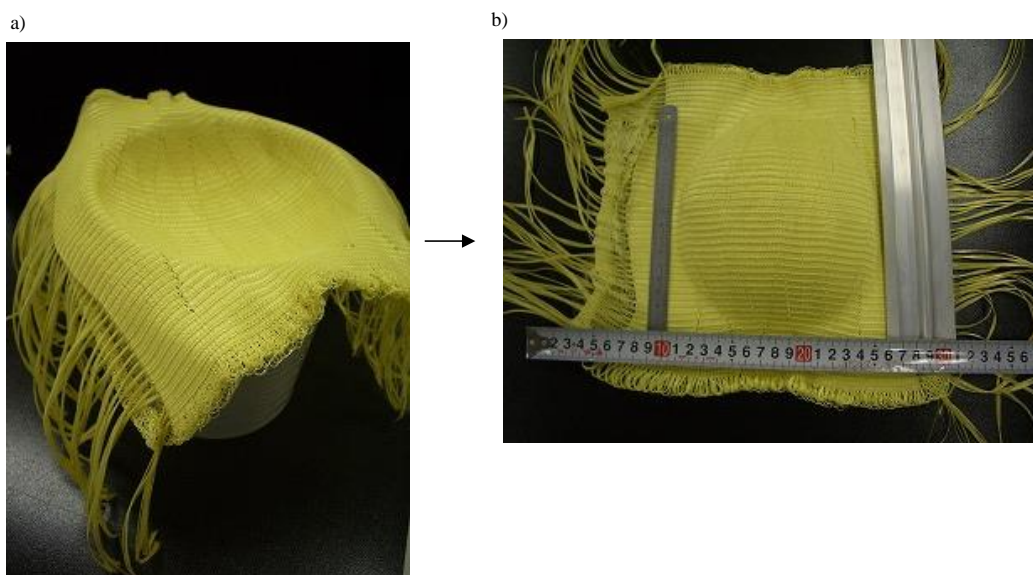


**Figure 3.** Photographs of preparation of 3-D dome shaped preforms

### 2.3 Locking Angle

The states of the fibres before and after deformation can be seen in Figure 4a, b. Before starting deformation of the fabric, the initial angle between the warp and weft biaxial fiber bundles was  $90^\circ$ . As the fabric deformed, the density of the warp and weft biaxial fiber bundles per unit area increased. After the first deformation, when we continued to further deformation, the critical shearing angle (locking angle) was reached. Thus, this angle can be used as a characteristic value for describing of the initial point of the wrinkles on the fabric surface.

## 3. RESULTS AND DISCUSSION

### 3.1 Effect of Locking Angle

In this part, the wrinkles on the surfaces of the composites were analyzed by quantitatively. Figure 5a, b demonstrates positions of the locking angles between the fiber bundles in the 3-D hemispherical BWK composite with dome shaped preform. Due to the wrinkles occurred on the surface of the 3-D composites with the BWK preforms, we understood

that the locking angles were reached for all the measurements. In Figure 5a, b, the locking angles were measured in 12 different positions from  $0^\circ$  to  $45.1^\circ$  in the 3-D hemispherical BWK composites.

A comparison of the locking angle versus is shown in Figure 6. During deformation without wrinkling is required for the forming into the complex shapes of the BWK composites, low locking angles are desired. The measured locking angles were agreed with amount of the wrinkle heights. The locking angles were reduced in both composites in positions from  $0^\circ$  to  $45.1^\circ$ .

At the same measured points, the composites with the dome shaped BWK preforms had lower locking angles, than the composites with the flat shaped BWK preforms. For example, the locking angles were  $45^\circ$  (flat shaped) and  $20^\circ$  (dome shaped) in positions at  $33^\circ$ . The ellipse shapes on the surface of the dome shaped BWK preforms in the dome shaped BWK composites would be reason of the lower locking angle compared to that was with the flat surfaced BWK preforms.

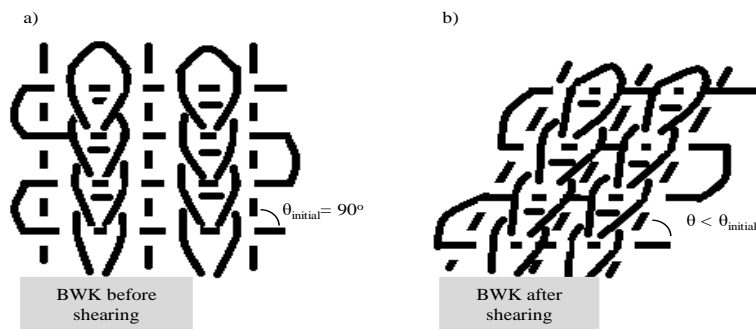


Figure 4. a and b states of the fibres before and after deformation

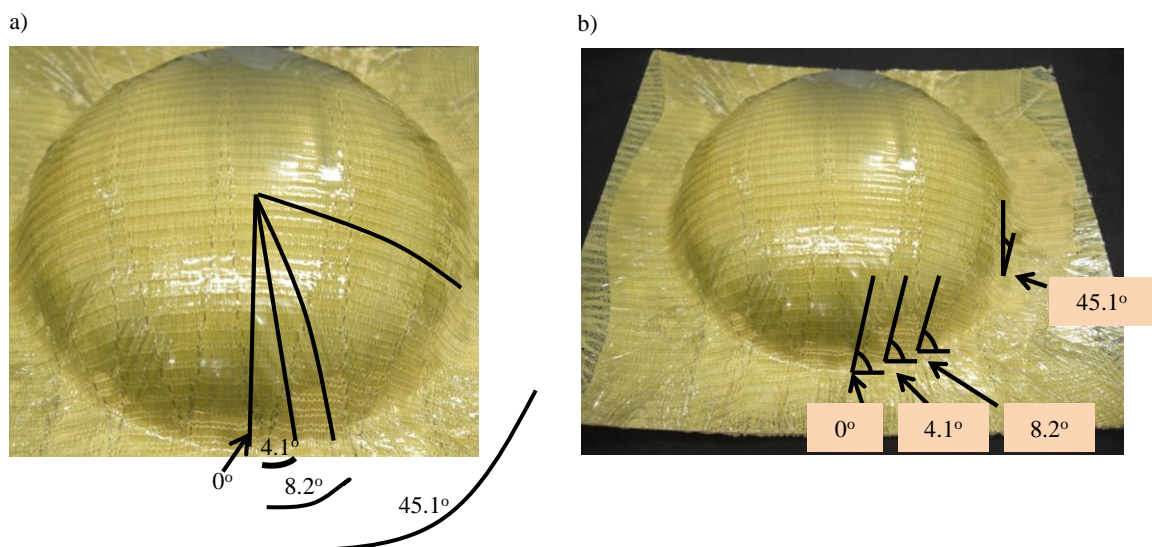
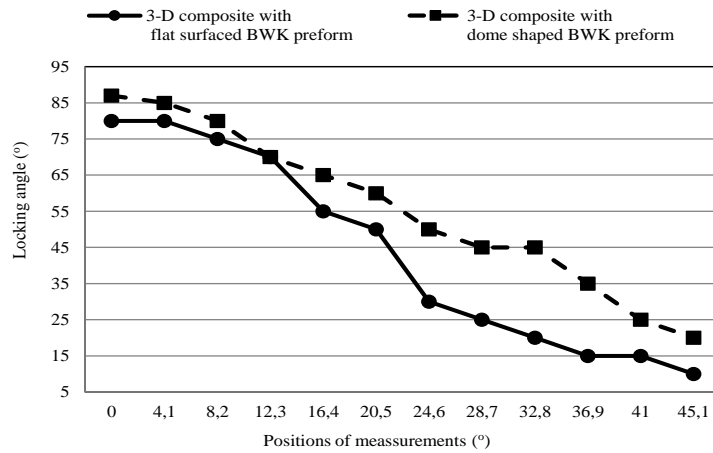


Figure 5. a and b positions of the locking angles between the fiber bundles in the 3-D hemispherical BWK composite



**Figure 6.** Comparison of locking angles of specimens

### 3.2 Surface Characteristics of the 3-D Composites

Two kinds of the composites, (i) 3-D hemispherical BWK composite with flat surfaced fabric (Figure 7a, b), (ii) 3-D hemispherical BWK composite with dome shaped fabric (Figure 7c, d), were produced with the same processing conditions, such as same weight pressure, PP film, curing conditions and etc. After fabricating of two kinds of the composite panels, amount of the wrinkles were analyzed by taking the digital photographs. The enlarged parts of the composites are shown in Figure 7b and 7d. Large numbers of wrinkle heights (10 heights/1 cm) were

observed on the flange of the 3-D hemispherical BWK composites with the flat surfaced preform (Figure 7b). However, small numbers of wrinkle heights (1 height/1 cm) were observed on the flange surface of the 3-D hemispherical BWK composites with the dome shaped preform, which is shown in Figure 7d. The pre-shaped BWK fabric can easier takes the hemispherical dome shape than the initially flat fabric which was stabilized by the knitted yarns. Therefore, pre-shaped BWK fabrics could be used to fabricate complex 3-D composite materials with a high quality.

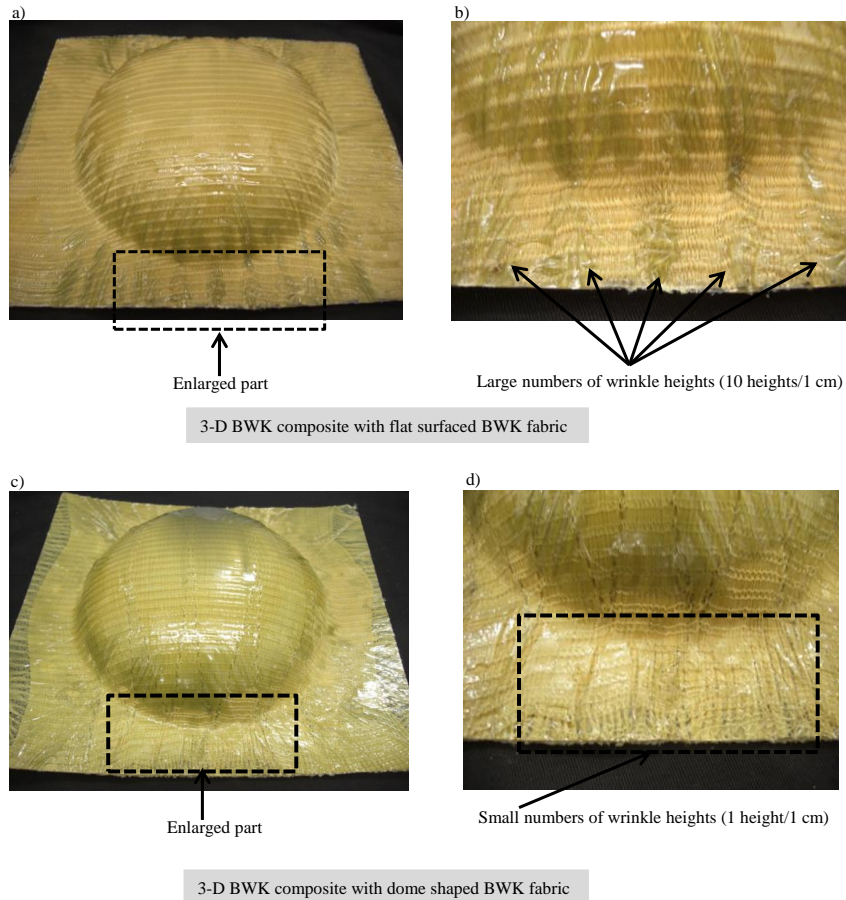


**Figure 7.** a) 3-D hemispherical BWK composite with flat surfaced preform, b) enlarged part of 3-D hemispherical BWK composite with flat surfaced preform, c) 3-D hemispherical BWK composite with dome shaped preform, d) enlarged part of 3-D hemispherical BWK composite with dome shaped preform

---

#### 4. CONCLUSION

The hand lay-up technique was applied to fabricate the 3-D hemispherical composites. Two kinds of the 3-D composites were produced with same processing conditions. The wrinkles characteristics of the composites were analyzed and found out the 3-D hemispherical BWK composites with the dome shaped preform had small numbers of wrinkle heights compared to the 3-D hemispherical BWK composites with the flat surfaced preform. This study showed that the complex 3-D structures can be produced by the biaxial weft-knitting technique and the quality of the composite materials, such as small numbers of wrinkle heights on the surface of the

composites, could be improved using 3-D preforms. In future study, thermoplastic biaxial weft-knitted hemispherical composites will be produced by hot compressing method and the influence of the different preform styles on the mechanical properties of the composites will be to investigated.

#### ACKNOWLEDGEMENT

The authors thank to Prof. Hiroyuki Hamada and Dr. Eng. Mohamed S. Aly-Hassan, Kyoto Institute of Technology for their help and support.

#### REFERENCES

1. Fangueiro R, Nunes P, Soutinho F, Araujo MD. 2009. Development of fibrous preforms for FRP pipe connections. *Composites Science and Technology* 69, 1412-1416.
2. Dufour C, Wang P, Boussu F, Soulat D. 2014. Experimental investigation about stamping behaviour of 3D warp interlock composite preforms. *Applied Composite Materials* 21, 725-738.
3. Wang P, Legrand X, Boisse P, Hamila N, Soulat D. 2015. Experimental and numerical analyses of manufacturing process of a composite square box part: Comparison between textile reinforcement forming and surface 3D weaving. *Composites Part B: Engineering* 78, 26-34.
4. Liu LS, Zhang T, Wang P, Legrand X, Soulat D. 2015. Influence of the tufting yarns on formability of tufted 3-Dimensional, composite reinforcement. *Composites Part A: Applied Science and Manufacturing* 78, 403-411.
5. Cherouat A, Borouchaki H, Laurence GM, 2010. Mechanical and geometrical approaches applied to composite fabric forming. *International Journal of Material Forming*. 3, 1189-1204.
6. Mossea L, Compstona P, Cantwell WJ, Cardew-Hall M., Kalyanasundaram S. 2006. Stamp forming of polypropylene based fibre-metal laminates: The effect of process variables on formability. *Journal of Materials Processing Technology* 172, 163-168.
7. Rozant O, Bourban PE, Manson JAE. 2000. Drapeability of dry textile fabrics for stampable thermoplastic preforms. *Composites Part A: Applied Science and Manufacturing* 31, 1167-1177.
8. Fiorotto M, Sorgente M, Lucchetta G. 2010. Preliminary studies on single point incremental forming for composite materials. *Journal of Materials Science* 3, 951-954.
9. Soulat D, Allaoui S., Chatel S. 2009. Experimental device for the preforming step of the RTM process. *Journal of Materials Science* 2, 181-184.
10. Vancloester K, Goidsenhoven GV, Lomov SV, Verpoest I. 2009. Optimizing the deepdrawing of multilayered woven fabric composites. *12th ESAFORM Conference on Material Forming*, Twente, the Netherlands.



# A Comparative Thermal Analysis of Fire-off Treated Cotton, PET and Co/PET Fabrics

Raziye Atakan, Gülay Özcan

Istanbul Technical University, Faculty of Textile Technologies and Design, Inonu Cad. No: 65 34437, Gumusuyu, Istanbul

**Corresponding Author:** Raziye Atakan, ratakan@itu.edu.tr

## ABSTRACT

The present paper investigates the capability of MCC and TGA methods by testing the thermal performance of commercially available flame-retardant chemical called Fire-off on polyethylene terephthalate (PET) and cotton (Co) fabrics and their corresponding blends (Co/PET). Fire-off was applied to the fabric through impregnation method and the resulting properties of these fabrics were assessed in terms of combustion behavior by use of micro combustion calorimeter (MCC) and thermogravimetric analysis (TGA). TGA results revealed that Fire-off could greatly enhance char residues of cotton, PET and Co/PET fabrics at high temperature region. MCC results indicated that Fire-off treatment could significantly decrease the heat release capacity (HRC), heat release rate (HRR), total heat release rate (THR) and peak heat release rate (pHRR) of cotton, PET and Co/PET fabrics. According to comparison results, a near-perfect agreement between MCC and TGA data were found in terms of degradation temperatures and mass loss rates of fabric samples

## ARTICLE HISTORY

Received: 02.07.2019

Accepted: 11.10.2019

## KEYWORDS

micro-scale combustion calorimeter, thermogravimetric analysis, thermal characterization tests, cotton, PET, Co/PET fabrics.

## 1. INTRODUCTION

With the development of science and technology and the improvement of people's living standard, the textile products show diversity in terms of application areas from the medical, military, home textiles to the common apparels. However, most of the textile products are composed of C, H, O, which are flammable and ignitable [1]. Especially, as we all know that the beddings and interior decoration of curtains with feature of flammability and ignitibility are the most of the fire hazard products worldwide [2]. Therefore, manufacturers are enforced by strict standards to look for new solutions [3]. Currently, it is evidently clear that flammable textile materials need to be tested by various independent thermal testing methods to assess the effectiveness of the FR formulations properly [4].

As a new and convenient thermal analysis technique for characterizing flammability properties of combustible materials developed in the early 2000's by the U.S.

Department of Transportation Federal Aviation Administration, the micro combustion calorimeter (MCC) test is a small-scale flammability testing method based on the principle of oxygen consumption [5–7]. The test is conducted in a laboratory environment in which milligram-scale specimen are heated at a controlled rate in an oxidizing atmosphere to achieve total material decomposition. Heat release rates associated with the combustion are then calculated by means of oxygen consumption. The temperatures over which combustion heat is released are also measured.

It serves as an alternative analytical test to verify material combustion consistency in end product. It is usually conducted in conjunction with the typical analytical tests such as fourier transform infrared spectrophotometer (FTIR), thermogravimetric analysis (TGA) or differential scanning calorimetry (DSC) used to validate formulation consistency in the most of research articles to achieve comprehensive evaluation of all kind of materials such as

**To cite this article:** Atakan R, Özcan G, 2019. A Comparative Thermal Analysis of Fire-off Treated Cotton, PET and Co/PET Fabrics. *Tekstil ve Konfeksiyon* 29(4), 311-316.

polymers, fillers, composites, fabrics, nanocomposites etc. [2,3,8–23].

It offers some benefits over other thermal tests of textile materials such as providing a quantitative comparison of combustion characteristics of textile materials such as peak heat release rate, the most significant parameter related to fire hazard of textile materials. This analysis is more difficult using cone calorimeter because of low thickness of textile fabrics [24]. Because, the experimental results of cone calorimeter are highly depended on the sample material thickness, ignition sources, orientations, ventilation and edge conditions. The cone calorimeter test requires repeated sampling of larger specimens (e.g., 10x 10 cm). Textile fabrics as thermally thin samples show larger heat release rate (HRR) values than thick samples. MCC test also provides quantitative information to correlate flammability behavior of new formulations during product development. It uses a fast cycle-time to obtain results in minutes [25], and it is capable of differentiating small differences amongst samples, which show similar flammability. In addition, fire growth index (FGI) of fabric samples can be calculated from the thermal combustion parameters measured by MCC in order to assess their burning hazard potentials. [26].

In the area of flame retardancy of textiles, the phosphorous based Flame Retardants (FRs) demonstrate lower toxicity profiles than the halogen-based compounds [27,28]. There have been ongoing attempts on synthesis and application of P-N containing eco-friendly FR systems, which are also more sustainable [1,29–31]. For instance, in a current study [32], P–N–Si synergistic flame retardant was synthesized with combining cyclodiphosphazane derivatives with silicon-containing compounds and applied to cotton fabrics. Effective FR properties were achieved with increased LOI values (from 18.2 to 52.9) and decreased total heat release (THR) and effective heat combustion (EHC) values. In another innovative study [33], casein-based, P-N containing FRs with  $-\text{COO}^-\text{NH}_4^+$  and  $-\text{P}=\text{O}(\text{O}^-\text{NH}_4^+)_2$  reactive groups, were synthesized based on a casein hydrolysis solution for cotton fabrics. Cotton fabrics, after the treatment, exhibited highly efficient flame retardancy by achieving 39.5% LOI value. The study also showed that the biomacromolecules can be flame retardant alternatives for textiles to synthetic chemicals as an environmentally friendly approach.

In our previous study [34], P-N synergetic FR agent (PVP (PR)-P-DCDA) was synthesized using polyvinyl alcohol, phosphoric acid, hydrophilic PET resin (PR), and dicyandiamide (DCDA). FR treated cotton, PET and Co/PET fabrics demonstrated no ignition with LOI values of +26 %. 100% PET fabric showed increased LOI values (from 22.5% to 33%) at very low add-ons (8–9%). In addition, investigation of mechanical properties of this FR, called Fire-off, treated fabrics exhibited an increase in abrasion, pilling, strength and elongation properties [35].

In this study, thermal properties and flame retardancy of Fire-off treated cotton, PET and Co/PET fabric samples were characterized by TGA and MCC in order to complete all thermal behaviors and product assessment of Fire-off. The capability of MCC and TGA was compared for analyzing FR performance of samples. In addition, FGI values of treated various samples were calculated using the combustion parameters of MCC in order to detect their fire risks.

## 2. MATERIAL AND METHOD

### 2.1 Material

Scoured 100% cotton (plain weave, 133 g/m<sup>2</sup>), 100% PET (plain weave, 172 g/m<sup>2</sup>) and 50/50% Co/PET fabrics (plain weave, 120 g/m<sup>2</sup>), which represent apparel and home textile fabrics were supplied from Zorlu Mensucat/ Turkey for experiments. P-N synergetic FR chemical Fire-off was supplied from Eksoy Chemical/Turkey.

### 2.2 Fabric Treatment Process

Each new section and subsection should have a heading consisting of an Arabic numeral followed by a period. Please a single space before and after the section title (see this template). Scoured fabrics were padded in Fire-off (400 g/L) solutions in three dips and nips using a two-roll laboratory padder (ATAÇ F-350 model) at room temperature, and squeezed to a wet pick-up of 85±2%. The padded fabrics were dried at 100°C for 3 min in an oven (ATAÇ EV 250 model) and subsequently cured using a mini ram (ATAÇ GK 40 model) at 180°C for 3 min. The add-on values of cotton, PET and Co/PET fabrics were obtained as 21-22%, 16-17% and 19-20%.

### 2.3 Thermal Characterization Tests

Thermogravimetric measurements were run on SEIKO Exstar 6200 TG/DTA instrument under a dry nitrogen atmosphere (purging rate 20 mL/min) and 10°C/min heating rate from 30 to 800°C using 4–5 mg sample amounts in open platinum pans.

The combustion performance of samples was measured by a MCC instrument (MCC, Turkey) equipped with a 40/L alumina pan in accordance with ASTM D7309, Method A. The samples (~ 5 mg) were first heated from room temperature to 750°C in an 80 cm<sup>3</sup>/min nitrogen stream with at a linear heating rate of 1°C. Then the thermal degradation products of the sample in nitrogen were mixed with a 20 cm<sup>3</sup>/min oxygen stream flow and combustion in a furnace at 900°C for 10 s. The heat of combustion of the pyrolysis products were measured by oxygen consumption principle. Each sample was run in three replicates and the averages of MCC parameters were calculated from the three measurements. The key fire parameters including heat release rate (HRR), total heat release (THR in kJ/g), heat release capacity (HRC in J/g K), peak heat release rate (pHRR in W/g) and temperature at maximum heat release rate (Tmax) were measured. The mass of specimen

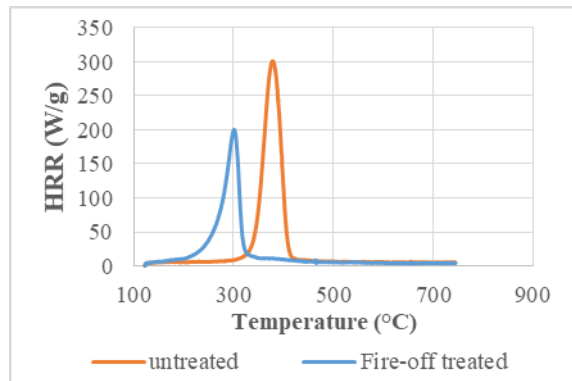
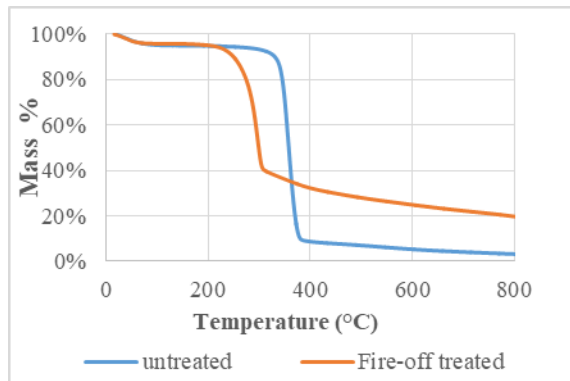
remaining after the test was also measured to evaluate char yield. The fire growth index (FGI) was also calculated using the ratio of pHRR of the material and Tmax (FGI=pHRR/ Tmax). The bigger the value of FGI, the greater the fire hazard.

### 3. RESULTS AND DISCUSSION

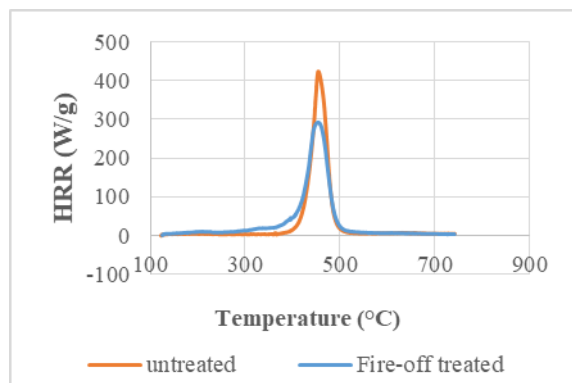
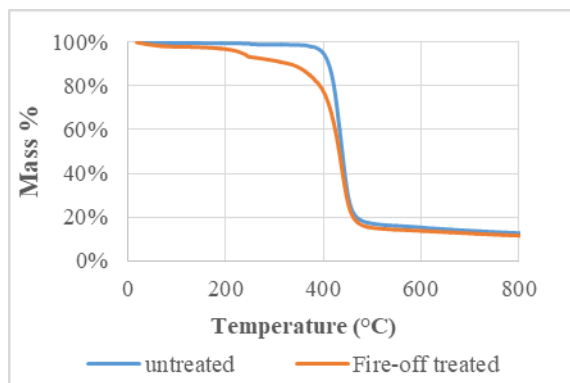
TGA is the most used method to rapidly evaluate the thermal stability of different materials, composites etc. It also exhibits the decomposition of polymers at various temperatures.

The thermal degradation and decomposition processes of untreated and treated fabrics were monitored by TGA. Subsequently, TGA measurement was compared with the MCC test in order to confirm the catalytic charring effect of the Fire-off treatments on cotton, PET and Co/PET fabrics. Both TG and MCC curves of untreated and treated samples are depicted in Figure 1, and the corresponding data of TGA and MCC are listed in Table 1 and 2, respectively.

#### 100% Cotton



#### 100% PET



#### 50/50% Co/PET

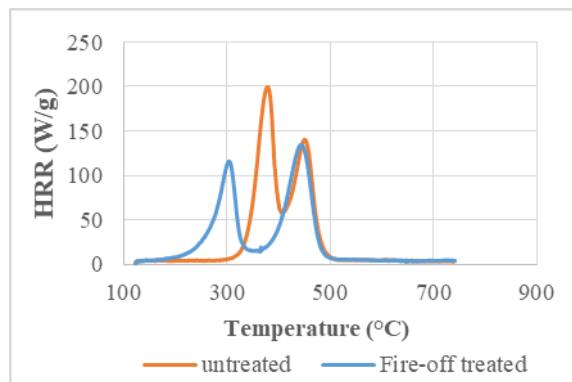
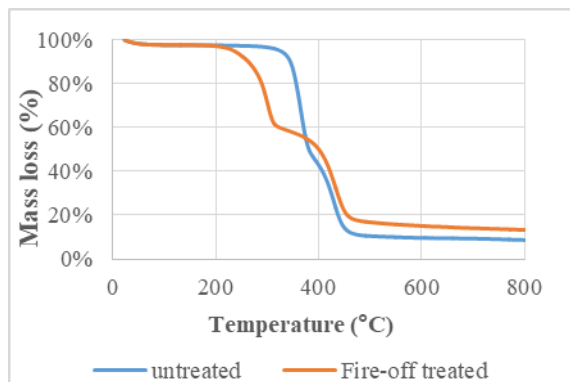


Figure 1. TG and HRR curves of untreated and treated fabrics.

**Table 1.** TGA data of untreated and treated fabrics.

Fabric Type	$T_1^*$ (°C)	$T_2^*$ (°C)	Residue at 750°C (%)
100% Cotton	342	373	3.6
100% Cotton- treated	273	310	21.04
100% PET	414	455	13.12
100% PET - treated	406	456	11.92
50/50% CO/PET	345-381	403-450	9.01
50/50% CO/PET- treated	272-311	395-456	13.69

**Table 2.** MCC data of untreated and treated fabrics.

Fabric Type	HR Capacity (J/g K)	pHRR (W/g)	$T_{max}$ (°C)	THR (kJ/g)	Mass Loss at 750°C (%)	Residue at 750°C (%)	FGI
100 % Cotton	315.33	287.4	377.6	14.57	94.94	5.06	0.76
100 % Cotton-treated	221.33	201.97	303.03	10.37	79.74	20.26	0.66
100 % PET	465.67	426.67	455.27	18.37	87.86	12.14	0.93
100 % PET -treated	333.33	305.13	451.93	19.2	90.45	9.55	0.67
50/50% Co/PET	219	202.03-	377.73-	16.57	91.48	8.52	0.53
50/50% Co/PET-treated	143.67	132.93-	442.23-	15.1	87.86	12.14	0.30

Phosphorous and nitrogen (P-N) containing FR systems can form a cross-linked network within the cellulose. Hence, they inhibit the release of volatile combustible fragments and enhance the formation of char. These systems are able to reduce cellulose inflammability by the mechanisms of dehydration, phosphorylation, and phosphate- ester decomposition. Generally, FR agents is supposed to decompose before the decomposition temperature of the textile substrates to interfere with the burning process [36,37].

As shown from TG curves in Figure 1, cotton begins to break down at 342°C ( $T_1$ ) and performs a one-step thermal degradation behavior because of the glycosyl units to char. The degradation is maximum at around 373°C ( $T_2$ ). Cellulose degradation involves the decomposition of the glycosyl units to an aliphatic char at lower temperatures and the depolymerisation of such units to volatile products containing levoglucosan at higher temperature [34,38]. Fire-off treatment leads to a strong reduction of the cellulose decomposition temperature, which is indicated by the initial decomposition ( $T_1$ ) value (342 to 273°C) for treated sample. While the char residue of untreated cotton was 3.60 %, around 21% char residue at 750°C was measured by TGA for treated cotton, which indicates high thermal stability due to the interaction of cellulose and Fire-off during combustion. This trend prevents cotton fabrics to further degradation. In parallel to TG curves, as clearly seen from HRR curves in Figure 1, cotton fabric goes through a one-step pyrolysis process due to the glycosyl units to char. The degradation of untreated cotton is maximum at 377°C ( $T_{max}$ ) and it presents the peak heat release rate (pHRR) of 287.4 W/g. On the other hand, degradation of treated cotton

starts earlier, is maximum at around 303 °C ( $T_{max}$ ), representing a lower pHRR value (201 W/g). The residue (%) obtained by MCC is 5.06, which is very close the one of TGA (3.6).

TG curve of untreated PET can be suitably fitted by a single stage reaction in nitrogen similar to cotton fabric. According to TGA data in Table 1, treated PET fabrics, demonstrated a slight decrease in maximum decomposition temperature (414 to 406°C). The char residue at 750°C were the approximately same percentage (13 to ~12%) for untreated and treated samples. MCC data confirms that the thermal decomposition started at around 375°C for the untreated PET fabric. The decomposition intensified as the temperature was increased, as indicated by rising HRR. It reached to maximum at 455°C with the HRR at 426 W/g (pHRR). The decomposition ended at 518°C, the char residue was measured as 12.14% at 750°C. On the other hand, some significant changes in the MCC parameters were observed after Fire-off treatment of on PET fabrics. For instance, the initial decomposition temperature was decreased to 300°C and a lowered pHRR of 305 W/g was obtained at 451°C ( $T_{max}$ ). The decomposition ended at 518°C same as the untreated one. The char residues were calculated around 12% and %10 for untreated and treated samples, respectively.

In case of Co/PET fabrics, as seen in TG curves, the pyrolysis proceeds in two independent steps, which exhibit a thermal degradation typical of a polymer blend: the former was attributable to cotton (345°C for untreated, 272°C for treated fabrics) and the latter to PET (403°C for untreated, 395°C for treated fabrics). The char residue at 750°C leads an increase from approximately 9 % to 13%

for treated Co/PET. HRR curves for Co/PET fabrics versus temperature exhibit two major degradation steps as same as the TG curves of Co/PET. For untreated Co/PET, the first peak (HRR<sub>1</sub>) is around 193 W/g and the second peak (HRR<sub>2</sub>) is around 132 W/g. Fire-off treatment demonstrate higher effectiveness in decreasing heat release rate after HRR<sub>1</sub> (from 193 to 120 W/g) than HRR<sub>2</sub> (from 132 to 130 W/g). It is obviously seen that Co/PET fabrics start degradation process earlier after FR treatments, at around 305°C, whereas untreated sample starts to degrade at around 380°C.

Additionally, as seen in Table 2, some other prominent changes in the MCC parameters were observed when all fabric types were treated with Fire-off. A strong reduction in HRC and THR was obtained for treated samples. Decreased THR values, which refer to the total available energy in the material in a fire situation, which suggest that more volatile products are catalytically carbonized to participate in the charring process, rather than transfer into the MCC combustor.

When compared FGI values of all fabrics, it should be noted that untreated PET fabric has the most burning hazard potential with the highest FGI value of 0.93, cotton fabric has 0.76 value and Co/PET has the lowest potential with a 0.53 FGI value. After Fire-off finishing treatment, FGI values of fabrics decreased (PET: from 0.93 to 0.67, cotton: from 0.76 to 0.66, Co/PET: from 0.53 to 0.30), thus fabrics became safer.

#### 4. CONCLUSION

In this study, a comparative assessment of MCC and TGA characterization techniques on the thermal and fire behavior of cotton, PET and Co/PET blends treated with FR agent-Fire-off- has been presented. The use of these techniques, TGA and MCC, allowed for the creation of small batch of materials and corresponding formulation as compared to the kilogram sample needed for cone calorimeter testing.

Results revealed that both TGA and MCC test methods provide very close data related to degradation behaviors and mass loss rates of textile fabrics, which was confirmed by cotton, PET and Co/PET blended fabrics in this study. TGA results indicate that FR treatment with Fire-off leads the decrease of degradation time of the treated samples than the untreated ones. This is in agreement with the MCC results, which also show the FR properties are improving with the decreasing HRR values.

As known very well, TGA data reflect the characteristics of thermal decomposition and degradation of all types of materials with changing temperatures, but not combustion. However, MCC technique covers TGA providing additional combustion characteristics such as HRC, THR and pHRR, which are the most prominent parameters related to fire hazard of textile materials in a shorter heating cycle and time. In addition, MCC data also enable to calculate the FGI of fabric samples. Therefore, the results of this study highlighted that thermal characteristics and combustion behaviors of FR textile materials can be assessed by MCC alone, without performing TGA. TGA could be used for more detailed mass loss assessment of the textile materials in terms of degradation steps with slow linear heating rate. However, both test technique should be conducted for comprehensive thermal evaluation.

#### ACKNOWLEDGEMENT

The work was financially supported by ITU BAP Program for the Doctoral Program of Higher Education (Project no: 39775). We wish to thank Zorlu Mensucat for fabric supply. We extend our appreciation to Prof. Dr. Nevin Çiğdem Gürsoy for laboratory facilities in “İ.T.Ü Universal Textile Design Center” to perform chemical finishing applications and Prof. Dr. Mustafa Üreyen for laboratory facilities to perform Micro Combustion Calorimetry (MCC) Test in “Anadolu University Civil Aviation Research Center”.

#### REFERENCES

1. A.R. Horrocks. 2011. Flame retardant challenges for textiles and fibres: New chemistry versus innovatory solutions. *Polymer Degradation and Stability* 96, 377–392. doi:10.1016/j.polyimdegadstab.2010.03.036.
2. Q. hua Zhang, J. Gu, G. qiang Chen, T. ling Xing. 2016. Durable flame retardant finish for silk fabric using boron hybrid silica sol. *Applied Surface Science* 387, 446–453. doi:10.1016/j.apsusc.2016.06.119.
3. M. Przybylak, H. Maciejewski, A. Dutkiewicz, D. Wesołek, M. Władysław-Przybylak. 2016. Multifunctional, strongly hydrophobic and flame-retarded cotton fabrics modified with flame retardant agents and silicon compounds. *Polymer Degradation Stability* 128, 55–64. doi:10.1016/j.polyimdegadstab.2016.03.003.
4. I. Šimkovic. 2012. TG/DTG/DTA evaluation of flame retarded cotton fabrics and comparison to cone calorimeter data. *Carbohydrate Polymers* 90, 976–981. doi:10.1016/j.carbpol.2012.06.030.
5. R.E. Lyon, R. Walters. 2002. A microscale combustion calorimeter (Report No. ADA401490). USA: Defense Technical Information Center.
6. B. Scharrel, K.H. Pawlowski, R.E. Lyon. 2007. Pyrolysis combustion flow calorimeter: A tool to assess flame retarded PC/ABS materials? *Thermochimica Acta* 462, 1–14. doi:10.1016/j.tca.2007.05.021.
7. J. Alongi, J. Tata, F. Carosio, G. Rosace, A. Frache, G. Camino. 2015. A comparative analysis of nanoparticle adsorption as fire-protection approach for fabrics. *Polymers (Basel)*. 7, 47–68. doi:10.3390/polym7010047.
8. C.Q. Yang, Q. He, R.E. Lyon, Y. Hu. 2010. Investigation of the flammability of different textile fabrics using micro-scale combustion calorimetry. *Polymer Degradation and Stability* 95, 108–115. doi:10.1016/j.polyimdegadstab.2009.11.047.
9. K. Apaydin, A. Laachachi, V. Ball, M. Jimenez, S. Bourbigot, D. Ruch. 2015. Layer-by-layer deposition of a TiO<sub>2</sub>-filled intumescent coating and its effect on the flame retardancy of polyamide and polyester fabrics. *Colloids and Surfaces A: Physicochemical and Engineering Aspects* 469, 1–10. doi:10.1016/j.colsurfa.2014.12.021.

10. L. Chen, L. Song, P. Lv, G. Jie, Q. Tai, W. Xing, Y. Hu. 2011. A new intumescent flame retardant containing phosphorus and nitrogen: Preparation, thermal properties and application to UV curable coating. *Progress in Organic Coatings* 70, 59–66. doi:10.1016/j.porgcoat.2010.10.002.
11. M. Zarrelli, A. Pullara, M. Codda, E. Amendola, A. Borriello, P. Fermi. 2012, June. Fireproof silicone sealants for shipbuilding. *ECCM15 - 15th European Conference On Composite Materials*, Venice, Italy.
12. H. Lu, C.A. Wilkie, M. Ding, L. Song. 2011. Flammability performance of poly(vinyl alcohol) nanocomposites with zirconium phosphate and layered silicates. *Polymer Degradation and Stability* 96, 1219–1224. doi:10.1016/j.polyimdeggradstab.2011.04.014.
13. H. Behniafar, S. Haghghat. 2008. Thermally stable and organosoluble binaphthylene-based poly(urea-ether-imide)s: one-pot preparation and characterization. *Polymers for Advanced Technologies* 19(8), 1040–1047. doi:10.1002/pat.1072.
14. H. Lu, C.A. Wilkie. 2010. Study on intumescent flame retarded polystyrene composites with improved flame retardancy. *Polymer Degradation and Stability* 95, 2388–2395. doi:10.1016/j.polyimdeggradstab.2010.08.022.
15. H. Lu, C.A. Wilkie. 2010. Synergistic effect of carbon nanotubes and decabromodiphenyl oxide/Sb<sub>2</sub>O<sub>3</sub> in improving the flame retardancy of polystyrene. *Polymer Degradation Stability* 95, 564–571. doi:10.1016/j.polyimdeggradstab.2009.12.011.
16. F. Fang, X. Zhang, Y. Meng, X. Ding, C. Bao, S. Li, H. Zhang, X. Tian. 2016. Boron-containing intumescent multilayer nanocoating for extinguishing flame on cotton fabric. *Cellulose* 23, 2161–2172. doi:10.1007/s10570-016-0928-8.
17. X.W. Cheng, J.P. Guan, R.C. Tang, K.Q. Liu. 2016. Phytic acid as a bio-based phosphorus flame retardant for poly(lactic acid) nonwoven fabric. *Journal of Cleaner Production* 124, 114–119. doi:10.1016/j.jclepro.2016.02.113.
18. F. Fang, X. Chen, X. Zhang, C. Cheng, D. Xiao, Y. Meng, X. Ding, H. Zhang, X. Tian. 2016. Environmentally friendly assembly multilayer coating for flame retardant and antimicrobial cotton fabric. *Progress in Organic Coatings* 90, 258–266. doi:10.1016/j.porgcoat.2015.09.025.
19. Q. Zhang, W. Zhang, J. Huang, Y. Lai, T. Xing, G. Chen, W. Jin, H. Liu, B. Sun. 2015. Flame retardance and thermal stability of wool fabric treated by boron containing silica sols. *Materials & Design* 85, 796–799. doi:10.1016/j.matdes.2015.07.163.
20. C.Q. Yang, Q. He. 2011. Applications of micro-scale combustion calorimetry to the studies of cotton and nylon fabrics treated with organophosphorus flame retardants. *Journal of Analytical and Applied Pyrolysis* 91, 125–133. doi:10.1016/j.jaap.2011.01.012.
21. Q. hua Zhang, G. qiang Chen, T. ling Xing. 2017. Silk flame retardant finish by ternary silica sol containing boron and nitrogen. *Applied Surface Science* 421, 52–60. doi:10.1016/j.apsusc.2017.01.283.
22. J. Alongi, J. Milnes, G. Malucelli, S. Bourbigot, B. Kandola. 2014. Thermal degradation of DNA-treated cotton fabrics under different heating conditions. *Journal of Analytical and Applied Pyrolysis* 108, 212–221. doi:10.1016/j.jaap.2014.04.014.
23. Q. Chen, C.Q. Yang, T. Zhao. 2014. Heat release properties and flammability of the nylon/cotton blend fabric treated with a crosslinkable organophosphorus flame retardant system. *Journal of Analytical and Applied Pyrolysis* 110, 205–212. doi:10.1016/j.jaap.2014.08.021.
24. C.Q. Yang, Q. He. 2011. Applications of micro-scale combustion calorimetry to the studies of cotton and nylon fabrics treated with organophosphorus flame retardants. *Journal of Analytical and Applied Pyrolysis* 91, 125–133.
25. X.W. Cheng, J.P. Guan, R.C. Tang, K.Q. Liu. 2016. Improvement of flame retardancy of poly(lactic acid) nonwoven fabric with a phosphorus-containing flame retardant. *Journal of Industrial Textiles* 46, 914–928. doi:10.1177/1528083715606105.
26. Z. Yang, H. Ai-Huayi, J.Y. Liu, X. Zhao. 2016. Study of Fire Hazard of Flooring Materials on Data of Cone Calorimeter. *Procedia Engineering* 135, 584–587. doi:10.1016/j.proeng.2016.01.113.
27. S. Gaan, L. Mauclair, P. Rupper, V. Salimova, T.-T. Tran, M. Heuberger. 2011. Thermal degradation of cellulose acetate in presence of bis-phosphoramidates. *Journal of Analytical and Applied Pyrolysis* 90, 33–41.
28. C. Hirsch, B. Striegl, S. Mathes, C. Adlhart, M. Edelmann, E. Bono, S. Gaan, K.A. Salmeia, L. Hoelting, A. Krebs, J. Nyffeler, R. Pape, A. Bürkle, M. Leist, P. Wick, S. Schildknecht. 2017. Multiparameter toxicity assessment of novel DOPO-derived organophosphorus flame retardants. *Archives of Toxicology* 91, 407–425. doi:10.1007/s00204-016-1680-4.
29. S. Nazare, B. Kandola, A.R. Horrocks. 2002. Use of cone calorimetry to quantify the burning hazard of apparel fabrics. *Fire and Materials* 26, 191–199.
30. A.R. Horrocks. 2013. Textile flammability research since 1980 - Personal challenges and partial solutions. *Polymer Degradation and Stability* 98, 2813–2824. doi:10.1016/j.polyimdeggradstab.2013.10.004.
31. K.A. Salmeia, S. Gaan, G. Malucelli. 2016. Recent advances for flame retardancy of textiles based on phosphorus chemistry. *Polymers* 8, 319.
32. M. Liu, S. Huang, G. Zhang, F. Zhang. 2019. Synthesis of P–N–Si synergistic flame retardant based on a cyclodiphosphazane derivative for use on cotton fabric. *Cellulose* 26, 7553–7567. doi:10.1007/s10570-019-02608-5.
33. F. Xu, L. Zhong, C. Zhang, P. Wang, F. Zhang, G. Zhang. 2019. Novel High-Efficiency Casein-Based P–N-Containing Flame Retardants with Multiple Reactive Groups for Cotton Fabrics. *ACS Sustainable Chemistry & Engineering* 7, 13999–14008. doi:10.1021/acsschemeng.9b02474.
34. R. Atakan, A. Bical, E. Celebi, G. Ozcan, N. Soydan, A.S. Sarac. 2018. Development of a flame retardant chemical for finishing of cotton, polyester, and CO/PET blends. *Journal of Industrial Textiles* 49 (2), 11–21. doi:10.1177/1528083718772303.
35. R. Atakan and G. Ozcan. 2018. Mechanical Assessments of Fire-off on CO/PET Fabrics. *IOP Conference Series: Material Science and Engineering* 460,012052. doi:10.1088/1757-899X/460/1/012052.
36. S. Gaan, G. Sun, K. Hutches, M.H. Engelhard. 2008. Effect of nitrogen additives on flame retardant action of tributyl phosphate: Phosphorus-nitrogen synergism. *Polymer Degradation and Stability* 93, 99–108. doi:10.1016/j.polyimdeggradstab.2007.10.013.
37. T.M. Nguyen, S.C. Chang, B. Condon. 2014. The comparison of differences in flammability and thermal degradation between cotton fabrics treated with phosphoramidate derivatives. *Polymers for Advanced Technologies* 25, 665–672. doi:10.1002/pat.3268.
38. A.R. Horrocks, D. Price. 2001. *Fire retardant materials*. UK: Woodhead Publishing.



# Performance and Characterization of Aloe Vera Microcapsules on Silk/Lyocell Blended Fabric

Mariyam Adnan<sup>1</sup>, Jeyakodi Moses J<sup>2</sup>

<sup>1</sup> Department of Apparel and Fashion Design, PSG College of Technology, Peelamedu, Coimbatore, 641004, Tamil Nadu, India

<sup>2</sup> Department of Applied Science, PSG College of Technology, Peelamedu, Coimbatore, 641004, Tamil Nadu, India

**Corresponding Author:** Mariyam Adnan, mariyam.ag@gmail.com

## ABSTRACT

In this study, silk and lyocell fibers were blended in the ratio of 50:50 and woven into a plain weave fabric. Aloe vera based microcapsules were used to impart antibacterial finish on silk/lyocell blended fabrics and assessed by SEM, EDX, FTIR, agar diffusion test, bacterial reduction test, and wash durability test. SEM analysis showed aloe vera capsules impregnated in the fabric. EDX also showed the presence of aloe vera in the fabric by showing the presence of chemical elements like Mg, Ca, K, Al and Fe which were not present in the untreated fabric. FTIR spectra of aloe vera treated samples showed an ether group, a secondary alcohol group, an aromatic group and a nitro group that reveal the probable chromophoric groups likely to be present in the aloe vera gel. The results of agar diffusion test clearly show that aloe vera treated fabrics have very good antibacterial properties and do not allow the growth of bacteria in the treated fabric. The zone of inhibition was found to be very good and ranged from 28 mm to 30 mm. Bacterial reduction test showed the percentage reduction values of both the microorganisms *S. aureus* and *E. coli* to be more than 97%. The wash durability of aloe vera treated fabrics lasted up to 25 washes.

## ARTICLE HISTORY

Received: 04.02.2019

Accepted: 11.10.2019

## KEYWORDS

aloe vera, lyocell, silk, microencapsulation, antibacterial

## 1. INTRODUCTION

Silk is a natural fiber priced for its vanity, versatility, wearability and comfort. In spite of all the wonderful properties silk possesses, it is extremely costly [1]. Lyocell is a regenerated cellulosic fiber which offers luxury, less cost and surpasses all other cellulosic fibers in terms of properties, aesthetics and importantly ecofriendliness in manufacturing [2]. Lyocell is 100% natural in origin, has better dyeability than other cellulose fibers, softness and drape, luxurious handle, good moisture retention and hence wearing comfort, and good dimensional stability. Notably, lyocell fiber blends well with various natural and synthetic fibers, like cotton, linen, rayon, polyester, lycra, nylon, silk and wool. The stress-strain characteristics of lyocell make it an ideal partner with the various textile fibers [2].

In this study, silk and lyocell were blended so that one can enjoy the richness of silk and excellent softness of lyocell. Since, silk and lyocell belong to the category of protein and

cellulosic fibers respectively; they are prone to microbial attack and can be damaged easily. Therefore, their protection against microbes becomes imperative to preserve their individual properties and widen its spectrum of applications [1, 2].

The use of natural agents such as chitosan, neem and natural dyes for antimicrobial finishing of textiles has been widely reported [3]. Aloe vera (*Aloe barbadensis*) is known 'Lily of the desert' and belongs to the family Liliaceae. The aloe leaf consists of two major parts, the outer green rind and the inner colourless parenchyma containing the aloe gel [4]. Polysaccharides in aloe gel are mainly responsible for their antimicrobial activity. There are different polysaccharides in aloe vera such as glucogalactan, glucomannan, galactogalacturan and lactomannan with different composition as well as acetylated acemannan. Acemannan is a long chain polymer consisting of randomly acetylated linear D-mannopyranosyl units having antibacterial and antifungal properties [5].

**To cite this article:** Adnan M, Moses J, 2019. Performance and characterization of aloe vera microcapsules on silk/lyocell blended fabric. *Tekstil ve Konfeksiyon* 29(4), 317-321.

Jayakumari et al [6] found some important bioactive constituents such as P-methyl benzoic acid, 2-thiophene carboxylic acid and dimethyl 4-chlorophenyl thiophosphate having antibacterial activities were found by subjecting the aloe vera extract to the Gas Chromatography Mass Spectroscopy (GC-MS). This study highlights the use of aloe vera as an effective antibacterial agent.

Irshad et al [7] studied the antibacterial activity of aloe vera which showed that aloe vera extract of methanol gave the maximum antibacterial activity as compared to other solvent extracts. A major limitation in antimicrobial finishing with natural agents is the non-durability of the finish. Finishing by microencapsulation method can increase the durability of antimicrobial finish on textiles as it offers many advantages compared to conventional process, in terms of economy, eco-friendliness and controlled release of substance [8-10].

Kamble et al [11] tested the antimicrobial activity of aloe vera extract against bacteria and found that methanol extract showed maximum inhibitory activity against *E. coli* and *Candida*. Fatemeh [12] identified, quantified, and compared the phytochemical contents, antioxidant properties, and antibacterial activities of Aloe vera lyophilized leaf gel and 95% ethanol leaf gel extracts.

Although considerable research work has been carried out in the past on the medical uses of aloe vera, its antibacterial activity on textile substrate is not widely reported. The present work aims at developing a natural antibacterial finish on silk/lyocell blended fabric using aloe vera microcapsules.

## 2. MATERIAL AND METHOD

### 2.1 Material

A blended yarn containing silk/lyocell in the ratio of 50:50 (S/L 50:50) was manufactured in a spinning unit in Coimbatore, Tamil Nadu, India and processed to produce 60s Ne (9.84 tex) yarn. The blended yarn was constructed into a plain woven fabric with the specifications of warp density 30 ends/cm, weft density 25 picks/cm, and fabric density of 71.8 g/m<sup>2</sup>. Aloe vera (*Aloe barbadensis*) was collected from the forest department, Coimbatore, Tamil Nadu, India. Acacia gum, citric acid, methanol and sodium sulphate were purchased from a chemical factory in Tirupur, Tamil Nadu, India.

### 2.2 Method

#### 2.2.1 Aloe vera extraction

The leaves of aloe vera were washed with lukewarm water. The aloe vera gel was then extracted from the leaves and stored in a clean glass vessel, dried in hot air oven at 75° C for two days and then powdered. 20 g of powdered aloe vera was dispersed in 100 ml of methanol (1: 5 ratio of aloe vera: solvent) and extracted after 24 hours. Methanol was removed, by exposing it to open air. This aloe vera extract was used as an antibacterial finishing agent [13-15].

#### 2.2.2 Microencapsulation finish

Microcapsules were done using aloe vera extract as core material (75% w / w) and gum acacia as wall material (25% w / w). 10g of gum acacia was allowed to swell for thirty minutes by mixing with 100ml of hot water. This mixture was stirred well for 15 min at 50°C by adding another 50 ml of hot water. 1.5% (owf) methanol extracts of aloe vera was then added slowly, stirred at 300-500 rpm for further 15 min followed by drop wise addition of 20% (owf) sodium sulphate solution. The stirrer speed was reduced and 6% (owf) citric acid was added as a binding agent. The stirrer was stopped and mixture was then kept in a freezer overnight to develop the microcapsules. The S/L 50:50 fabric was immersed in the microcapsule solution for one hour using pneumatic padding mangle with a wet pick up of 80%, dried at 80°C for 3 min and cured at 110°C for 2 min on a lab model curing chamber [8].

#### 2.2.3 Characterization of treated fabrics

Surface morphology of the untreated and aloe vera treated fabric samples were examined by scanning electron microscope (SEM) JEOL JSM 6396, Japan. Energy dispersive X-ray (EDX) was carried out using a system fitted on the SEM which allowed identification of the elements present in the surface of the S/L 50:50 blended fabrics. The Fourier transform infrared (FTIR) spectrum for the untreated and aloe vera treated samples was obtained using Shimadzu FTIR - 8400S, Kyoto, Japan.

#### 2.2.4 Assessment of antibacterial activity

The antibacterial activity of untreated and aloe vera treated fabrics by microencapsulation method were evaluated qualitatively using the AGAR diffusion method according to AATCC 147-2004 and quantitatively using the Shake Flask method according to AATCC 100-2004. The bacterial species *Staphylococcus aureus* (*S. aureus*) and *Escherichia coli* (*E. coli*) were used as a representative gram positive and gram negative bacteria respectively.

#### 2.2.5 Wash durability

The wash fastness of the aloe vera treated S/L 50:50 blended fabrics in terms of percentage reduction of bacteria was evaluated quantitatively by shake flask method (AATCC 100-2004) after subjecting the samples to 1, 5, 10, 15, 20 and 25 home launderings as per the AATCC 135-2004 method. The samples were washed using a standard detergent (2% owf) at 40°C for 10 min [13].

## 3. RESULTS AND DISCUSSION

### 3.1 Characterization

#### 3.1.1 SEM analysis

The SEM photographs of untreated and aloe vera treated S/L 50:50 blended fabrics are shown in Figures 1(a) and 1(b) respectively. The treated fabric clearly shows a heavy

deposition of aloe vera microcapsules on the fiber surface as seen from the Figure 1(b) when compared to the untreated fabric in Figure 1(a). It is in correlation to the earlier results that the microcapsules are fixed firmly on the fiber assembly of the fabric [13, 16].

### 3.1.2 EDX analysis

An elemental analysis of the particles was carried out by scanning electron microscope equipped with energy disperse X-ray spectrum (EDS), which provides a rapid

qualitative and quantitative analysis of the elemental composition. Figure 2 shows the EDX graphs of untreated and aloe vera treated fabrics. Figure 2(b) reveals the presence of aloe vera in the treated fabric when compared to the untreated fabric (Figure 2a). The aloe vera treated fabric shows the presence of inorganic elements such as calcium, chlorine, iron, magnesium, potassium, phosphorous and sodium which are not present in the untreated fabric [1].

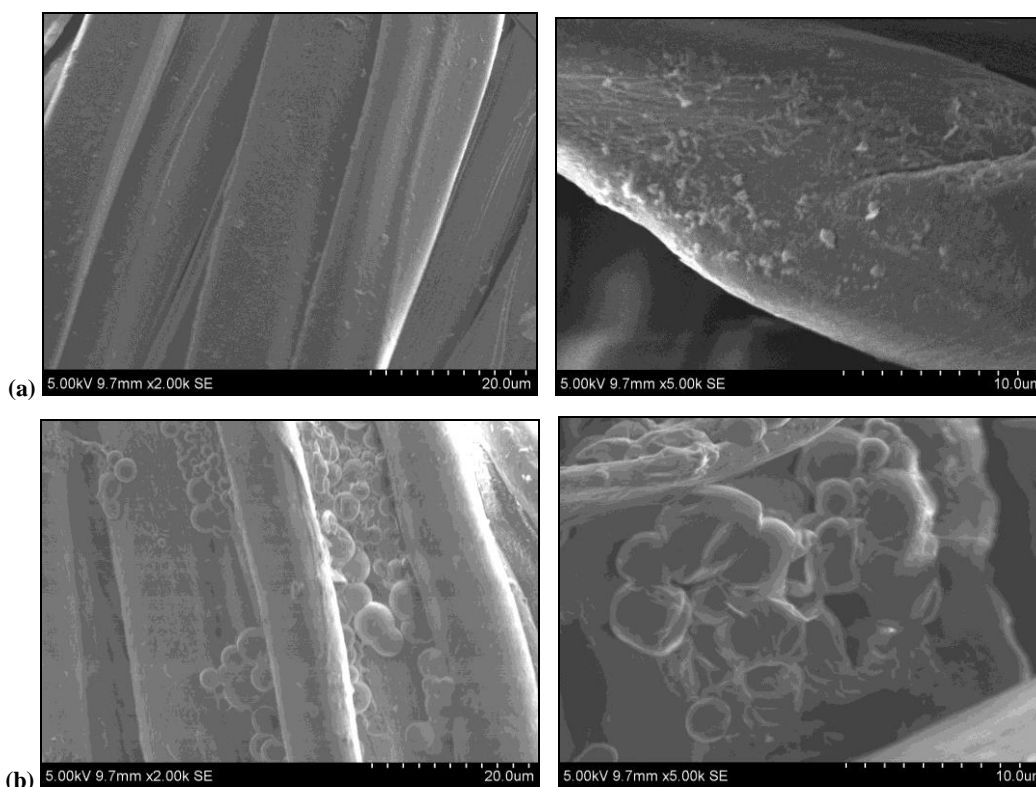


**Figure 1.** SEM images of (a) Untreated and (b) Aloe Vera Treated S/L 50:50 blended fabrics

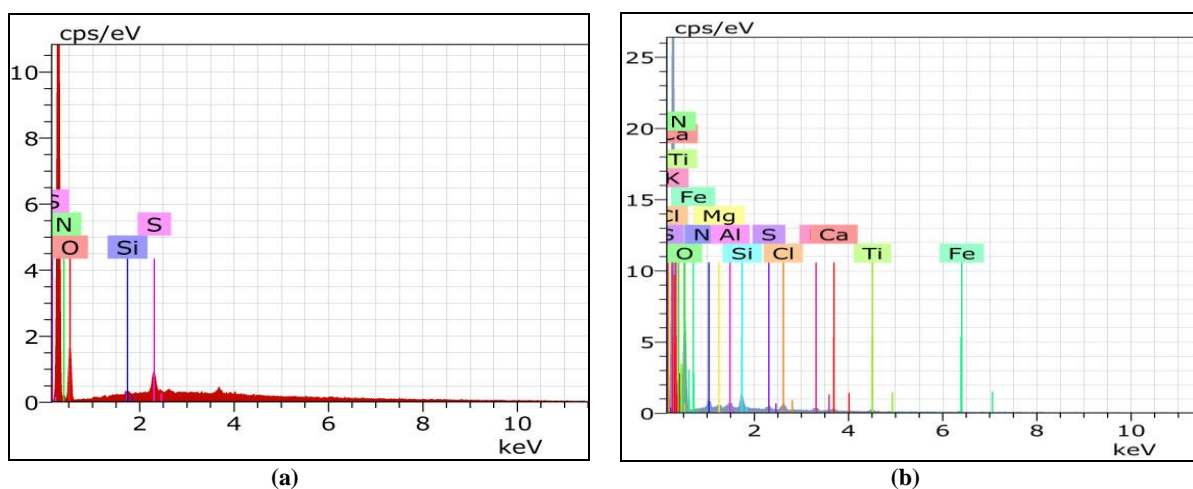


**Figure 2.** EDX Graphs of (a) Untreated (b) Aloe Vera Treated S/L 50:50 Blended Fabrics

### 3.1.3 FTIR analysis

FTIR analysis was carried out using FTIR spectrophotometer. Figure 3 shows the FTIR spectra of both untreated and aloe vera treated S/L 50:50 blended fabric. In comparison with the FTIR spectra of untreated S/L 50:50, the spectrum of aloe vera treated S/L 50:50 samples show bands of ether R-OR group at 1047 cm<sup>-1</sup> and secondary alcohol R-OH group at 1158 cm<sup>-1</sup>. An ether ROOR group is seen at 1230 cm<sup>-1</sup> and an aromatic group is seen at 1443 cm<sup>-1</sup>. A band of nitro NO<sub>2</sub> group is also seen at 1516 cm<sup>-1</sup>. These bands show the probable chromophoric groups likely to be present in the gel of aloe vera [17]. The strong absorption band at 1620-1610 cm<sup>-1</sup> is due to C = C stretching which indicates the presence of vinyl ether and aloin compound [18].

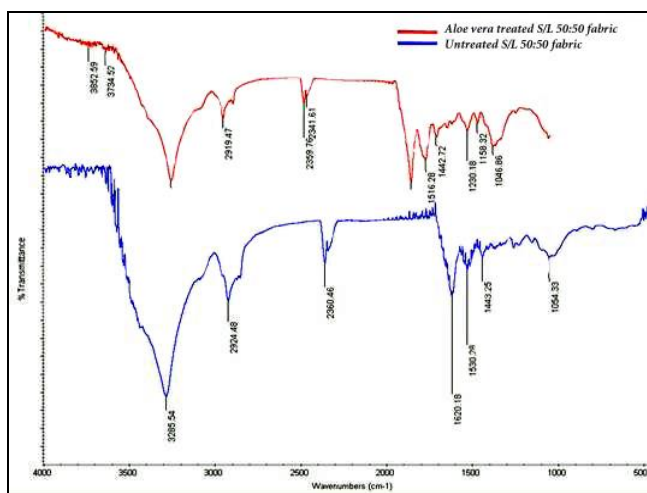


**Figure 3.** FTIR Spectra of Untreated and Aloe Vera Treated S/L 50:50 Blended Fabrics

## 3.2 Antibacterial efficacy of aloe vera treated fabrics

### 3.2.1 Qualitative evaluation

Antibacterial activities of aloe vera were determined qualitatively using Agar Diffusion Test on S/L 50:50 blended fabrics. The results are shown in Table 1.

**Table 1.** Qualitative Evaluation of Antibacterial Activity on Untreated and Aloe Vera Treated S/L 50:50 Blended Fabrics

Silk/Lyocell Fabrics	Zone of inhibition (mm)	
	<i>S. aureus</i>	<i>E. coli</i>
Untreated S/L 50:50	Nil	Nil
Aloe Vera Treated S/L 50:50	30 ± 0.2	28 ± 0.2

The results of qualitative analysis by microencapsulation method clearly show that the aloe vera treated S/L 50:50 blended fabrics have very good antibacterial properties to both gram positive (*S. aureus*) and gram negative (*E. coli*) bacteria. The aloe vera treatments do not allow the growth of bacteria on the treated fabric. The microencapsulation treated fabrics reveal a zone of inhibition of 30 mm for *S. aureus* (Figure 4a) and 28 mm for *E. coli* (Figure 4b). The antibacterial efficacy of aloe vera is found to be better against *S. aureus* than *E. coli*.

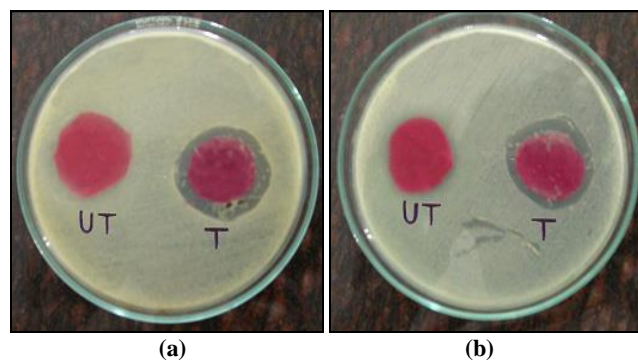


**Figure 4.** Antibacterial Activity of Untreated (UT) and Aloe Vera Treated (T) S/L 50:50 Blended Fabrics for (a) *S. aureus* and (b) *E. coli*

### 3.2.2 Quantitative evaluation

Antibacterial activities of aloe vera were determined quantitatively using Shake Flask Method by bacterial reduction percentage on S/L 50:50 blended fabrics. The results are shown in Table 2.

**Table 2.** Quantitative Evaluation of Antibacterial Activity on Untreated and Aloe Vera Treated S/L 50:50 Blended Fabrics

Silk/Lyocell Fabrics	Bacterial reduction (%)	
	<i>S. aureus</i>	<i>E. coli</i>
Untreated S/L 50:50	0	0
Aloe Vera Treated S/L 50:50	97.8	97.5

Quantitative results indicate that the percentage reduction value of both the microorganisms *S. aureus* and *E. coli* were found to be more than 97% as seen from Table 2. The untreated S/L 50:50 blended fabric showed 0% reduction to both the microorganisms. The zone of inhibition values as seen in Table 1 indicates that the aloe vera treatment not only prevents the growth of bacteria in the S/L 50:50 fabric, but also leaches out and reduces the growth of bacteria. This is in agreement with the test results of % reduction values. Similar results were obtained by Sathianarayanan et al [16, 19] in an earlier study.

### 3.3 Wash durability

The wash durability of aloe vera finishes by microencapsulation method on S/L 50:50 blended fabric is tested quantitatively by shake flask method in terms of bacterial reduction % and are shown in Table 3.

**Table 3.** Wash Durability of Aloe Vera Treated S/L 50:50 Blended Fabrics by Quantitative Method

Number of Washes	<i>S. aureus</i>	<i>E. coli</i>
0	97.8	97.5
1	92.2	90.4
5	89.2	85.3
10	79.6	76.1
15	67.1	55.3
20	50.7	42.6
25	42.1	39.3

It is seen from Table 3 that the aloe vera microencapsulation treated fabrics are found to be excellent in the initial stage, and after subsequent washing up to 25 cycles also the effect is not reduced much. After every wash cycle, the antibacterial activity gradually decreases and at the end of 25th wash cycle the percentage reduction goes down to 42.1% and 39.3% for *S. aureus* and *E. coli* respectively. The reason of good durability to washing may be attributed to the sustained release of aloe vera microcapsules over repeated laundering from the aloe vera extract because of the microencapsulation technique [20, 21]. These results were similar to reports of microencapsulation of neem, Mexican daisy, tulsi, pomegranate and ajwain applied on cellulosic materials in an earlier study [16, 19].

#### 4. CONCLUSION

Following conclusions were drawn from the study conducted to evaluate the efficacy of antibacterial finish using aloe vera. Aloe vera microcapsules were found to

have good antibacterial properties on silk/lyocell 50:50 blended fabrics to gram positive *S. aureus* as well as gram negative *E. coli* bacteria. S/L 50:50 fabrics treated with microcapsules of aloe vera were also found to have good wash durability up to 25 washes. SEM study revealed a better penetration of finish and bondage between the fibre molecules. EDX and FTIR analysis confirm the presence of aloe vera on silk/lyocell 50:50 blended fabrics by exhibiting compounds present in aloe vera gel. Also, both silk/lyocell blended fabric as well as aloe vera is 100% natural, having eco-friendly properties thereby giving economic, social and environmental benefits and can very well serve as a suitable alternative to conventional harmful chemicals.

#### ACKNOWLEDGEMENT

The authors wish to thank the Management and the Principal, PSG College of Technology, Coimbatore for given the permission and providing the necessary infrastructure. Thanks are also due to The Head, Department of Textile Technology for the kind help in department laboratory supports.

#### REFERENCES

1. Vinay GN, Sanjeev RS. 2015. Antimicrobial activity of silk treated with aloe-vera *Fibers and Polymers* 16(5), 1012-1019.
2. Vinay GN, Sanjeev RS. 2017. Antimicrobial treatment of silk with silver nanoparticles using acrylic binder *Indian Journal of Fibre & Textile Research* 42, 465-473.
3. Joshi M, Ali SW, Rajendran S. 2007. Antibacterial finishing of polyester/cotton blend fabrics using neem (*azadirachta indica*): a natural bioactive agent *Journal of Applied Polymer Science* 106, 793-800.
4. Reynolds T. 2004. *Aloes: the genus aloe*. Florida: CRC Press LLC.
5. Jothi D. 2009. Experimental study on antimicrobial activity of cotton fabric treated with aloe gel extract from aloe vera plant for controlling the *Staphylococcus aureus* (bacterium). *African Journal of Microbiology Research* 3(5), 228-232.
6. Jayakumari S, Prabhu K, Rao MRK, Bhupesh, Kumaran D, Ramesh A. 2017. The GC MS analysis of a rare medicinal plant aloe barbadensis *Journal of Pharmaceutical Sciences and Research* 9(7), 1035-1037.
7. Irshad S, Butt M, Younus H. 2011. In-vitro antibacterial activity of aloe barbadensis miller (aloe vera) *International Research Journal of Pharmaceuticals* 1(2), 59-64.
8. Thilagavathi G, Krishna Bala S, Kannaian T. 2007. Microencapsulation of herbal extracts for microbial resistance in healthcare textiles *Indian Journal of Fibre & Textile Research* 32, 351-354.
9. Haufe H, Muschter K, Siebert J, Böttcher H. 2008. Bioactive textiles by sol-gel immobilized natural active agents *Journal of Sol-Gel Science and Technology* 45(1), 97-101.
10. Karolia A, Mendapara S. 2007. Imparting antimicrobial and fragrance finish on cotton using chitosan with silicon softener *Indian Journal of Fibre & Textile Research* 32, 99-104.
11. Kamble KKM, Vishwanath B, Patil CCS. 2013. Antimicrobial activity of aloe Vera leaf extract *International Journal of Applied Biology and Pharmaceutical Technology* 4, 286-290.
12. Fatemeh NB. 2013. Antibacterial activities and antioxidant capacity of aloe vera. *Organic and Medicinal Chemistry Letters* 3, 1-8.
13. Krishnaveni V, Aparna B. 2014. Microencapsulation of copper enriched aloe gel curative garment for atopic dermatitis *Indian Journal of Traditional Knowledge* 13(4), 795-803.
14. Ibrahim W, Sarwar Z, Abid S, Munir U, Azeem A. 2017. Aloe vera leaf gel extract for antibacterial and softness properties of cotton *Journal of Textile Science and Engineering* 7(3), 1-6.
15. Ganesan P, Tamil Selvi C, Ramachandran T. 2010. Microencapsulation of copper enriched herbals for curative garments *Indian Journal of Traditional Knowledge* 11(3), 532-536.
16. Sathianarayanan MP, Bhat NV, Kokate SS, Walunj VE. 2010. Antibacterial finish for cotton fabric from herbal products *Indian Journal of Fibre & Textile Research* 35, 50-58.
17. Narsih, Kumalaningsih S, Wignyanto, Wijana S. 2012. Identification of aloin and saponin and chemical composition of volatile constituents from aloe vera (l.) peel *Journal of Agricultural Food and Technology* 2(5), 79-84.
18. Ravi S, Kabilar P, Velmurugan S, Kumar RA, Gayathiri M. 2011. Spectroscopy studies on the status of aloin in aloe vera and commercial samples *Journal of Experimental Sciences* 2(8), 10-13.
19. Sathianarayanan MP, Bhat NV, Chaudhari BM. 2011. Development of durable antibacterial agent from ban-ajwain seed for cotton fabric *Indian Journal of Fibre & Textile Research* 36, 234-241.
20. Lebre, Filipa, Bento D, Jesus S, Borges O. 2012. Chitosan-based nanoparticles as a hepatitis B antigen delivery system *Methods in Enzymology* 509, 127-142.
21. Hildebrand GE, Tack JW. 2000. Microencapsulation of peptides and proteins *International Journal of Pharmaceutics* 196(2), 173-176.



# Experimental and Numerical Study of Sewing Seams of Automobile Seat Covers Under Unidirectional and Multiaxial Loading

Natalia Kovalova<sup>1</sup>, Petr Kulhavý<sup>2</sup>, Josef Vosáhlo<sup>2</sup>, Antonin Havelka<sup>1</sup>

<sup>1</sup> Technical University of Liberec, Faculty of Textile Engineering, Studentska 2, 46117 Liberec 1, Czech Republic

<sup>2</sup> Technical University of Liberec, Institute for Nanomaterials, Advanced Technologies and Innovation, Studentská 2, 46117 Liberec 1, Czech Republic

**Corresponding Author:** Natalia Kovalova, natalia.kovalova@tul.cz

## ABSTRACT

In industrial textiles, knowing the exact characteristics and behaviour of materials is important. For car seats, industrial textiles not just cover the underlying foam but also increase rigidity of the seat cushion and influence viscoelastic behaviours of foams. Moreover, strength of sewn seams is one of the main quality parameters. Herein, four polyester and polyamide threads were sewn on a material used for car seat covers through lockstitch sewing. Combinations of these materials were studied using static tests in the unidirectional and multiaxial variants. The experimental measurements recorded using a high-speed camera and computer tomography were used to create CAD models. Numerical simulations were conducted using these models and the obtained material models. These model studies help predict and describe the stresses emerging within various types of textile and the threads in their connections. The simulation results agree well with the experimental results.

## ARTICLE HISTORY

Received: 11.12.2018

Accepted: 01.10.2019

## KEYWORDS

sewing seam; strength, 3D curves, parts contact, numerical model

## 1. INTRODUCTION

Automotive textiles represent the most valuable market worldwide for technical textiles. Within this segment, a broad spectrum of products having novel textile structures with performance properties and attractive design is available [1]. Car seat covers are perhaps the most familiar automotive textiles. Considerable technical input is necessary to develop materials that must withstand rigorous use (and abuse) and yet last for the lifetime of the car seat [2].

The exact knowledge about mechanical properties of the used materials is the basic prerequisite for successful product construction. The mechanical properties of materials play a crucial role in the control of production technology, quality control and development of new

materials. In addition, in a few cases, human life may be placed in danger owing due to a malfunction of these products (such as parachutes, airbags, and safety belts). Therefore, it is necessary to understand not only the strength characteristics of textile materials and threads but also the performance of seams.

The seam characteristics include strength, elasticity, durability, safety, and appearance. Inconsistencies in these characteristics can lead to significant differences in seam behavior and can affect seam deformation characteristics. These characteristics originate from four principal sources: speed, needle, thread, and fabric. It has been found that fundamental interactions among these factors exist [3].

Mazari et. al. [4] confirmed that the friction between the needle and sewing thread is one of the major sources of

**To cite this article:** Kovalova N, Kulhyvy P, Vosahlo J, Havelka A. 2019. Experimental and numerical study of sewing seams of automobile seat covers under unidirectional and multiaxial loading *Tekstil ve Konfeksiyon* 29 (4),322-335.

---

needle heating. High needle temperature during sewing weakens the thread because thread tensile strength is a function of temperature as well, and this leads to decreased production. In addition, the strength of the final stitched thread is 30–40 % lower than that of the parent threads. A very high needle temperature can damage the materials as well, for example, a few synthetic fabrics or plastics that come into direct contact with the needle during sewing. Zak [5] described the principles of mutual fabric interaction by using Pierce's model and numerically by using the finite element method (FEM).

According to Midha [6], during high-speed sewing, the strength of sewing threads decreases substantially. Any change in thread strength is closely connected to the thread's passage over the guiding elements of the sewing machine and, consequently, the friction and bending originating between the needle's thread and the touching areas, as well as friction with the bobbin thread [7]. These pressure and friction forces result from internal tension.

One of the major quality factor associated with seams is fabric type. At present, different types of materials are used for upholstering car seats. These include technical textiles for car seat covers, such as woven, knitted, and nonwoven fabrics; natural and artificial leather from synthetic polymers such as polyester, polyamide, and viscose; and blends of wool and cotton with synthetic fibres. Woven and knitted structures are two main fabric forming methods used for manufacturing car seat upholstery manufacturer [8]. Ujevic et al. [9] studied the influence of fabric type on the mechanical properties of the seam, and they found that technical woven fabrics have higher breaking force and penetration resistance than knitted fabric, but knitted fabric is softer and more elastic. Sewing thread accounts for a small percentage of the final product cost but accounts for 50% of the seam strength. Hence, thread plays an important role in seam quality, especially in car seat covers, where it is necessary to consider the following factors: thread fiber type, thread construction, thread finish, and thread size.

For creating a high-quality seam it is necessary to consider all abovementioned parameters. This is a fairly time-consuming process because of the wide variety of existing materials. Therefore, the aim of this study is to develop a numerical model of sewing seams considering all necessary parameters. When studying literature and the latest world research, it is possible to find some numerical models that relate to the textiles connections, however they are simplified by local homogenization of the entire seam as one local area with usually orthotropic properties or some studies of just small segment of the yarn. No model that interprets the thread in its entirety, including individual yarn twists and holes in the fabric has been found.

There are many types of fabric constructions used in automobiles as seat cover fabrics. One type of twill fabric and four types of sewing threads were used for determination of the mechanical properties with using

different measuring methods. Together with that, twill fabric type and one type of polyamide sewing thread were used for creating numerical model of sewing seam. The twill fabric used is the most common fabric used by researchers and its possible to compare with the findings of the previous researchers. In future the numerical model can be tested for multiple textile fabrics.

The required material properties have been measured using a designed multiaxial apparatus. Seam strength was determined by conducting the standard uniaxial static experiments. However, because automobile seat covers are subjected to various loadings, especially, multi-axis load, a special testing device was designed and constructed [3,10]. This device operates on the principle of extrusion of a spherical cap into a cylindrically clamped sample. Each type of test was recorded on a high-speed camera and the samples before and after testing were screened using computer tomography to obtain precise geometric parameters of the created CAD model. Based on this CAD geometry and by using the commercial software ANSYS, several nonlinear contact numerical simulations were conducted to predict the behaviour of the stitched seams instead of the classical experiments [11]. Therefore, the main aim of this article is to thoroughly describe the behaviour of stitched seams for various textile materials and various loading conditions, as well as to develop the corresponding simulation model that can predict the real behaviour of a selected combination of threads and fibres instead of having to conduct expensive experiments.

## 2. MATERIAL AND METHOD

### 2.1 Material

During the process of product usage, sewn seams and materials are subjected to variable loads, leading to various deformations. For textile materials, which show considerable anisotropy or orthotropy, testing along one axis is generally insufficient, and it is necessary to load two axes simultaneously. According to Quaglini [12], because of the small thickness of fabric, it is usually a neglected component of strain along the thickness direction of the material, and technical textiles are mainly thought to be affected by plane stress [13,14].

#### 2.1.1 Threads

To investigate the effect of different sewing threads on seam strength, four different threads were used for specimen preparation (Table 1). Threads of Type B, Type C, Type H, and Type M1 were used to investigate seam strength under multiaxial loading. Other types of threads were used for static measurements. These threads are commonly used in the industry to sew car seat covers. According to ISO 2060 [15] and ISO 2061 [16], the values of fineness and twist of the sewing threads were investigated experimentally.

For preparing all samples tested in this study, seam parameters were selected precisely, and the sewing machine was set up accordingly. A Dürkop Adler sewing machine with an upper thread tension of 4 N and lower thread tension of 1 N was used. Classes of seams and stitching are defined in the international standards ISO 4916 and ISO 4915 respectively. The parameters of the sewing process were as follows: superimposed seam with width of 10 mm and 301 Lockstitch with a density of 3.3 mm. These parameters of stitches and seams are most commonly used for sewing car seat covers.

### 2.1.2 Fabric

Sandwich-type fabrics are used for preparing samples to test the mechanical properties of sewing seams under different type of loading. The material consists of the PES face fabric, foam core and the weft knit fabric as the back. Material thickness was defined using the method given in the standard ISO 5084 [17]. The exact parameters of the fabric are listed in Table 2.

### 2.1.3 Experimental samples for unidirectional and multiaxial loading

The samples for uniaxial loading were prepared according to the norm CSN EN ISO 13935-1 [18]. Laboratory samples of size 700 mm × 350 mm were prepared of the material used to industrial manufacturing of car seat covers (Figure 1a). The samples were folded, such that the edge of the fold was parallel to the shorter side of the sample. The samples were prepared in the warp and the weft directions. Finally, the real width of the sample was 50 mm, and the length of the sample used for investigation was 330 mm (Figure 1b).

The production of experimental samples for measuring seam strength under multiaxial stress begins in the same way as that for uniaxial stress. Parts of the fabric are sewn together, and the remaining parts are prepared for each set of experiment on the test samples by cutting out the desired shapes (Figure 1b). The shaded area in Figure 1b shows the

portion of the test sample on which the spherical cup is pushed [19].

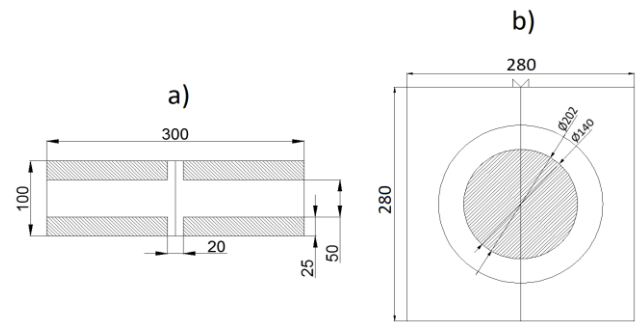


**Figure 1.** Laboratory specimens: a) The UD sample and b) experimental sample

## 2.2 Experimental Devices and Methods

As Reinhardt pointed out [20], in terms of textile testing, the materials are almost always loaded and should be tested biaxially. According to Novak and Hanus [21], anisotropic materials such as the tested coating materials show noticeable hysteresis and different deformations according along different loading directions owing to specific mechanical properties. In tensile tests of textiles along one axis in the longitudinal direction, the main stress concentrators are formed, and the fabric subsequently ruptures near the clamping jaws. By contrast, the tension along the transverse direction is more uniformly concentrated at the sample centre.

According to Escárpita [22], testing of multiaxial loaded samples is necessary to ensure that the test device meets the basic requirements. There must be strictly tension or compression, and spurious shear or bending loads must be avoided. Generally, the use of a hydraulic or mechanical system comprising linear motors, cable system, pulleys, and bearings is recommended.

**Table 1.** Properties of threads used in this study

Property	Type B	Type C	Type H	Type M1
Tread content	PA6.6	PA6.6	PES	PES
Actual thread density T [Tex]	107.8	79.0	94.8	78.7
Twist [t/m]	347	409	375	416

**Table 2.** The fabric specifications

Parameter	Value	Weave type
Width [mm]	1800 ± 20	 Twill (2/1) weave
Weight [g/m <sup>2</sup> ]	490 ± 50	
Thickness [mm]	4.5 ± 0.5	
Face [g/m <sup>2</sup> ]	330 ± 30 (100% PES)	
Lamination	Polyester foam	
Backing [g/m <sup>2</sup> ]	38 (100% PES)	

In the tests, a sample of certain dimensions with the seam in the middle is stretched in a direction perpendicular to the seam at a constant rate until seam breakage.

### 2.2.1 Unidirectional tests

The most common tests applied to automotive seat upholstery were specified by the Society of Automotive Engineers (SAE) and the American Society for Testing Material (ASTM) [23]. For determining the mechanical properties associated with seam sewing, the Strip tests [18] are used. For these experiments, it was necessary to select and condition the samples according to the standard ISO 139 [24].

During the static tests, the maximum force for seam rupture is determined using the strip method when the applied force is perpendicular to the seam. In the tensile test that is a part of this method, the entire width of the test specimen is gripped in the jaws of the testing machine (Figure 2). The feed speed of the jaws was set to 100 mm/min [18].



Figure 2. Experimental device for unidirectional testing

### 2.2.2 Multiaxial testing

A device that can be used to measure sewing seam strength under multiaxial stress has been developed (Figure 3a, 3b). The device consists of a spherical cup (1), an upper jaw (2), a lower jaw (3), screws (4), a hook clamp (5), light source (6), and cylindrical frame (7). In this case, the essential requirement is applied pressure at seam sample, and therefore, it is necessary to choose appropriate settings of the tensile machine. A laboratory-made seam sample was clamped between the two circular jaws and fixed using hook clamps. Then, during the tests, the indenter was

moved vertically downward toward the seam connection at a constant velocity of 100 mm/min.

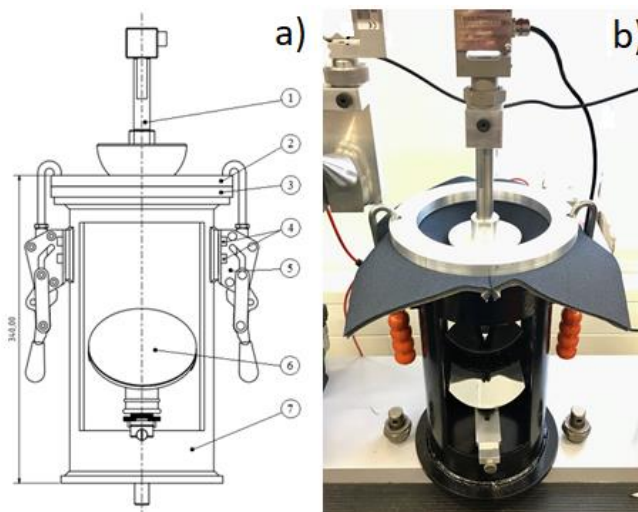


Figure 3. Laboratory instrument for measuring seam strength under multiaxial stress: a) Schematic view of the created device and b) photograph of constructed device

## 2.3 Model Creation

Given the fact that using conventional imaging devices, it is not possible to simply show the mutual thread connections, the computer tomography (Figure 4a, Figure 4b) was used. However, it is not possible to simply convert the obtained graphical data into a CAD-compatible format. Therefore, the images were used mainly as shape templates. Simultaneously pictures obtained using a macro camera was used to measure the fundamental dimensions of the seam.

### 2.3.1 CAD model

For creating the models, the Creo software application was used. Creo is the one of the only few CAD modellers that allows supports direct manual and parametric input for creating 3D curves, including their transition parameters and enhanced control of their base polygons [25].

For creating so complex CAD models, it is important to find the most appropriate forming and carrier curves that can respond to sudden changes in the direction vectors and radius of curvature. Generally, it is possible to express a curve in space by using the explicit expression  $z = f(x, y)$  or implicitly by using  $F(x, y, z) = 0$ . In computer graphics, the parametric curves are expressed by using the point equation  $P(t) = [x(t); y(t); z(t)]$  or with the steering vectors  $\vec{p}(t) = [x(t); y(t); z(t)]$  [26].

The design concept was compiled using B-splines and the Bezier curve (Figure 5). A B-Spline is a generally controlled modification of piecewise polynomial functions and their approximations. It is in fact a curve that passes

through the specified points, while seeking to achieve the lowest values of the radii of curvature in each part. By contrast, the Bezier curve is firmly defined by the end and start points, which create the so-called control polygon and other (internal) points that indicate and allow for direct control of the internal curvature. Currently, the Bezier plate is one of the most popular curves used, for example, in

various font styles [26, 27]. By changing the magnitudes of the Bezier curve parameters, it is possible to obtain and check, for example, the main characteristics of lines, ellipses, parabolas, and hyperbolas. The common feature of the two curves is that by changing any one point, the entire curve can be varied.

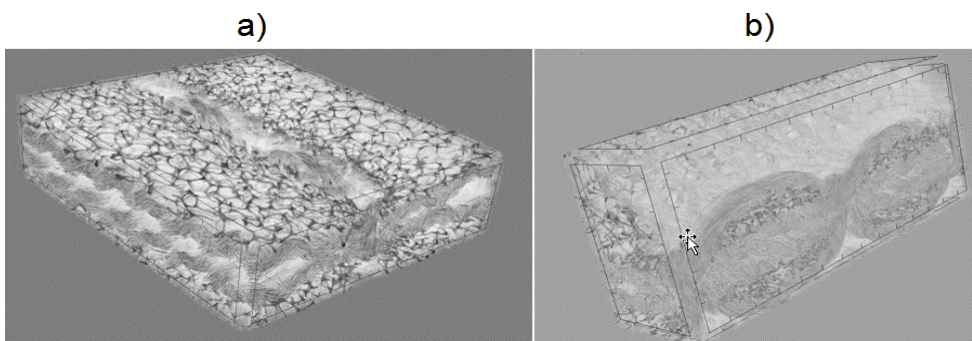


Figure 4. Example of CT scan of seam: a) Internal and b) external view of seam

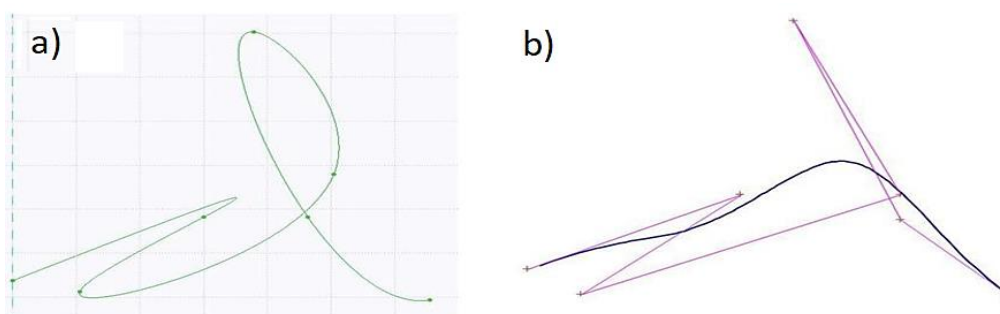
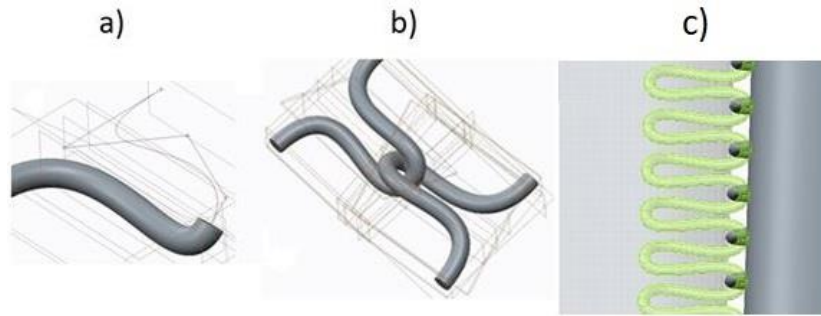


Figure 5. Same points interlayered using a) a spline and b) the Bezier curve

The spline curve has been found to be unsuitable for the thread model, Possible because during model creation, the individual parts are connected together, and the curve is sensitive to any local change. This could cause unwanted changes to the entire geometry, even when only a tiny local variation occurs. This leads to interference among the assembly parts and possibly to errors during FEM computation. The Bezier curve was found to be suitable because of firmly specified start/finish points and because the curvature is independent of the adjacent connected segments. For a required connection, it is possible to simply use the adjustable parameters of normality, tangentiality, or parametric settings of the transitions. A very important parameter of the model is the setting of the parametric classes of the continuity transitions between individual segments that define the continuous derivatives in the three classes. Connection C0 refers to a common point with two arbitrarily passing vectors and two curves of different radii

of curvature. Continuity C1 is characterized by one common tangential vector  $\vec{t}_1$  at the transition point, but two curves having different radii of curvature. Completely analogously, class C2 is characterized by a common tangent vector and constant value of the curvature at the transition point.

At first, the yarns (Figure 6a) were interconnected. For connection of the yarns, the merged surfaces were used, and the whole geometry was formed using the assembly cut-off with the offset surfaces (Figure 6b). The CAD model of the entire assembly was verified by tracking global interferences of all parts, where any intersections could not occur. Checking the geometry of the entire assembly this way was necessary, especially for solving the future numerical contact model. The assembly of mutual thread connections and implementation on fabric are shown in Figure 7c.



**Figure 6.** Model of a) thread and b) binding point of upper and lower thread c) assembly of mutual threads connection and implementation on fabric

## 2.4 Numerical Model Theory

An appropriate choice of a material model is very important. For the materials used in this study, it was necessary to determine the elastic and shear moduli [GPa], tensile strength [GPa], and set the Poisson ratio [-] by conducting various experiments. For creating the numerical model of the fabrics, the spatial ten square node tetrahedron SOLID 187, which is suited for modelling irregular structures (created, e.g., in CAD systems), was used. It is defined by eight nodes having three degrees of freedom at each node and the orthotropic material properties. The default element coordinate system is along global directions. The element is usually used for modelling plastic elastic deformation, shrinkage, creep and initial stress, initial deformation, and large deformation. The truss element was selected for modelling the yarns, which are subjected to tensile loads only and do not transfer any type of moment [28, 29]. As the truss element the Link 180 – 3D finite strain spar was used. This element is similar to link8 but with improved nonlinear capabilities. The curved truss element in 3D space has six deformation parameters in each node. The element's deformation parameter matrix has a total of twelve elements. This element transmits only the axial force, but it is deformed by bending and torsion. In technical practice, an uniform distribution of shear deformation on the cross-section originates is assumed for the truss element, but according to the Midlin hypothesis with possible deviation of the perpendicularity to the centerline of the element. Therefore, unlike for the straight bar (Link8), it was necessary to consider the curved truss element (Link180), which is based on the decomposition principle of the centerline elongation and the change of curvature.

For the static analysis, owing to the duration of the entire process, an automatic step control scheme was used. Generally, because of the small thickness of the fabric component, the stress in the thickness direction of the material can be neglected. Therefore, technical textiles are thought to be affected by plane stress.

### 2.4.1 UD model

Unidirectional loading was modelled using FEM in ANSYS. Owing to the complexity of the geometry and the lengthy calculation, the model was divided and solved in half axial symmetry. Gradually, the material properties of the fabric, structural steel, and PA fibre were introduced into the model (Table 3). For such a complicated geometry, it was necessary to create a mesh by using a combination of triangular polygons, geometric smoothing, and sweep methods.

In the critical parts of the geometry, the mesh of the thread was optimized using the Body Size function in the marked areas of the model. For body sizing, the definition of type element sizing 0.23 mm with coarse behaviour was introduced. In addition, the hex dominant method was used to generate the final mesh of the labelled geometry [30].

With regard to the same textile materials for all experiments, the same material model for multi axis simulation was used.

The FEM mesh was optimized so that individual elements did not overlap with the optimized meshes that were already created (Figure 7). In the Table 4 there is a specification of the optimized mesh.

**Table 3.** Material models used in unidirectional model

Material	Density [kg.m <sup>-3</sup> ]	Elastic modulus [GPa]		Shear modulus [GPa]		Poisson ratio [-]		Tensile strength [Gpa]
		$F_{11}^{f,m}$	$F_{22}^{f,m}$	$G_{12}^{f,m}$	$G_{23}^{f,m}$	$V_{12}^{f,m}$	$V_{23}^{f,m}$	
Fabric	1250	4.9	4.4	1.96	1.1	0.32	0.35	2.1
Uniaxial Structural steel	7850	200		76.9		0.3		0.25
PA fibre	1140	1.8		0.74		0.21		0.23



Figure 7. The mesh of the unidirectional model

Table 4. Specification of the created mesh in the UD model

The UD	1 <sup>st</sup> fabric	2 <sup>nd</sup> fabric	1 <sup>st</sup> thread	2 <sup>nd</sup> thread
Nr of nodes	22 797	27 454	24 864	16 465
Nr of elements	101 620	128 000	17 595	10 637

When two separate faces touch each other, they become tangential to each other and should therefore be considered in contact (Figure 8). They can transmit pressure normal forces and tangential friction. The higher the contact stiffness  $K$  [N m<sup>-1</sup>], the lower is the mutual penetration  $x$  [m]. The ideal case for infinite stiffness would have been zero penetration. However, when using Penalty Methods, this is numerically impossible [31]. In the real case, however, when the penetration  $x$  is very small, the result will still be sufficiently accurate. The frictional contacts with the coefficient  $f = 0.3$  [32] was used for the modelled yarn (Figure 9a) and assembly completely (Figure 9b). The main difference, however, is the introduction of variable  $\lambda$ , in which the Lagrangian method adds low sensitivity to the contact stiffness and this way provides an easier solution in the case of such complicated contacts. Another advantage of minor penetration is that when the penetration is not allowed, the contact is either opened or closed, that is, it can be represented using a step function. This can lead to problems in convergence or the solution oscillates between the open and closed statuses. Therefore, the basic Penalty Method was employed in the UD models. Normal stiffness is another essential contact parameter. In general, the higher the stiffness, the better is the accuracy.

However, solution convergence becomes difficult [29]. Concerning the definition of a contact pair, it is necessary to determine the distribution of stress in the two parts of the fibre. Therefore, for representing the mutual interactions of the fibres, symmetrical behaviour of the contact pair was selected. In a comparison of the interaction of yarn and fabric, it is possible to use automatic or asymmetric expressions. In the end, for derivation of integration points, the nodal-normal definition has been used [30]. The value of the maximum tensile stress depends on the displacement (Figure 17), as was observed in the results.

#### 2.4.2 Multiaxial model

A smooth uniform mesh should be sought in the regions of interest for the analysis. Elsewhere, coarsening of the ambient mesh may help reduce the overall size of the problem to be solved [31]. The rigid and flexible parts of the model were meshed sequentially by using the sweep method in combination with triangular polygons. To optimize it, the mapping features were inserted. The input value of an element was set to 0.18 mm. The mesh was optimized to the values specified in the Table 5.

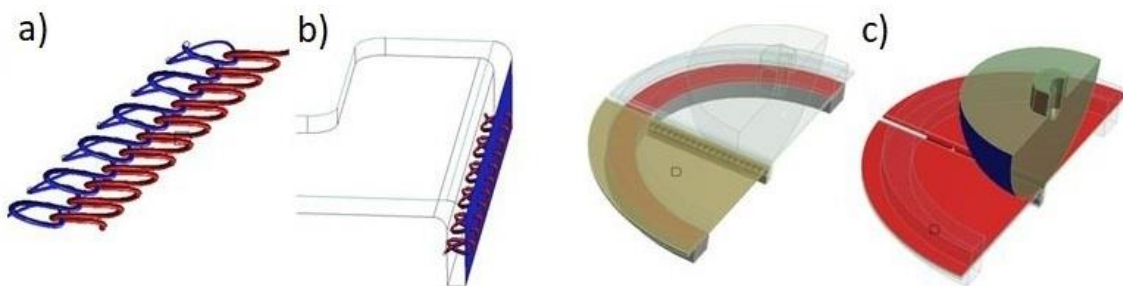


Figure 8. Scheme of solved numerical contact for uniaxial (a and b) and multiaxial (c) models

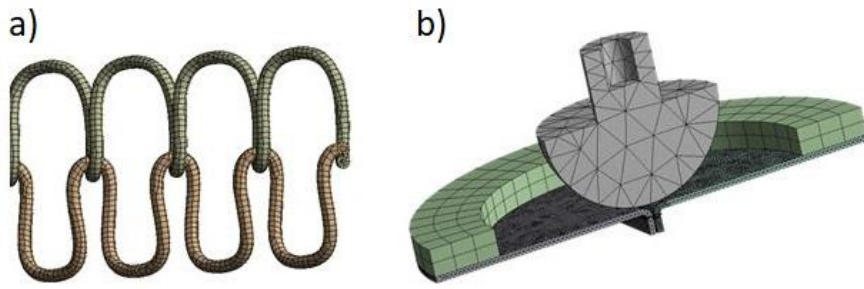


Figure 9. The mesh of the: a) sewing seam in detail b) whole multidirectional model

Table 5. Specification of the created mesh in the multiaxial model

The multiaxial	Indentor	Jaw	1st fabric	2nd fabric	1st thread	2nd thread
Nr of nodes	12 281	800	3 650	3 715	25 402	13 661
Nr of elements	2 763	1 275	1 902	1 915	8 986	8 913

Between the rigid and flexible parts of the model, the friction was set. Selected contact surfaces were defined using the friction coefficient  $f = 0.3$  and Normal Lagrange formulation (Figure 8c) [32]. After optimization of the contacts, the indentor, which was in contact with the tested fabric, was set to undergo remote displacement in one direction. The value of the maximum tensile stress depends on the displacement (Figure 22), as was observed in the results.

#### 2.4.3 The introduction of models boundary conditions

For simulation of the both models (unidirectional and multiaxial), different boundary conditions were introduced. In the case of uniaxial loading modelling of at the bottom of the surface, the model was fixed in all movements and rotations. On the opposite side of the surface the displacement in uniaxial direction was set. This boundary condition has been defined to the maximum length in the displacement  $u \rightarrow$  depends on time. In the other directions, the displacements have been fixed to avoid some undesirable shift. The feed value  $u \rightarrow$  corresponds to the

maximum elongation achieved during the real tests of the uniaxial fabric.

In case of the modelling of uniaxial loading at the bottom of the surface, the model was fixed for all movements and rotations. On the opposite side of the surface, the displacement along the uniaxial direction was set. This boundary condition was defined such that the maximum length along the displacement  $u \rightarrow$  depended on time. Along the other directions, the displacements were fixed to avoid any undesirable shift (Figure 10a). The feed value  $u \rightarrow$  corresponds to the maximum elongation achieved during real tests of the uniaxial fabric.

In the case of multiaxial loading modelling, the model was divided into two parts, namely, rigid and flexible. The rigid part of the model formed a jaw and indentor, into which the material properties of the structural steel were introduced. In the flexible parts of the model, the material properties of the fabric and PA 30 sewing threads were inserted (Figure 10b).

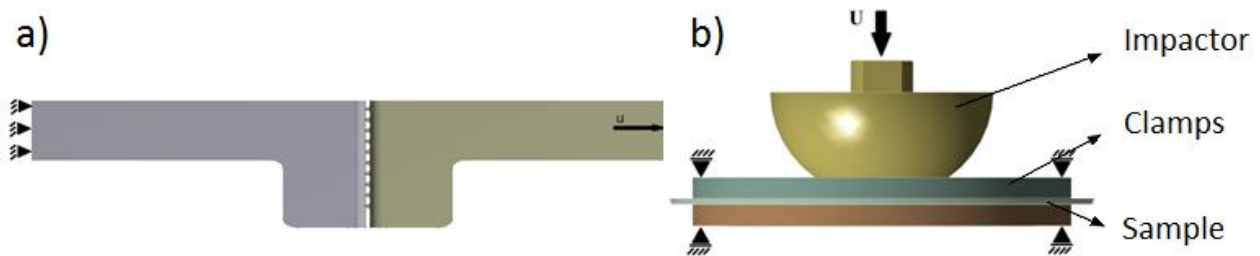


Figure 10. Defined boundary conditions: a) uniaxial measurements and b) multiaxial measurements

To improve the efficiency of analyses involving large number of bodies, is advantageous to suppress the default frictionless interaction that is scoped to all bodies, and insert additional body interaction objects, which limit interactions to specific bodies instead. The value of the displacement  $\vec{u}$  was the maximal value of displacement, equal to the on measured when the yarn was broken during the experiments. The determined value corresponds to mean values of the measured displacements during which breach of threads in real samples occurred. The observed results were the values of maximum tensile stress in dependency on the displacement (Figure 20). Two kinds of stepping control of the static analysis have been used. The

first one with a constant time step size and the second with substeps adjustments. As could be seen in the Figure 11, the chosen approach has little bit changed the convergence of solution, however there was no impact to the duration or precision of the results.

The most important step to the successful convergence in the studied case were not any very precise mesh neither the setting of the solver, but definition of the contact, especially the detection of the integration points on the contact surfaces. This could be caused by the fact, that as could be seen in Figure 12 the contact is mostly sliding and the integration contact points varying for the each step.

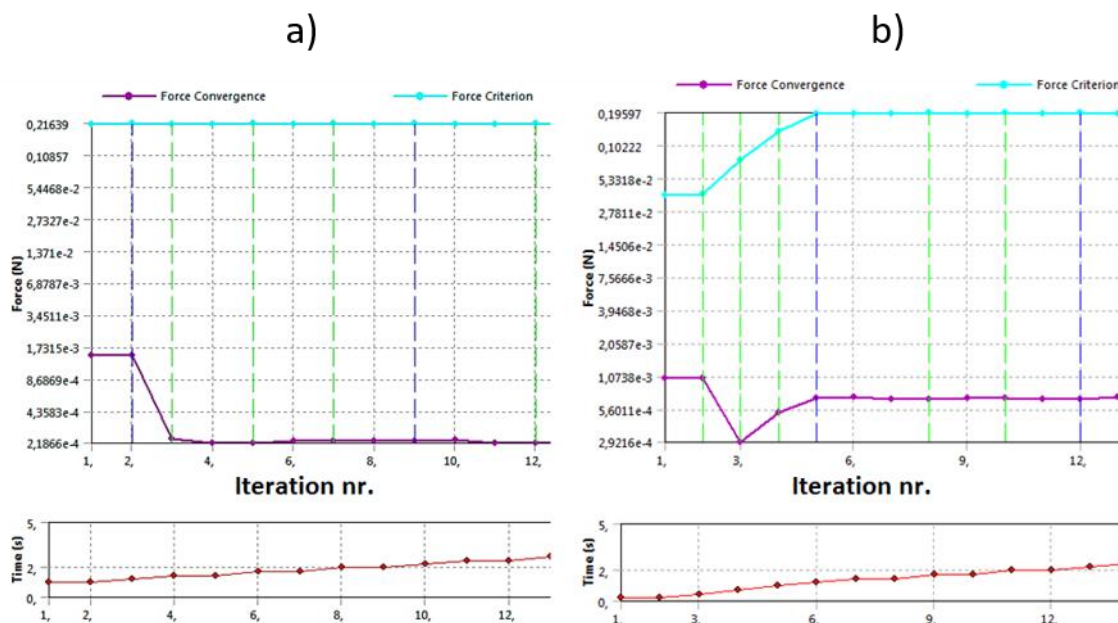


Figure 11. Convergence of the model solver for the a) Constant b) Variable step control

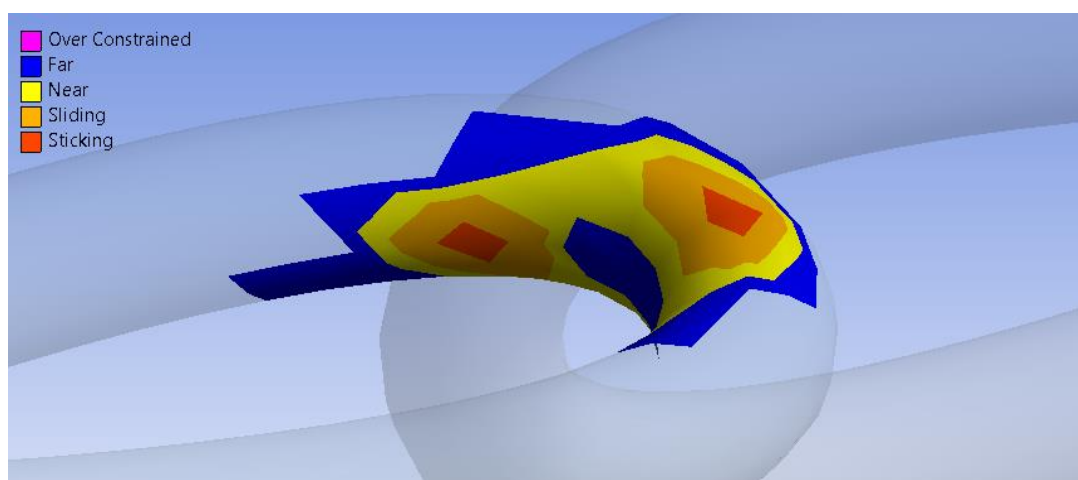


Figure 12. The status of the mutual threads contact

### 3. RESULTS AND DISCUSSION

In this work, the mechanical characteristics of seams were analysed experimentally for various types of stresses. The device that can be used to test seam strength and monitor the mechanical characteristics of seams under multi-axial loading was developed. Then also the experimental analysis of the dynamic characteristics of the seam was performed to compare the strength of sewed seams under static and dynamic stresses.

#### 3.1 Experimental Results

##### 3.1.1 Unidirectional tests

The ultimate strength tests under different types of loading are summarized in Figure 13, where the loading curves are shown (as an example for seams with PA 30 thread). The fiber strength was determined based on the known cross section area, normal stress and the ultimate strength known from the experiments.

A correlation can be observed between the results of static loading in warp and weft directions. However, based on the experimental results it was found that for static loading in the warp direction, the maximal forces were approximately 10% higher than in the weft direction (Figure 14). In all seams with the various sewing threads were used. The material is strongest when the seam is perpendicular to the warp direction and weakest when the seam is perpendicular to the weft direction.

This is probably related to the fact that the density expressed by the number of threads per unit length is higher in warp direction (28 ends per cm and 22 picks per cm).

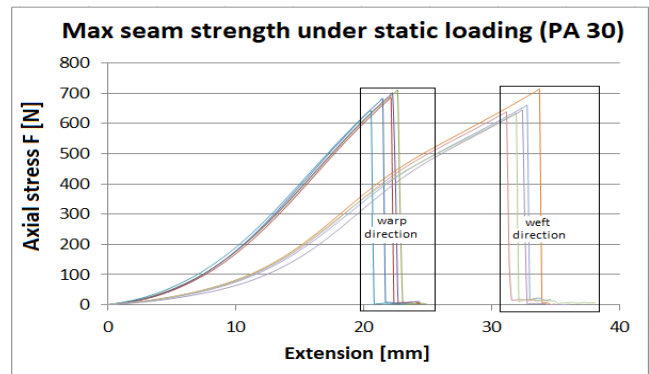


Figure 13. Force–elongation curves of seams with PA 30 threads in warp and weft directions (unidirectional static test)

##### 3.1.2 Multiaxial tests

Four types of polyester and polyamide sewing threads were used for sewing the sandwich material, which is used directly for sewing car seat covers. The axial stress and elongation of seams under multiaxial stress were measured. The test results in the form of stress-strain curves for seams using PA 30 threads, as an example, are shown in Figures 15 and 16.

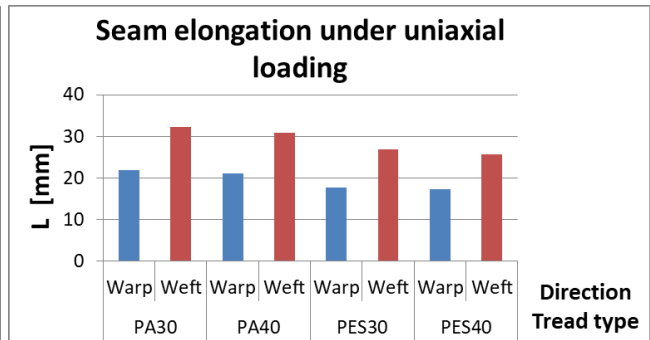
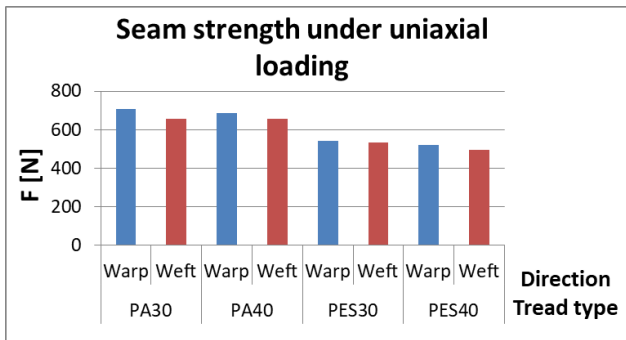


Figure 14. Changes in seam breaking forces and elongation depending on thread type and test direction

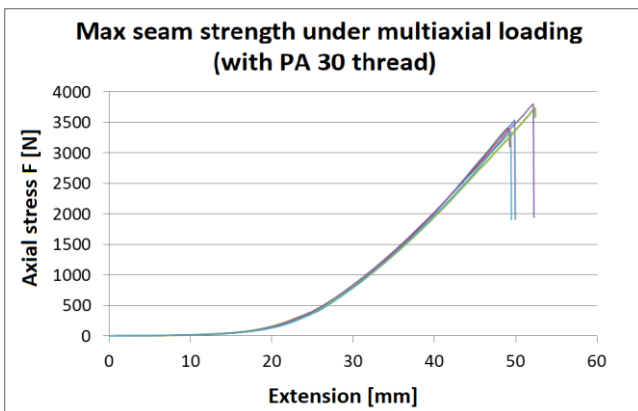


Figure 15. Axial stress to seam break under multiaxial load

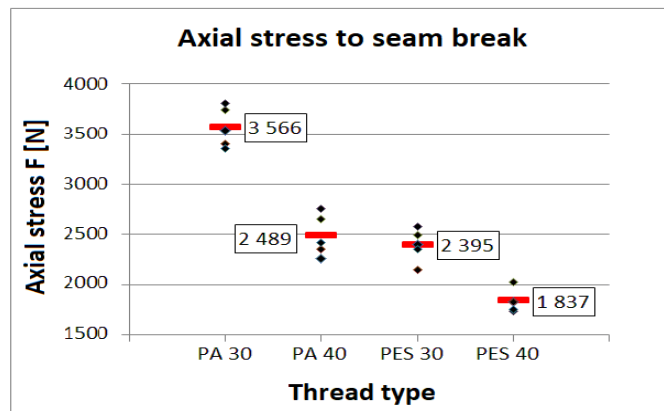


Figure 16. Experimentally determined value of axial stress to seam break with dependency on thread type under multiaxial stress (red lines are averages of axial stress to seam break)

### 3.2 Static Uniaxial Loading

The first step before the main modelling was exploring how real seam rupture occurs. For better comprehension, seam rupture was monitored using high-speed cameras i-SPEED 3 over the course of the experiments. Examples of seam rupture observed sewed with PA30 thread type under uniaxial static loading are shown in Figure 17. In the image,

locations of seam rupture are visible clearly at the recording speed of 10,000 fps for static loading.

The solution of this model was the maximum tensile stress observed in the added fabric yarns (Figure 18) and the resultant computed force compare with the experiment in the Figure 19.

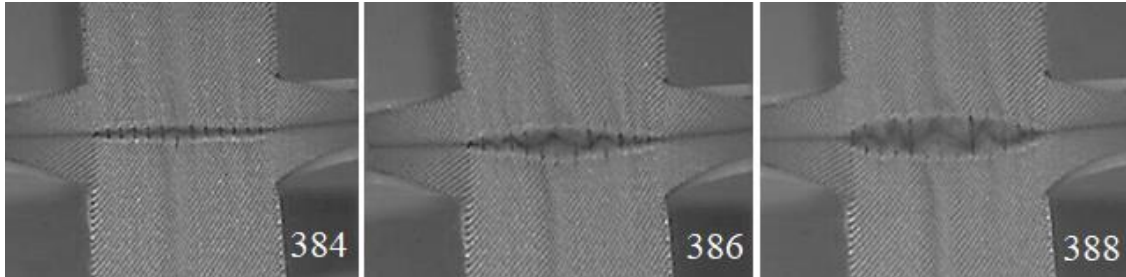


Figure 17. Moment of rupture under static uniaxial loading (384<sup>th</sup> frame, 386<sup>th</sup> frame, and 388<sup>th</sup> frame)

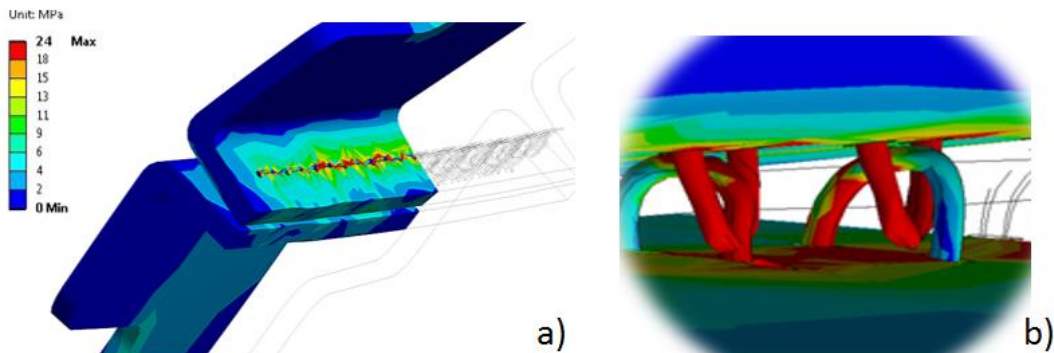


Figure 18. Normal stress in uniaxial model

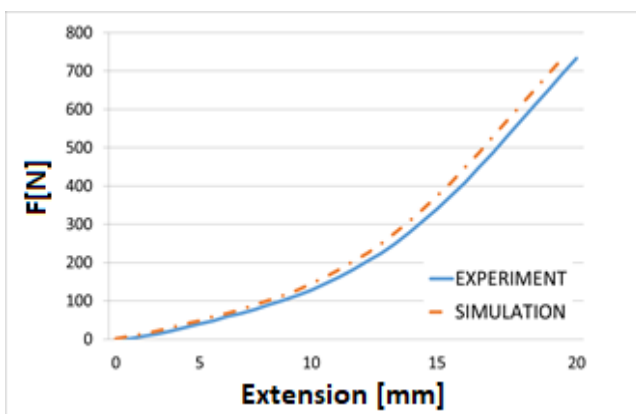


Figure 19. Results of for static loading

### 3.3 Static Multiaxial Loading

The location of rupture of the seam with PA30 thread type during multiaxial loading was monitored using a high-speed camera with a recording speed of 10,000 fps. Examples of seam rupture are shown in the Figure 20.

The maximum tensile stress observed in the added fabric yarns (Figure 21) together with the position of the indenter and the resultant computed forces are shown in Figure 22.

The results of the conducted experiment and the simulations under static unidirectional loading with PA 30 sewing thread in a seam were compared to each other (Figure 22).

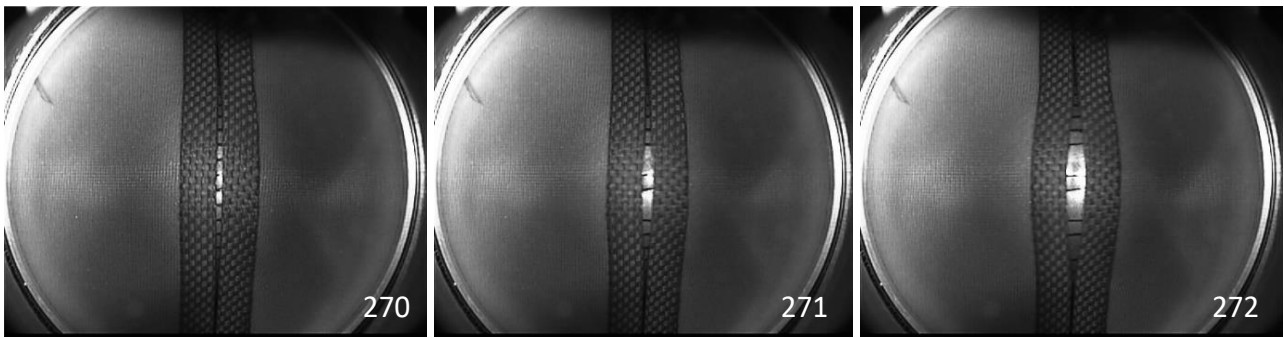


Figure 20. Moment of growing rupture under dynamic uniaxial loading

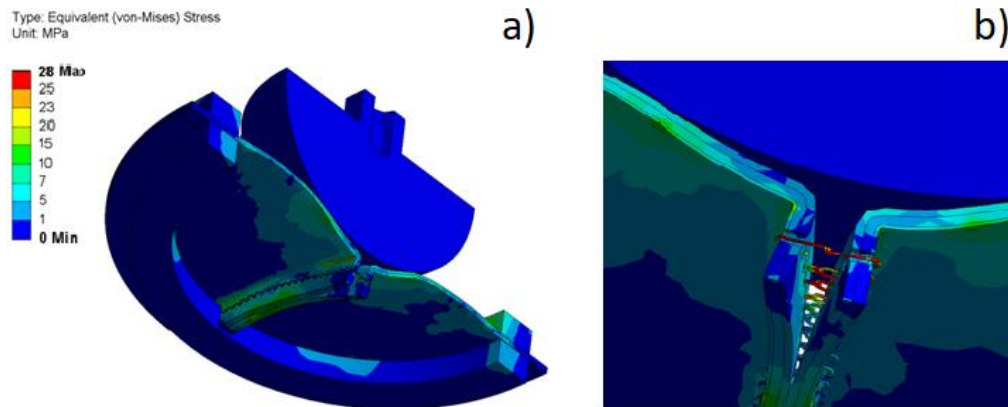


Figure 21. Normal stress in uniaxial model

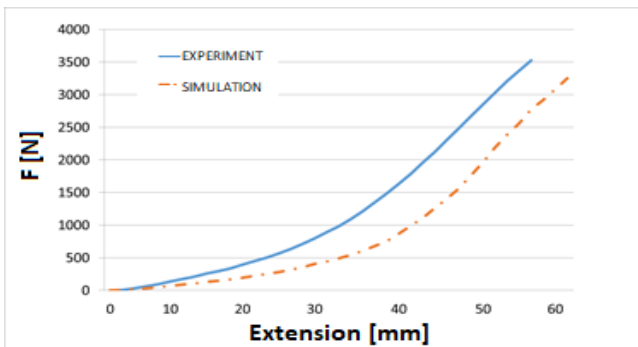


Figure 22. Results of model and experiment under multiaxial static loading

The outputs of the experiment for determining the strength of sewing seams in car seat covers revealed that seams with PA 30 threads have the highest strength and elongation, and they are the most suitable for sewing covers compared to other threads. In the simulation results, the maximum normal stress in the seam area could be observed. The simulated values correspond to the experimental values with a deviation of 8% in force and 10% in displacement.

#### 4. CONCLUSION

In this study, a method of measuring the strength of sewing seams was proposed. The device for seam strength measurement under unidirectional and multiaxial stress in

static and dynamic loading was developed. This is useful because of the anisotropy of sandwich structures in the technical textiles used, for example, in car seat covers.

Based on the experimental measurements, the mechanical properties of several combinations of yarns and fabrics were determined. To predict behaviour of the seam in real conditions and to verify the experimental results, the unidirectional and multiaxial tensile tests were simulated numerically. At first, the CAD model based on the real microstructure obtained by CT and micro capture, with the lockstitch threads connections, was designed and imported to ANSYS 18.0, where the model was subjected to real loading and boundary conditions. Based on the experiments, the material models of the yarns and fabric used herein were determined. The simulation results agree well with the results of the real tensile test. Based on these results, it can be said that the given sewing seams exceeded the limit of proportionality of 680 N in the in static mode, respectively, in the model of unidirectional loading, and this led to their rupture, as shown in Figure 18. Furthermore, the maximum tensile stress in the threads and the textile materials was investigated. The model of multiaxial stress of the seam yielded the maximum normal stress of 28 MPa, which corresponds approximately to 3500 N, as shown in Figure 22.

Every model and technique has default estimations. In the unidirectional test the simulation overestimates the strength

and on the multidirectional it underestimates it as seen on Figures 19 and 22. Additionally it differentiates more in the multidirectional test, what is primarily associated with a large number of parameters and contacts in multidirectional modeling. The predictability of mode is in the reasonably good, but it is necessary to find ways to improve the models. The solution of the problem of optimization of a mathematical models of sewing seam under different loadings is consist the following stages: the choice of an optimization method, a directed search for a combination of the values of the parameters of a mathematical model ensuring the achievement of the desired goals, the accuracy of the models in particular.

This work provides new insights into the physical and mechanical properties of sewing seams, which are especially useful for the production and testing of technical textiles. Actuality of work is due to the high demands on the quality of technical textile products especially the demands on the strength of the seams, as one of the most important properties. The high cost of testing already finished products necessitates determining the sewing seam strength theoretically or testing appropriate samples by using a convenient device. In the future, research is needed to improve the developed apparatus for measuring the

strength of a seam under multiaxial strain, correcting the seam numerical model to shorten the development cycle, which consists of preparing sample prototypes, testing the prototypes, and re-sampling. Another task will be modification of the materials used, which consist of composite parts. The newly created material models will be subjected to testing to improve the parameters and strength of the existing seams.

## ACKNOWLEDGEMENT

This publication was written at the Technical University of Liberec as part of the results of this project Of the Ministry of Education, Youth and Sports of the Czech Republic and the European Union – European Structural and Investment Funds in the frames of Operational Programme Research, Development and Education – project Hybrid Materials for Hierarchical Structures (HyHi, Reg. No. CZ.02.1.01-0.0-0.0-16\_019/0000843) and through the financial support of the Ministry of Education, Youth and Sports of the Czech Republic and the European Union (European Structural and Investment Funds - Operational Programme Research, Development and Education) in the frames of the project “Modular platform for autonomous chassis of specialized electric vehicles for freight and equipment transportation”, Reg. No. CZ.02.1.01/0.0/0.0/16\_025/0007293.

## REFERENCES

1. Shishoo R. 2008. *Textile advances in the automotive industry*. The Textile Institute. Boca Raton Press: Woodhead, ISBN 9781845693312.
2. Fung W. 2000. *Textiles in automotive engineering*. Cambridge: Woodhead, ISBN 1855734931.
3. Barbulov-Popov D, Cirkovic N, Stepanovic J. 2012. The Influence of Stitch Density and of the Type of Sewing Thread on Seam Strength *TEM Journal* 2, 104–110.
4. Mazari A, Kausik B, Havelka A. 2016. Prediction of needle heating in an industrial sewing machine *Textile Research Journal* 86(3), 302–310.
5. Zak J. 2015. Modelling of textile structures *Fibres and Textiles*, Slovak University of Technology in Bratislava, Vol. 22, 2015, ISSN 1335-0617.
6. Midha VK, Chatopadhyay R, Kothari VK. 2009. Studies on the changes in tensile properties of sewing thread at different sewing stages *Textile Research Journal*. 79(13), 1155–1167.
7. Rudolf A, Gersak J. 2011. The effect of drawing on PET filament sewing thread performance properties *Textile Research Journal* 82(2), 148–160.
8. Gülşah P, Çeken F. 2009. Research on the breaking and tearing strength and elongation and elongation of automobile seat cover fabrics *Textile Research Journal* 79(1), 47–58.
9. Ujevic D, Kovacevic S. 2004. Impact of the seam on the properties of technical and nonwoven textiles for making car seat coverings *International Nonwovens Journal* 13(1), 31–41.
10. Germanova-Krasteva D, Petrov H. 2008. Investigation on the seam's quality by sewing of light fabrics *International Journal of Clothing Science and Technology* (20), 57–64.
11. Bagnaci B, Shanbeh M, Ghareaghaji A. 2010. Effect of tensile fatigue cyclic loads on bagging deformation of elastic woven fabrics *Indian Journal of Fibre & Textile Research* 35, 298–302.
12. Quagliani V, Corazza C, Poggi C. 2008. Experimental characterization of orthotropic technical textiles under uniaxial and biaxial loading. Composites Part A *Applied Science and Manufacturing* 39(8), 1331-1342.
13. Kawabata S, Niwa M. 1984. Validity of the linearizing method for describing the biaxial stress-strain relationship of textile. The University of Shiga Prefecture..
14. Wang Y, Zhang P, Zhang Y. 2014. Experimental investigation the dynamic pressure attenuation of elastic fabric for compression garment *Textile Research Journal* [online] 84(6), 572–582 [cit. 2016-03-28].
15. ISO 2060: 1994. Textiles: Yarn from packages-Determination of linear density (mass per unit length) by the skein method.
16. ISO 2061: 2010. Textiles: Determination of twist in yarns - Direct counting method.
17. ISO 5084: 1996. Textiles-Determination of thickness of textile and textile products.
18. ISO 13935-1: 2014. Textiles - Seam tensile properties of fabrics and made-up textile articles - Part 1: Determination of maximum force to seam rupture using the strip method.
19. Kovalova N, Kulhavý P, Vosáhlo J, Havelka A. 2016. Numerical Model and Analysis of Multiaxial Stress on the Sewing seam. Proceeding of International Conference AUTEX. University of Ljubljana, Ljubljana.
20. Reinhard HW, Corazza C, Poggi C. 1976. On the biaxial testing and strength of coated fabrics *Experimental Mechanics* 16(2), 71–74.
21. Novak O, Hanuš J. 2010. 3D nonwovens in medicine-simulation of mattresses behavior under loading. Liberec: Technical university in Liberec, 112.
22. Escarpita D, Koenders EAB, Carvalho DBF. 2012. Biaxial tensile strength characterization of textile composite materials *Composites and Their Properties*. InTech, 08-22.

- 
23. Mukhopadhyay SK., Jeffrey FL. 1999. *Partridge automotive textiles*. The textile Institute, Oxford,
  24. ISO 139: 2005. Textiles — Standard atmospheres for conditioning and testing.
  25. Kulhavy P, Kovalova N, Vosahlo J. 2015. Numerical model of the static loading of a stitched seam in the composite cover of car seat *Applied Mechanics and Materials* 827, Trans tech publication.
  26. Matousek I. 2005. *Computer modelling in the automated production of molded glass*. Technical University of Liberec: Liberec, 28s. ISBN 80-708-3988-0.
  27. Zára J., Benes B. 2004. *Modern computer graphics*. Computer Press: Brno, 609 p. ISBN 80-251-0454-0.
  28. Vosahlo J, Novak O, Petru M, Lepsik P. 2014. Experimental and numerical study of mechanical properties of artificial blood vessel, EAN- 52nd International Conference. on Exp. Stress Analysis. Mariánské Lázně; Czech Republic, 175-176.
  29. Madenci E, Guven I. 2006. *The Finite Element Method and Applications in Engineering Using ANSYS*. Springer, ISBN-13: 978-0387282893.
  30. Talia M, Lankarani H, Talia JE. 1999. New experimental technique for the study and analysis of solid particle erosion mechanisms *Wear* pp. 225-229, pp.1070–1077.
  31. Jirasek M, Bazant Z. 2002. *Inelastic analysis of structures*, Wiley, ISBN 0-471-98716-6.
  32. Zavarise G, Wriggers P, Schrefler BA. 1995. On augmented Lagrangian algorithms for thermomechanical contact problems with friction *International Journal for Numerical Methods in Engineering* 38 (17), 2929–2949.



## Colorimetric changes of thermochromic ink printed on smart textile materials exposed to different heat transfer methods

Stefan Đurđević<sup>1</sup>, Dragoljub Novaković<sup>1</sup>, Savka Adamović<sup>1</sup>, Nemanja Kašiković<sup>1</sup>, Neda Milić<sup>1</sup>,  
Branko Štrbac<sup>2</sup>, Miodrag Hadžistević<sup>2</sup>

<sup>1</sup>University of Novi Sad / Faculty of Technical Sciences, Department of Graphic Engineering and Design / Novi Sad, Serbia

<sup>2</sup>University of Novi Sad / Faculty of Technical Sciences, Department of Production Engineering / Novi Sad, Serbia

**Corresponding Author:** Stefan Đurđević, djurdjevic@uns.ac.rs

### ABSTRACT

This research aims to determine the influence of heat and printing substrate type on the colorimetric properties of the thermochromic ink printed on various textile materials while subjected to heating simulating realistic conditions of usage. The results of the research can be used as a recommendations for the development of a smart temperature indicators for textile packaging. Four specific groups of textile materials were used as printing substrates and magenta leuco thermochromic water-based screen printing ink (activation temperature 31°C) in order to analyze resulting colorimetric properties. Experiment based on analysis of resulting color differences confirmed that the screen thread count influences the rate of the material color change. Namely, the higher the thread count the faster the color change i.e. the sample returns faster from the discolored to the colored state. It was also confirmed that the lower the fabric weight of the material is, the sample returns faster from discolored to the colored state. In addition, this article presents a comparison of the contact and contactless method of sample heating at the same temperature. It was shown that the samples were cooled slower and consequently changed the colorimetric values after the contact method.

### 1. INTRODUCTION

The most commonly accepted definition of smart materials is that such materials can be activated by physical, chemical or mechanical environmental influences and react to their surroundings predictably and beneficially. Some of the most important smart materials are piezoelectric, shape memory, chromatic and magnetic-rheological [1]. Chromatic materials are materials that change color under the influence of external factors (temperature, light, the presence of solvents, pressure, electricity, friction, etc.) [2]. Material that changes color due to the temperature change is called thermochromic material. Thermochromism finds its application in the textile industry, but textiles produced from thermochromic fibers have not appeared on the market yet. So far the thermochromic effect on textiles is mainly achieved by screen printing with thermochromic inks [3].

In this article, the term activation temperature will be used to define the temperature at which the coloration/discoloration process occurs. Leuco dye-based thermochromic ink is a thermochromic composite that consists a color-former and a color-developer dissolved in a solvent. The composite is microencapsulated in a protective coating to protect the content from the environment [4]. The color-former has two forms in dependence of the temperature – colored and colorless form. In a non-heated state, the composite remains in solid form, and the color-former adopts its colored form. In heated state, the solvent melts and the interaction between the solvent and the color-former destroy the composite, thus causing the color-former to adopt its colorless form. The activation temperature is defined by the temperature at which the solvent changes from solid to liquid state [5].

### ARTICLE HISTORY

Received: 26.02.2018

Accepted: 09.11.2019

### KEYWORDS

printing, thermochromic, ink, smart textiles, materials properties

**To cite this article:** Durdevic S, Novakovic D, Adamovic S, Kasikovic N, Milic N, Strbac B, Hadzistevic M. 2019. Colorimetric changes of thermochromic ink printed on smart textile materials exposed to different heat transfer methods. *Tekstil ve Konfeksiyon* 29(4), 336-343.

Thermochromic leuco dyes are available with different activation temperatures, from -15 to 65 °C. However, the majority of applications are limited to the three standard temperature ranges, cold (~ 10 °C), human body temperature (~ 31 °C) and warm (~ 43 °C) [6]. Usually, the leuco dyes are colored beneath activation temperatures and become discolored or transparent above the activation temperature. All the main types of inks, both water-based and UV-based, are available for paper, plastic and textile applications [7].

Although the colorimetric characteristics of thermochromic inks on textiles are significant from the perspective of the application, the influence of temperature on colorimetric values of thermochromic inks has not been studied to a great extent. Friškovec et al. [8] confirmed that thermochromic inks have poor stability against light and high temperatures. They used the white inked aluminum plate as a substrate for heating at the high temperatures and paper substrate for exposure to light. The stability tests showed that the thermochromic prints were affected by UV light and the temperatures well above 150 °C. Kulčar et al. [9] after tests on paper samples, noted that the discoloration process was not completely finished at the highest temperatures, even far beyond the activation temperature. The samples retained a bright pastel color from the ink on the sample, and this effect increased with the increase of the ink layer thickness. Kulčar et al. [10] also shown that the color values of thermochromic samples are the function of the temperature. They concluded that the thermochromic samples does not depend only on temperature, but also on its thermal history, so the thermochromic materials belong to several physical systems with a hysteresis. In all this research samples were printed with screen printing technique. Chowdhury et al. [11] applied thermochromic inks to a conductive cotton fabric made of nichrome/cotton core-spun yarn and show the temperature dependence of colorimetric properties on the thermochromic inks. The heat generation and the temperature rise were controlled by the voltage applied. The research related to colorimetric characteristics of thermochromic inks were normally carried out in a controlled manner by precisely varying temperature through specially designed heating and cooling systems. Generally, the samples were heated and cooled on plate materials [6,8,9,10].

In this article, we developed a system for testing the temperature dependence of colorimetric properties based on multipurpose universal devices without specially designed heating and cooling systems. Since textile materials in real use may or may not have be in a direct contact with the heated body, the tests on the samples are carried out after the air heating process under controlled conditions without direct contact between the fabric and the heating surface. In this way, the real conditions in which the product finds itself in practical application are emulated. In this article, the thermochromic sample property will be examined as a function of the temperature in the cooling process, to show the dependence of the material type and the screen mesh selection during printing to achieve a quality print with desired characteristics.

## 2. MATERIAL AND METHOD

### 2.1 Materials

Four types of textile materials with dimensions 250 x 350 mm were used in this study. For each of the material samples, the following are determined: fabric weight (ISO 3801:1977) [12], number of threads per unit length (EN 1049-2:1993) [13], linear density of yarn removed from fabric (ISO 7211-5:1984) [14] and material composition (EN ISO 1833-1:2010) [15]. The characteristics of the samples are given in Table 1. In the printing process, commercial SFXC magenta ink (activation temperature 31°C) and acrylic based binder were used [16]. The ratio of the dye and binder was 1:1.

### 2.2 Color Measurement

Using the diffuse geometry colorimeter HP200 (D65/10°, measurement geometry d/8°), CIELAB values of thermochromic ink were determined over time. Figure 1 shows the experimental setup with the position of devices during the measurements. Color measurement was done in two experiments. In the first experiment samples were heated in laboratory drying oven COLO DRY53A, while in another experiment the samples were heated using the heating press. After heating, the samples were placed on the Styrofoam. A temperature change of the material was recorded with a thermal imaging camera, and during the cooling process, the color change was measured with the HP200 spectrophotometer.

**Table 1.** Fabric weight, number of threads per unit length, the linear density of yarn removed from fabric and material composition of the samples

Textile material	Fabric weight [g/m <sup>2</sup> ]	Number of threads per unit length [threads/cm]		The linear density of yarn removed from fabric [tex]		Material composition	
		Warp	Weft	Warp	Weft	Type	[%]
Sample 1	208	44	21	27.00 x 1	26.40 x 1	Cotton	100
Sample 2	123	23	16	30.20 x 1	29.20 x 1	Cotton, Polyester	98.60, 1.40
Sample 3	81	39	25	8.10 x 1	18.20 x 1	Cotton	100
Sample 4	120	52	28	13.60 x 1	12.60 x 1	Cotton, Polyester	14.40, 85.60
Standard	ISO 3801:1977	EN 1049-2:1993		ISO 7211-5:1984		EN ISO 1833-1:2010	

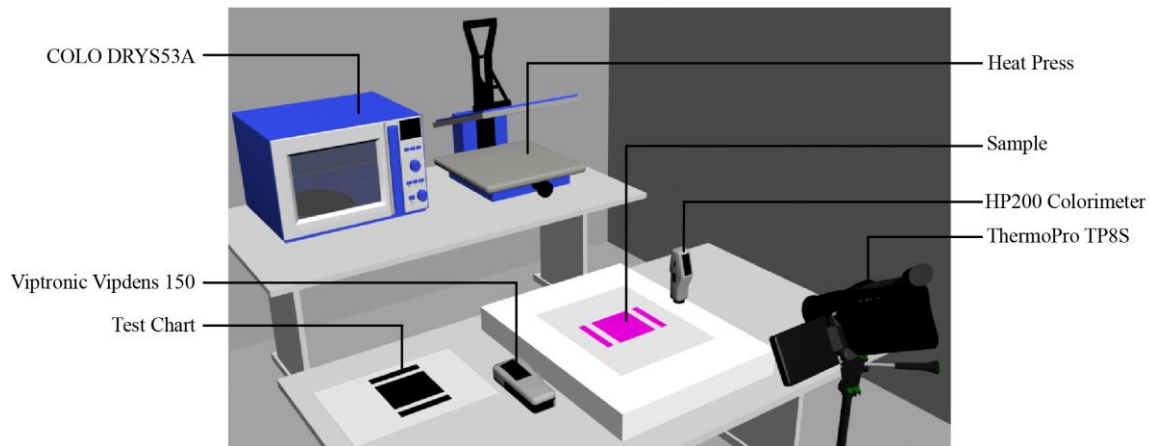


Figure 1. Experimental setup

### 2.3 Test Chart

The test chart (164 x 100 mm) consists of two 26 x 100 mm surfaces for color measurement, and 100 x 100 mm field for temperature analysis (Figure 1). It was developed on a glossy positive film ColorGate Screenfilm with photosensitive layer Sericol Dirasol 915, 50 lpi, at the angle of 90°. The film was illuminated using the Linotype Hell Linotronic 300 Red laser at its working temperature for 120 s, developed on the Esco Fot Gluns & Jensen machine with a process bath temperature of 32 °C for 30 s and fixed at 25 °C for 30 s. The shape of the raster dot on the film was ellipse. The concentration of the process bath was satisfactory as the regeneration was carried out on time. Minimum and maximum density values were measured on the film using the Viptronic Vipdens 150 densitometer. Obtained values of  $D_{min} = 0.06$  and  $D_{max} = 2.70$  confirmed that the film was well developed.

### 2.4 Screen Development

For the fabrication of the screen, silk net finishes (thick fibers), dimensions 500 x 700 mm and two different monofilament weave weights of 54 threads/cm and 120 threads/cm were used. The fabric was attached to the measuring aluminium frame size of 580 x 840 mm. The tensile force of the screen on the frame was 21 N/cm<sup>2</sup> during the making of the screen. After screen mesh tightening, the tensile force was 18 N/cm<sup>2</sup>. The emulsion thickness was 0.30 mm for 54 threads/cm and 0.10 mm for 120 threads/cm, and it was exposed on a screen mesh through an indirect screening process and a drying time of 2 hours at 35 °C.

### 2.5 Printing Process

The samples were printed on screen printing machine S550. For the printing process, a neoprene-shaped squeegee edged at an angle of 45° was used, hardness 80A. The thickness of the squeegee was 5 mm, and the length 25 mm. The weight of the squeegee was 180 g every 100 mm in length, the total length of the blade was 255 mm. The printing speed was 150 mm/s, the return speed of the squeegee and the ink carrier was 150 mm/s, the distance of the exposed emulsion

from the substrate was 4 mm, the distance of the ink application from the substrate 2 mm and the distance of the squeegee from the substrate was 2 mm. The ink (50 ml) and the binder (50 ml) were homogenized using the IKA KS 130 basic orbital shaker at a mixing rate of 400 rpm for 5 min. During the homogenization, printing and measuring process, the following ambient conditions were measured: temperature  $22 \pm 2$  °C, pressure  $101 \pm 1$  kPa and relative humidity  $40 \pm 2\%$ . For these measurements, we used Extech RH520A.

### 2.6 Temperature Measurement

In order to measure the temperature values during the cooling of analyzed samples the IR ThermoPro TP8S camera was used. Selected camera has a microbolometric sensor with a resolution of 640 x 840 pixels and generates wavelengths in the range of 8 to 14  $\mu\text{m}$  with a sensitivity of 0.08 at 30°C. The temperature measurement process takes place in such a way that the infrared sensors integrate electromagnetic IR radiation in the wavelength range of operation, and then generate the corresponding electrical signal [17]. The application of IR cameras in this experimental study is particularly useful because the emissivity coefficient of the tested materials, which is determined experimentally, is quite significant and ranges from 0.89 to 0.95. In order to increase the accuracy of the temperature measurement, the values of the relative air humidity, the ambient temperature and the distance between the IR sensor and the object of measurement should be entered as the input parameters in the IR camera. The distance between the IR sensor and the samples was 100 cm (Figure 1).

### 2.7 Ambient Conditions Measurement

In order to reduce the radiation from the additional sources in the surroundings, the temperature measurement should be performed in the dark environment [18]. Using the Eye-One Pro device (D65/10°, measuring geometry 45°/0°), the spectral curves and ambient lighting characteristics were measured (Figure 2). The intensity of light was 5.4 lux while the color temperature was 4594.50 K (corresponds to standard illuminant D50). In the visible spectrum, the light

is almost uniform, which confirms that the conditions in which the measurement was performed were favourable and controlled.

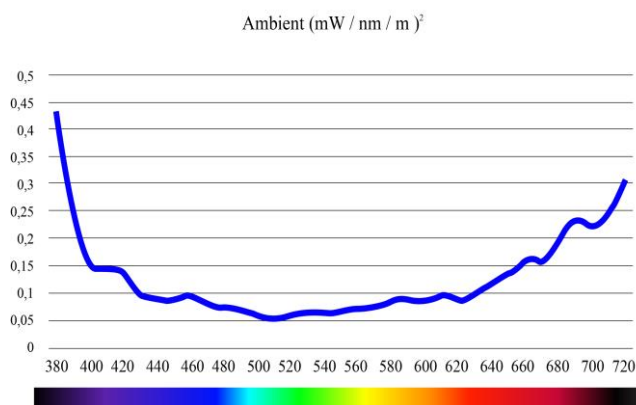


Figure 2. The spectral curve and ambient characteristics

### 3. RESULTS AND DISCUSSION

#### 3.1 Thermovision Measurements

After heating the samples inside the COLO DRY53A for 3 minutes at the temperature of 50 °C, the samples were pulled out and left to cool. It was noticed that after one minute of the cooling process, all the samples reached the ambient temperature. The surface temperature of the analyzed material was measured every 10 seconds, and the temperature was measured at the same time as color characteristics. Figure 3 gives an example of the thermal image.

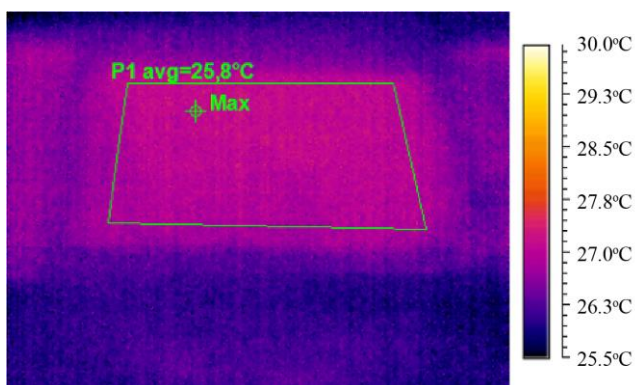


Figure 3. Thermal image of sample 3 printed using 54 threads/cm screen, second measurement, after 40s cooling

Figure 4 shows the dependence of time and temperature for the samples used in the study printed with different screens (differed by screen thread counts). The obtained results show that the cooling process of the printed samples is influenced by choice of a screen thread count, in such a way that the smaller screen thread count leads to the greater samples temperature retention time and, consequently, slower cooling. The cooling rate was slowing down when the screen mesh value decreases because of the larger openings that allow more ink to flow through. [19]. The selection of the screen thread count had the smallest effect

on sample 3, where the temperature did not change significantly over time (Figure 4).

#### 3.2 Spectrophotometric Measurements During Cooling of Heated Samples

After heating the samples for 3 minutes in a multi-purpose device, COLO DRY53A at a temperature of 50 °C, the samples were cooled to ambient temperature (24 °C). During the cooling process, the samples were measured every 10 seconds. In order to minimize the effect of heat transfer from the sample to the measuring surface, the samples were placed on Styrofoam (10 cm thick). During the cooling, CIELAB values for all samples were measured. The results are shown in Figure 5. The same figure also shows color differences. The color difference was calculated using the CIEDE2000 formula [20]. In addition to the color coordinate values and color differences, the relationship between colorimetric values (lightness and chroma) and the cooling time was investigated using Pearson correlation (correlation coefficients (r) and the corresponding degrees of determination (r<sup>2</sup>) are presented in Table 2).

There was a strong, negative correlation between lightness and cooling time and a strong positive correlation between chroma and cooling time in cases of all four materials and both screen thread counts. This means that the color is gradually getting darker and more saturated with enhancing time interval after exposing samples to the heat. The high coefficients indicate that colorimetric values can be used with a high level of confidence to determine the time elapsed from the beginning of the cooling process. The higher correlation coefficients in the case of lightness indicate that the lightness value is a more precise parameter for the cooling time prediction than chroma. Furthermore, the extremely high correlation coefficient values in the case of sample 1 indicate that the confidence degree of prediction depends on the choice of material. The influence of material and screen thread count on lightness value was investigated with ANOVA analysis with repeated measures for intervals 10, 20, 30, 40, 50, 60 and 70 seconds after exposure to the heat source. Besides determined significant effect of time interval on lightness,  $F= 319.34$ ,  $p<0.0005$ , multivariate partial eta squared = 0.99, it was confirmed that there a significant influence of the material type on behavior of lightness ( $F= 319.34$ ,  $p<0.0005$ , multivariate partial eta squared = 0.99), and also of screen thread count ( $F= 42.17$ ,  $p<0.05$ , multivariate partial eta squared = 0.79). The influence of the textile material type on the color difference change in relation to the first measured value during the cooling process for the tested screen thread count of 54 and 120 threads/cm are shown in Figure 6.

**Table 2.** Pearson's correlation coefficient (r) and the corresponding degree of determination (r<sup>2</sup>) between the lightness and time, as well as the chroma and time for all samples

	Sample 1	Sample 2	Sample 3	Sample 4	Sample 1	Sample 2	Sample 3	Sample 4
<b>Screen thread count (threads/cm)</b>								
	r(r <sup>2</sup> ) correlation L i T				r(r <sup>2</sup> ) correlation C i T			
<b>54</b>	-0.95 (0.90)	-0.87 (0.75)	-0.93 (0.86)	-0.89 (0.79)	0.92 (0.85)	0.84 (0.70)	0.82 (0.68)	0.77 (0.60)
<b>120</b>	-0.94 (0.88)	-0.91 (0.83)	-0.86 (0.73)	-0.83 (0.69)	0.92 (0.84)	0.88 (0.77)	0.74 (0.54)	0.75 (0.57)

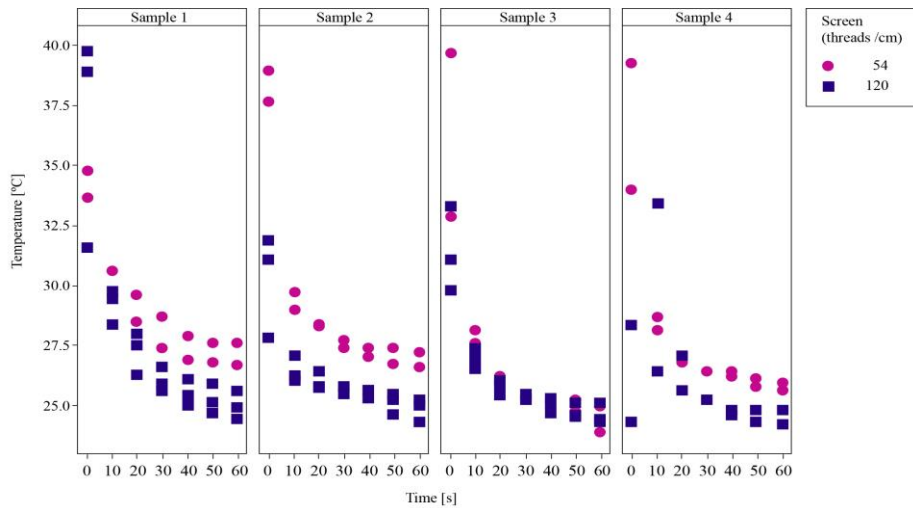


**Figure 4.** Time and temperature comparison of the samples printed with two different screens

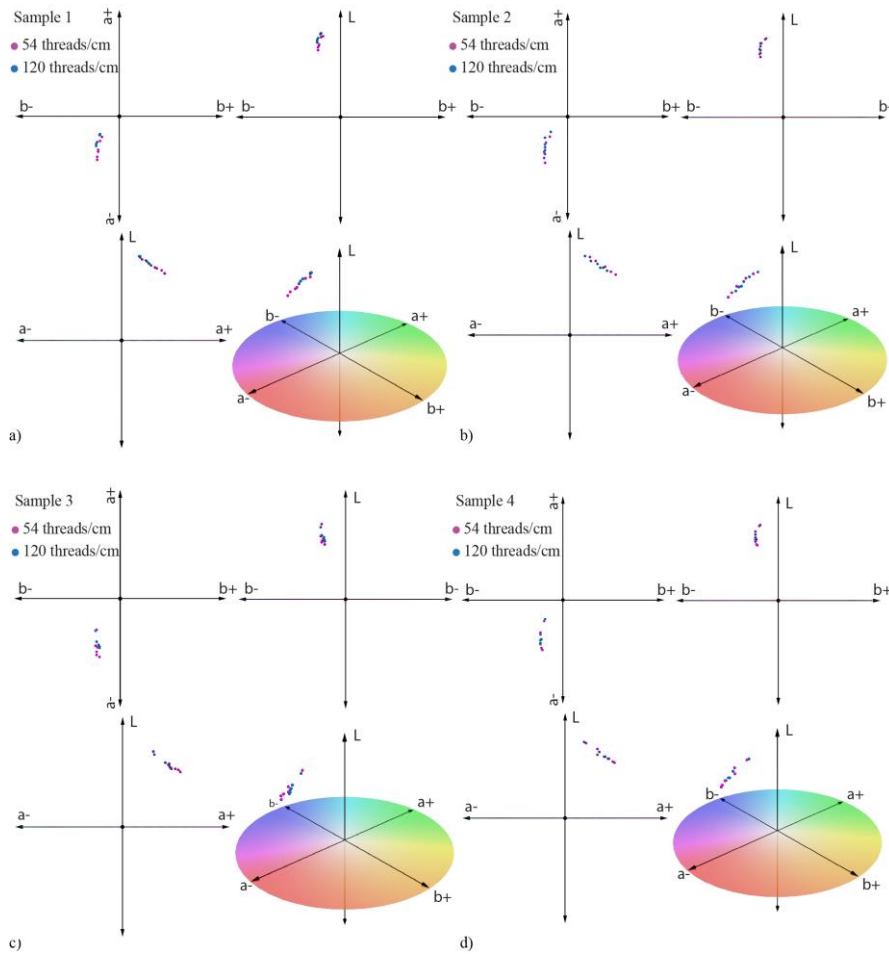


**Figure 5.** CIELAB values of the a) Sample 1, b) Sample 2, c) Sample 3, d) Sample 4 during the cooling process

After color differences analyzing, it was observed that sample 4 (54 threads/cm) and sample 2 (120 threads/cm) had the most significant color difference change compared to the first measured value. These fabrics are distinguished by the non-linearity of the color difference value between each subsequent measurement. In terms of the linearity of the changes over time, the lowest color difference between each subsequent measurement is characterized by sample 1 (54 threads/cm and 120 threads/cm), and at the same time these samples are characterized by the slightest change in the color difference and the smallest effect of the screen thread count on the color difference. With reducing the screen thread count, the color difference between each subsequent measurement is lower, but the color difference in relation to the first measured value is higher. Thus, for each fabric type, the color difference change in relation to the first measured value is higher for the screen thread count of 54 threads/cm.

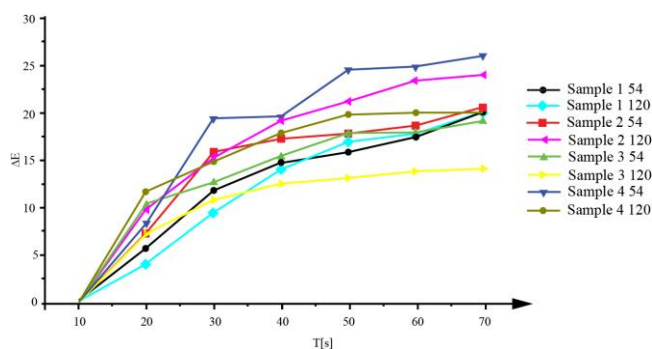


**Figure 6.** The color difference in relation to the first measured value for screens of 54 threads/cm and 120 threads/cm

In the analysis of color differences between each subsequent measurement, it was determined at which moment the most significant color change occurred, and then this change was slightly reduced until the ambient temperature was reached. For samples printed with a screen of 54 threads/cm, it was noted that the most significant change occurred in the first 30 seconds of measurement, excluding the cotton material with the smallest fabric weight at which the most significant color change occurred in the first 20 seconds of measuring. On samples with a screen 120 threads/cm, this change took place at 20 seconds of measurement, excluding the cotton material with the most significant fabric weight at which this change took place for 30 seconds of measurement. Compared to materials with polyester additives, cotton materials are characterized by higher absorption, resulting in a higher amount of thermochromic ink in the material and longer

temperature retention. To determine how the type of material influences the change of thermochromic ink, four specific groups of materials applicable to various textile packaging were used in the experiment. In this way, we created the basis for precise temperature identification via thermochromic ink printed on various textile packaging materials. Based on this analysis, it has been confirmed that the screen thread count influences the change of the thermochromic ink on the material in such a way that the higher the screen thread count is, the faster the color change, meaning that the sample returns faster from the discolored to the colored state. The screen with the higher thread count transfers less ink, and therefore the material, will release the heat faster. With the higher screen thread count, screen the ink will return faster from the colored to the discolored state [21]. It has also been confirmed that the smaller the fabric weight of the material, the faster is the return from the discolored to the colored state. It was shown that depending on the fabric weight of the material, the heat changes was different. The material with a greater fabric weight had the ability to absorb a larger amount of ink, so it kept the heat for a longer period of time [22]. Higher volume of thermochromic ink absorbed in the fabric causes higher color changes in thermochromic effect as a result of higher concentration of thermochromic pigments inside the material. The liquid absorption of fabrics decreases with increasing warp and weft densities as the fabric structure become very compact and dense. The effect of fabric constructions without any hydrophilic finish on liquid or water absorption was studied by researchers [23, 24, 25].

To compare the contact and contactless heating method, the measurements were repeated under the same conditions on samples that were cooled after heating using the heating press. Color differences were estimated between the first measured color value and the consequent measurements. The relation between color difference and temperature for the samples printed with different screens and dried within the drying oven and using heat press are shown in Figure 7a and 7b, respectively.

By analyzing the relation of color difference and temperature, it is noticeable that the samples measured after heating with heat press linearly increased the color difference with decreasing the temperature because they maintain the heat within the material for a longer time. These results show that the heating method influences the samples' cooling time. Hence, in order to create real conditions in which the smart textile packaging material could be found, it is necessary to use a device for contactless heating.

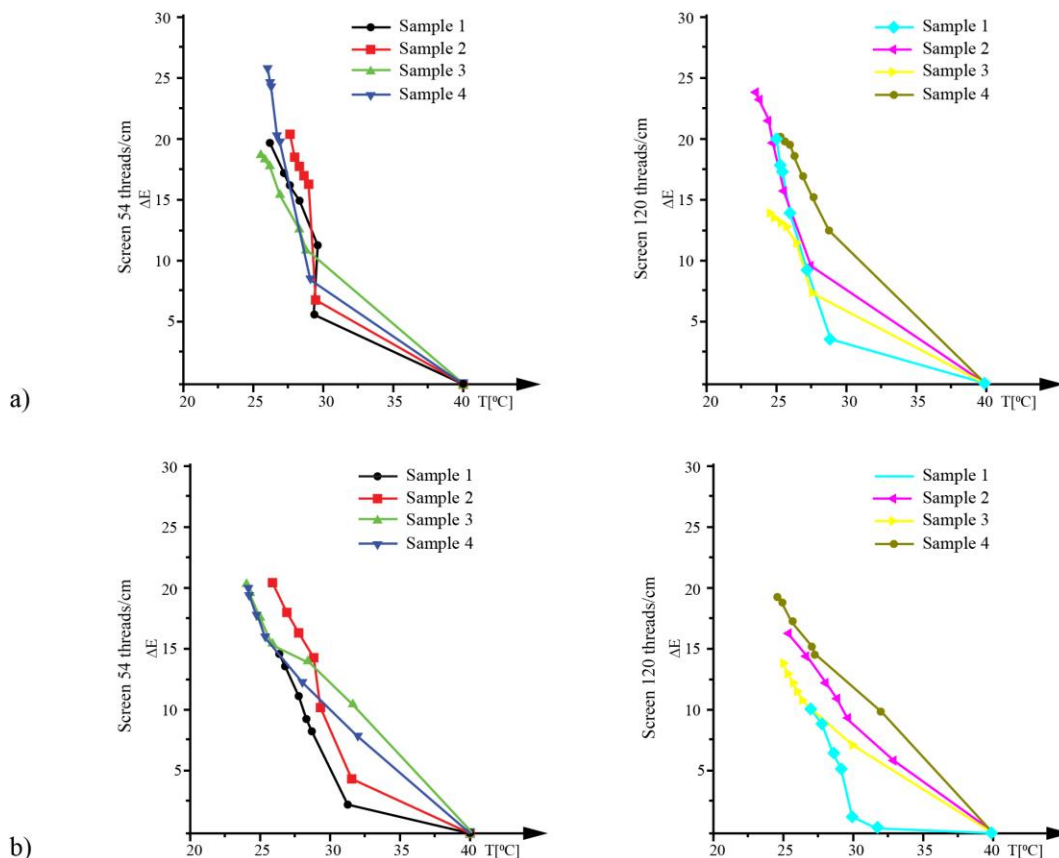


**Figure 7.** The color difference in relation to the first measured value for screens of 54 threads/cm and 120 threads/cm: a) samples dried within the drying oven, b) samples dried using heat press

#### 4. CONCLUSION

In this article we assessed the change of the colorimetric values of leuco thermochromic ink in screen printing with the change of the temperature during cooling. The printed samples were heated by contact and contactless method. The color measurement was done after the heating, during the cooling of the samples. The samples changed from achromatic to the chromatic after lowering the temperature below the activation temperature. During the cooling, the colors changed significantly in the first 30 s of the measurement. After that time and until the ambient temperature was reached the color difference was very small. It was also noticed that in almost all the samples (excluding cotton fabric with the small fabric weight) the influence of the screen thread count on the material temperature is noticeable. It is observed that using the lower screen counts in screen printing led to higher

temperature retention within the printed material, and vice versa. The choice of screen thread counts in printing did not have a significant influence on the temperature change during cooling in case of the cotton sample with small fabric weight.

In addition, it was shown that the heating method influences the cooling time. Although the samples were heated to the same temperature in both methods, the samples were cooled more slowly and therefore slowly changed the colorimetric values after the contact heating.

#### ACKNOWLEDGEMENT

This work was supported by the Serbian Ministry of Science and Technological Development, Grant No.:35027 "The development of software model for improvement of knowledge and production in graphic arts industry".

#### REFERENCES

1. Sun B. 2015. *Smart Materials and Structures*. Cape Town: Cape Peninsula University of Technology.
2. Bamfield P. 2001. *Chromic Phenomena: The Technological Applications of Colour Chemistry*. Cambridge: The Royal Society of Chemistry.
3. Kooroshnia M. 2013. Leuco dye-based thermochromic inks: recipes as a guide for designing textile surfaces. In Proceedings of the 13th AUTEX World Textile Conference. Dresden, Germany.
4. Gregor-Svetec D. 2018. Intelligent Packaging. In M. Cerqueira (1st Ed.). *Nanomaterials for food packaging: Materials, Processing Technologies, and Safety Issues*. 203-247. Netherlands: Elsevier.
5. Kooroshnia M. 2013. Demonstrating color transitions of leuco dye-based thermochromic inks as a teaching approach in textile and fashion design. In Proceedings of the Nordic Design Research Conference. Copenhagen, Denmark.

6. Kulčar R, Friškovec M, Knešauere, N, Sušin B, Gunde M. 2009. Colour changes of UV-curable thermochromic inks. In Proceedings of the 36th International Research Conference of iarigai. Advanced in Printing and Media Technology. 429-434. Stockholm, Sweden.
7. Kulčar R, Friškovec M, Hauptman N, Vesel A, Gunde, M. 2010. Colorimetric properties of reversible thermochromic printing inks. *Dyes and Pigments* 86 (3), 271-277.
8. Friškovec M, Kulčar R, Gunde, M. 2013. Light fastness and high-temperature stability of thermochromic printing inks. *Coloration Technology*. 129 (3), 214-222.
9. Kulčar R, Friškovec M, Gunde M, Knešauerek N. 2009. Colorimetric properties of UV-thermochromic inks. In 13th International Conference on printing, design and graphic communications Blaž Baromić. 89-93. Senj, Croatia.
10. Kulčar R, Gunde M, Knešauerek N. 2012. Dynamic Colour Possibilities and Functional Properties of Thermochromic Printing Inks. *Acta Graphica* 202, 23 (1-2), 25-36.
11. Chowdhury M, Butola B, Joshi M. 2013. Application of thermochromic colorants on textiles: temperature dependence of colorimetric properties. *Coloration Technology* 129 (3), 232-237.
12. ISO 7211-5:1984. Textiles: Woven fabrics - Construction - Methods of analysis Determination of linear density of yarn removed from fabric.
13. ISO 1833-1:2006. Textiles: Quantitative chemical analysis Part 1: General principles of testing.
14. ISO 3801:1977. Textiles: Woven fabrics - Determination of mass per unit length and mass per unit area.
15. ISO 7211-2:1984. Textiles: Woven fabrics - Construction - Methods of analysis Part 2: Determination of number of threads per unit length.
16. SFXC. 2019. Thermochromic screen printing ink magenta 31°C. Retrieved from <https://www.sfxc.co.uk/products/thermochromic-screen-printing-ink-magenta-31-c?variant=6850976961>.
17. Dawson TL. 2008. Beyond the visible: ultraviolet and infrared radiation. *Coloration Technology* 35 (1), 31-41.
18. Lanc Z, Štrbac B, Zeljković M, Živković A, Hadžistević M. 2018. Emissivity of aluminium alloy using infrared thermography technique. *Materiali in Tehnologije* 52 (3), 323-327.
19. Ružičić B, Stančić M, Kasikovic N, Majnaric I, Novaković D, Milošević R. 2015. The influence of thermal load on the print quality of screen printed knitted fabrics. *Advanced Technologies* 4 (1), 78-83.
20. Luo MR, Cui G, Rigg, B. 2001. The development of the CIE 2000 colour-difference formula: CIEDE2000. *Color Research & Application* 26 (5), pp. 340-350.
21. Kašiković N, Stančić M, Vladić G, Grujić D, Novaković D, Milošević R, Pinčjer I. 2017. The influence of heat treatment on the quality of screen printed textile substrates *Revista Materia*, 22 (1).
22. Stancic M, Kašiković N, Novakovic D, Dojcinovic I, Vladic G, Dragic M. 2014. The influence of washing treatment on screen printed textile substrates, *Textile and Apparel* 24 (1), 96-104.
23. Karahan M, Eren R. 2006. Experimental investigation of the effect of fabric parameters on static water absorption in terry fabrics. *Fibres & Textiles in Eastern Europe* 14 (2), 59-63.
24. Petruyte S, Baltakyte R. 2009. Static water absorption in fabrics of different pile height. *Fibres & Textiles in Eastern Europe* 74 (3), pp. 60-65.
25. Cruz J, Leitão A, Silveira D, Pichandi S, Pinto M, Fangueiro R. 2017. Study of moisture absorption characteristics of cotton terry towel fabrics. *Procedia Engineering* 200, 389-398.



# Supplier Selection Under Fuzzy Environment

Çağdaş Gündüz<sup>1</sup>, Gonca Şimşek Gündüz<sup>2\*</sup>

<sup>1</sup>Pamukkale University, School of Applied Sciences, Denizli, Turkey;

<sup>2</sup>Pamukkale University, Denizli Vocational School of Technical Sciences, Denizli, Turkey

**Corresponding Author:** Çağdaş Gündüz, cgunduz@pau.edu.tr

## ABSTRACT

Selecting the right supplier in supply chain is of great importance for firms. Because, when the supplier is a piece of a well-organized supply chain, this relationship may affect the competition power across the entire supply chain. Supplier selection is so critical process that it requires to evaluate many factors like quality, delivery time, cost, technology, payment due, flexibility and corporate reputation. Decision makers must consider these factors to select ideal suppliers. At this point, multi-criteria decision making methods (MCDM) help them to solve supplier selection problems. In this paper, considering the fuzziness in group decision making process, fuzzy set theory is used to deal with supplier selection problem of textile manufacturing firm. Ratings and weights of the criteria are expressed by linguistic variables. According to the proposed method fuzzy Technique for Order Preference by Similarity to Ideal Solution (TOPSIS), a closeness coefficient is calculated for obtaining supplier performance rankings.

## 1. INTRODUCTION

The meaning of being a supplier for firms has changed in today's market conditions where competition takes place among the supply chains. Firms desire to construct long-term relations based on mutual trust with their stakeholders like suppliers. Since, to work with the right supplier can reduce purchasing costs for the firm and can increase customer satisfaction. In this way, the firm is able to gain a chance to strengthen its competitiveness and performance [1, 2]. Therefore, supplier selection process is of great importance for firms in today's global market conditions and firms must achieve this process effectively for their future. Firms also must be flexible against changing market conditions and customer demands. A well-organized supply chain management helps firms to realize these goals. Because, supply chain management controls whole products and information flowing through the supply chain of the firm. It is a process which involves the firm's selection of a supplier for its production operations. In other words, supplier selection targets to select the supplier with the highest potential for meeting demands of a firm at an acceptable cost. The most important topic here is to construct the closeness and long term reliable relations with

the optimal supplier among a number of suppliers [3-5]. To select a supplier is one of most difficult and critical decisions for the buyer because it has some factors in it. Also, these factors may differ according to firm's needs. If the firm wants to complete this selection in an effective way, so it evaluates many criteria [6]. Among those criteria considered by decision makers in supplier selection, quality, delivery time, cost, production capability, service management, technology, research and development, finance, flexibility, reputation and risk are the most popular ones. As it is seen, it may involve different types of criteria, various decision models to select a supplier so it is a multi-criteria decision problem for the firm [7].

The supplier selection process covers different steps. First of all, the firm requires a new supplier so it is very important for the firm to expose exactly what it wants to achieve in supplier selection problem. Secondly, the firm should decide on selection criteria in accordance with its own needs and also it has adequate knowledge about alternatives. Third, the firm should select the one that meets the needs at the maximum level among the alternatives [8]. Briefly, it is very difficult to find the best way for the firm to eliminate alternatives and select supplier because it is required to use a variety of different methods for achieving

## ARTICLE HISTORY

Received: 10.04.2019

Accepted: 21.08.2019

## KEYWORDS

supplier selection, supply chain, fuzzy TOPSIS method, linguistic variables, MCDM

**To cite this article:** Gündüz Ç, Gündüz GŞ. 2019. Supplier selection under fuzzy environment, *Tekstil ve Konfeksiyon* 29(4), 344-352.

---

it. So, the main issue in this process is to find the most appropriate method among many selection methods to select the ideal supplier.

Actually, the supplier selection problem is the process of finding the best option among all suitable alternatives. When firms make an effort to find the ideal option, they should be cared for the number of alternatives and decision makers, the degree of uncertainty and environmental conditions effecting criteria [9]. By means of MCDM methods, decision makers can reach the ideal solution. For instance, MAXMIN, MAXMAX, AHP, TOPSIS, SMART, ELECTRE are the most known methods among these methods. While information technologies are developing rapidly, the usage of computers have become widespread so these methods have found great acceptance in selecting suppliers [10]. But, there may exist some differences between methods in solving problems. The ratings and the weights of criteria are measured exactly in classical MCDM models. In other words, those kind of models assume precise data [11, 12]. However, human judgments cannot be predicted with precise numerical values. Also, they are often uncertain. For this reason, the exact data will not be sufficient to model real life conditions under many circumstances [13, 14]. For example, decision makers set to decide under time pressure or limited knowledge capacity. In this situation, the use of linguistic variables instead of numerical values can be a more realistic approach. The ratings and weights of the criteria may be expressed by linguistic variables [15, 16]. According to Zadeh [17], a linguistic variable is a variable that is expressed in words or sentences in natural or artificial language. Language variables are also expressed statements like very high, very good, high, good, normal, very low, very bad [18]. According to Saghafian and Hejazi (2005) [19], this kind of linguistic expressions are a natural representation of human judgments. These characteristics represent the feasibility of fuzzy set theory of Zadeh in constructing the decision maker's preferred structures. The fuzzy set theory is related with the human's ability to understand and analyze inaccurate information. Zadeh developed it based on the idea that the key elements of human thought are linguistic expressions rather than numbers [16, 17].

Fuzzy set theory helps to measure the uncertainty in concepts through the subjective judgments of human beings [19, 20]. To Bellman and Zadeh [21], a fuzzy set is a class of objects in which there is no sharp boundary between those objects in terms of being member or non-member. From this point, the classes of objects can be characterized by some adjectives that are commonly used as large, small, important, serious, simple, accurate, approximate. The theory models linguistic uncertainty related to human perception and subjective judgment. It provides the interpretation of qualitative parameters and mathematical expression of linguistic uncertainty with fuzzy numbers [22].

Fuzzy set theory applications are increasing day by day in the solution of uncertain fuzzy problems by means of Zadeh's fuzzy set theory in 1975 and also Bellman and

Zadeh's decision-making methods in fuzzy environments in 1970 [18].

Supplier selection process have received great attention in the supply chain management literature recently. When the literature is examined, it is seen that there are various studies on both supplier selection and fuzzy TOPSIS method. Chen, Lin and Huang (2006) [9] developed a model to cope with the supplier selection problem of a high technology manufacturing company based on the concept of fuzzy TOPSIS method. They used the linguistic variables in order to assess the ratings and weights for the supplier evaluating factors. These linguistic variables were expressed in both trapezoidal and triangular fuzzy numbers. By applying the fuzzy TOPSIS, they calculated closeness coefficient of each supplier and selected the suitable supplier for the company.

Zouggari and Benyoucef's (2012) [23], study is conducted by using both supplier selection and fuzzy TOPSIS method. The criteria required is quantitatively evaluated for order allocation among the selected suppliers in the study. Fuzzy TOPSIS is applied to determine the weights for order allocation. Singh and Benyoucef (2012) [24], proposed the use of fuzzy TOPSIS for group decision making method to select the best supplier among several alternatives.

Orji and Wei (2014) [25], considered the importance of sustainability in supplier selection process to improve organizational performance in one of Chinese gear manufacturing company. In the study, the researchers developed a model based on integrated MCDM methods to solve supplier selection problem. TOPSIS methodology which is the most preferred for capturing all objective and subjective criteria is applied to choose the best possible sustainable supplier in fuzzy environment. Then, they analyzed the interdependencies between some sustainability factors including social, economic and environmental factors. And then, they tried to select the best sustainable supplier in fuzzy environment effectively. The findings demonstrated that the company considered frequently on work safety and quality factors of the respective suppliers.

Kannan, Jabbour, and Jabbour (2014) [26], used fuzzy TOPSIS method to select the most suitable supplier among a set of potential green suppliers for a Brazilian electronic company. They ranked the suppliers. The results of the proposed framework are compared with the ranks obtained by both the geometric mean and the fuzzy TOPSIS methodology. In order to examine the influence of preferences given by stakeholders as decision makers about selecting various suppliers a sensitivity analysis has been performed.

Igoulalene, Benyoucef and Tiwari (2015) [27], addressed the strategic supplier selection problem. They formulated the supplier selection problem as a fuzzy multi criteria decision making problem and solved it by using one of two approaches including fuzzy TOPSIS methodology. They computed the weights of the criteria for fuzzy TOPSIS. To show the applicability of this methodology, they presented

a simple supplier selection problem and analyzed numerical results. Finally, they listed the advantages and disadvantages of each approach they used in the study.

Other studies using TOPSIS, which is a frequently used model in supplier selection, can be listed as Wang, Cheng and Cheng (2009) [28]; Razmi, Songhori and Khakbaz (2009) (29); Shahanaghi and Yazdian (2009) [30]; Liao and Kao (2011) [31]; Li and Zabinsky (2011) [32]; Rouyendegh and Saputro (2014) [33]. All of these studies cope with the supplier selection problem to make a judgment about optimum supplier among the other alternatives by applying fuzzy TOPSIS methodology. The ideal supplier selection is obtained by integrating the closeness coefficients to the fuzzy TOPSIS model. In the end, the supplier who received the top ranking is defined as the optimum supplier.

TOPSIS method is one of the most frequently used method to select appropriate supplier the literature. But, the uncertainty effect upon decision criteria is the main problem for this method. In this paper, considering the fuzziness in group decision making process, we used fuzzy set theory.

The paper aims to evaluate the supplier selection problem of a textile manufacturing firm by using the fuzzy TOPSIS method. The paper is formed four sections. Next section gives some details about the fuzzy decisionmakingmethod to deal with the supplier selectionproblem in the study. In section 3, the proposed method isillustrated with an example. Finally, some conclusionsare pointed out at the end of the paper.

## 2. MATERIAL AND METHOD

TOPSIS method proposed by Hwang and Yoon (1981) [12] is one of the well known methods in the literature for MCDM. This method was later developed by some authors like Chen (2000) [15], Zavadskas, Turskis and Tamosaitiene (2008) [34], Hung and Chen (2009) [35]. The main point of TOPSIS is to identify the ideal solution which consists of all of best values accessible of criteria and the negative ideal solution which is composed of all worst values accessible of criteria [36]. In other words, unlike other methods, TOPSIS is based on logical thinking which gives the most appropriate results for both the positive ideal solution and the negative ideal solution. According to Hung and Chen (2009) [35]; Bottani and Rizzi (2006) [37], compared to other MCDM methods, TOPSIS has some advantages. Some of these advantages can be explained as being rational and simple, efficiency in computation, flexibility in ranking of alternatives and to calculate the best and worst alternatives ability for measuring the relative performance of alternatives in a simple mathematical form.

In addition to these aforementioned positive aspects of TOPSIS method, a different method called the Fuzzy TOPSIS is used in order to prevent the negative conditions caused by the changes in the decision criteria against some changes in environmental conditions and uncertainty especially. The basis of the fuzzy TOPSIS method is that the decision criteria used by decision makers to evaluate

alternatives have different weights. Using the fuzzy TOPSIS method, the decision coefficients and their evaluations about alternatives are converted into triangular or trapezoidal fuzzy numbers. Then the proximity coefficient of each alternative is calculated [9]. In classical TOPSIS, the rating and weight of the criteria are known precisely. In fuzzy TOPSIS, all the ratings and weights are defined by means of linguistic variables [10, 38, 39]. If it is decided to use fuzzy TOPSIS instead of TOPSIS, a number of weaknesses can be eliminated. Firstly, results may fail to comply with basic considerations sometimes. In this case, the best solution is the closest option to the positive ideal solution and the uttermost option to the negative ideal solution. Secondly, in fuzzy TOPSIS method, it is required for each criterion to assign initial weight for calculation. Finally, when fuzzy numbers are 1 and 0, it is directly assumed that they are both positive ideal solution and negative ideal solution. When the weights of criteria are extremely small, the closeness between the criteria and fuzzy positive and negative ideal solutions increase [38].

It is understood from the aforementioned statements that fuzzy TOPSIS is suitable for decision making in fuzzy environments where uncertainty prevails. Membership functions are given to linguistic expressions by using fuzzy numbers, thus uncertainty is eliminated. Theselinguistic expressions are most commonly expressed in triangular or trapezoidal fuzzy numbers [9]. The degree of membership for a continuous variable is expressed by the membership function and it is determined subjectively [38]. The membership function grade approaches 1 as the degree to which an element belongs to a certain set increases, otherwise it approaches 0 in the fuzzy set theory [3]. Because of the linear simple membership function, Hanns (2005) [40] stated thatthe use of triangular fuzzy numbers is generally preferred. Sanchez and Gomez (2003) [41] expressed that triangular fuzzy numbers are most commonly used fuzzy numbers because they provide ease of operation and also they can be created intuitively. Therefore, to avoid complexity of operations, the calculations were made using triangular fuzzy numbers in the study.

For example, if  $n_2 = n_3$  in a trapezoidal fuzzy number  $n = (n_1, n_2, n_3, n_4)$ , then the new number  $n$  is occurred and called triangular fuzzy number. Given any two positive fuzzy numbers called  $m$  and  $n$  and a positive real number  $r$ ,  $m_l^a$  and  $n_l^a$  is the lower limit of range,  $m_u^a$  and  $n_u^a$  is the upper limit of range, the  $\alpha$ -cut of two fuzzy numbers are  $m^a = [m_l^a, m_u^a]$  and  $n^a = [n_l^a, n_u^a]$  ( $\alpha \in [0; 1]$ ), respectively. Some main operations made using triangular fuzzy numbers  $m$  and  $n$  can be summarized as follows [9, 15, 42]:

$$(m(+))n^a = [m_l^a + n_u^a, m_u^a + n_l^a] \quad (1)$$

$$(m(-))n^a = [m_l^a - n_u^a, m_u^a - n_l^a] \quad (2)$$

$$(m(\cdot))n^a = [m_l^a \cdot n_l^a, m_u^a \cdot n_u^a] \quad (3)$$

$$(m(:))n^a = [m_l^a / n_u^a, m_u^a / n_l^a] \quad (4)$$

$$(m^a)^{-1} = [1/m_u^a, 1/m_l^a] \quad (5)$$

$$(m(\cdot))r^a = [m_l^a \cdot r, m_u^a \cdot r] \quad (6)$$

$$(m(:))r^a = [m_l^a / r, m_u^a / r] \quad (7)$$

$$\tilde{x}_{ij}^k = \frac{1}{k} [\tilde{x}_{ij}^1 \oplus \tilde{x}_{ij}^2 \oplus \dots \oplus \tilde{x}_{ij}^k] \quad (8)$$

$$\tilde{w}_j^k = \frac{1}{k} [\tilde{w}_{ij}^1 \oplus \tilde{w}_{ij}^2 \oplus \dots \oplus \tilde{w}_{ij}^k] \quad (9)$$

The fuzzy TOPSIS method has some computational steps which is summarized as follows [9, 15, 43, 44]:

*Step 1.* Determine the objectives, form decision makers group and then identify the evaluation criteria.

*Step 2.* Choose the linguistic variables according to the importance of the criteria and the linguistic ratings for alternatives.

*Step 3.* Weights of criterion are aggregated to obtain aggregated fuzzy weight  $W_j$  of  $C_j$  criterion. Get aggregated fuzzy ratings  $x_{ij}$  of alternative  $A_i$  under criterion  $C_{ij}$  in the opinion of decision makers.

*Step 4.* Construct the fuzzy decision matrix and calculate the normalized fuzzy decision matrix for each decision maker. Linguistic variables in the fuzzy decision matrix are defined as triangular fuzzy numbers

$$[x_{ij} = (a_{ij}, b_{ij}, c_{ij})w_{ij} = (w_{j1}, w_{j2}, w_{j3})].$$

Here, the various criteria scales transform into comparable scales for avoiding complexity of mathematical operations in decision process. For this reason, the set of criteria can be divided into benefit (B) and cost (C) criteria. Therefore, the normalized fuzzy decision matrix can be represented under B and C criteria as:

$$\tilde{r}_{ij} = \left( \frac{a_{ij}}{c_j^*}, \frac{b_{ij}}{c_j^*}, \frac{c_{ij}}{c_j^*} \right), j \in B \quad (10)$$

$$\tilde{r}_{ij} = \left( \frac{a_j^-}{c_{ij}^*}, \frac{a_j^-}{b_{ij}^*}, \frac{a_j^-}{a_{ij}^*} \right), j \in C \quad (11)$$

$$c_j^* = \max_i c_{ij} \text{ if } j \in B \quad (12)$$

$$a_j^- = \min_i a_{ij} \text{ if } j \in C \quad (13)$$

*Step 5.* Construct weighted fuzzy decision matrix as:

$$\tilde{v}_{ij} = \tilde{r}_{ij} \otimes \tilde{w}_j \quad (14)$$

*Step 6.* Determine the positive ideal and negative ideal solutions for each decision maker.

$$\tilde{v}_j^+ = (1, 1, 1) \quad (15)$$

$$\tilde{v}_j^- = (0, 0, 0) \quad (16)$$

*Step 7.* Calculate the distance of each alternative from the positive ideal solution and thenegative ideal solution.

$$d_i^* = \sum_{j=1}^n d(\tilde{v}_{ij}^+, \tilde{v}_j^+), i=1,2,\dots,m \quad (17)$$

$$d_i^- = \sum_{j=1}^n d(\tilde{v}_{ij}^-, \tilde{v}_j^-), i=1,2,\dots,m \quad (18)$$

where  $d_v(.,.)$  is the measurement of distance between two fuzzy numbers.

*Step 8.* Calculate the closeness coefficient of each alternative.

This coefficient shows the distances to the fuzzy positive ideal solution ( $A^*$ ) and fuzzy negative ideal solution ( $A^-$ ) synchronously by taking therelative closeness to the fuzzy positive ideal solution [9]. In other words, it is defined to set the ranking order of whole alternatives. The coefficient ( $CC_i$ ) is calculated for each alternative as follows:

$$CC_i = \frac{d_i^-}{d_i^* \oplus d_i^-}, i = 1, 2, \dots, m \quad (19)$$

*Step 9.* Rank the preference order for each alternative according to the closeness coefficient.

This empirical study evaluates the supplier selection problem of a textile manufacturing firm operating in Denizli by using the fuzzy TOPSIS method at first. Secondly, some advices are given to the managers about the results of this selection process. Four companies (alternatives) which are supplying knitted fabric and sewing yarn to the company in the study were evaluated. Two meetings were realized with procurement, production and marketing managers of the company. In the first meeting, managers were provided information on the supplier selection criteria in the literature. Company managers indicated cost (C1), payment due (C2), discount (C3), quality (C4), healthy product (C5), having quality certificate (C6), delivery time (C7), flexibility for changing in orders (C8), flexibility for delivery time (C9), easy contact (C10) and problem solving capability(C11) as the importance criteria in supplier selection process as a result of the first meeting. In the second meeting, managers were informed about the scales used in the evaluation of the criteria and alternatives. Then, they were asked to fill in the prepared questionnaire. Seven-point Likert scale (1= "very low (very poor)" to 7= "very high (very good)") was used to measure all items in the questionnaire. In this study, the questionnaires were sent through e-mail to the procurement manager, production manager and marketing manager of the surveyed textile firm. These three managers who are directly responsible for supply chain management of the firm evaluated the four suppliers separately. The questionnaire was administered in Turkish. The responses

were collected from March to April in 2018. Finally, Microsoft Excel2007 was used for evaluating data.

### 3. RESULTS AND DISCUSSION

TOPSIS is widely used in many different areas in MCDM problems. In this paper, TOPSIS method proposed by Chen (2000) [15] was used to assist the top management of the firm to solve the supplier selection problem under a fuzzy environment.

The importance weights of each criteria presented in Table 1 as linguistic variables are assessed by three department managers as decision makers. The decision makers also use the linguistic rating variables, which is presented in Table 2 to assess ratings of alternatives with respect to each criteria.

**Table 1.** Linguistic variables for the importance weight of each criteria

Very low	(0,0,0.1)
Low	(0,0.1,0.3)
Medium low	(0.1,0.3,0.5)
Medium	(0.3,0.5,0.7)
Medium high	(0.5,0.7,0.9)
High	(0.7,0.9,1.0)
Very high	(0.9,1.0,1.0)

**Table 2.** Linguistic variables for ratings

Very poor	(0,0,1)
Poor	(0,1,3)
Medium poor	(1,3,5)
Fair	(3,5,7)
Medium good	(5,7,9)

**Table 3.** The fuzzy decision matrix

	C1	C2	C3	C4	C5	C6	C7	C8	C9	C10	C11
Alternative 1	2,6667	7,6667	6,0000	2,6667	3,3333	7,6667	6,6667	3,0000	2,6667	7,3333	2,0000
	3,6667	8,6667	7,0000	3,6667	4,3333	8,6667	7,6667	4,0000	3,6667	8,3333	3,0000
	3,6667	8,6667	7,6667	3,6667	4,6667	8,6667	8,0000	4,0000	3,6667	8,3333	3,3333
	4,6667	9,6667	8,6667	4,6667	5,6667	9,6667	9,0000	5,0000	4,6667	9,3333	4,3333
Alternative 2	7,6667	6,0000	2,6667	3,3333	7,6667	6,6667	3,0000	2,6667	7,3333	2,0000	3,0000
	8,6667	7,0000	3,6667	4,3333	8,6667	7,6667	4,0000	3,6667	8,3333	3,0000	4,0000
	8,6667	7,6667	3,6667	4,6667	8,6667	8,0000	4,0000	3,6667	8,3333	3,3333	4,0000
	9,6667	8,6667	4,6667	5,6667	9,6667	9,0000	5,0000	4,6667	9,3333	4,3333	5,0000
Alternative 3	6,0000	2,6667	3,3333	7,6667	6,6667	3,0000	2,6667	7,3333	2,0000	3,0000	3,0000
	7,0000	3,6667	4,3333	8,6667	7,6667	4,0000	3,6667	8,3333	3,0000	4,0000	4,0000
	7,6667	3,6667	4,6667	8,6667	8,0000	4,0000	3,6667	8,3333	3,3333	4,0000	4,3333
	8,6667	4,6667	5,6667	9,6667	9,0000	5,0000	4,6667	9,3333	4,3333	5,0000	5,3333
Alternative 4	2,6667	3,3333	7,6667	6,6667	3,0000	2,6667	7,3333	2,0000	3,0000	3,0000	7,3333
	3,6667	4,3333	8,6667	7,6667	4,0000	3,6667	8,3333	3,0000	4,0000	4,0000	8,3333
	3,6667	4,6667	8,6667	8,0000	4,0000	3,6667	8,3333	3,3333	4,0000	4,3333	8,3333
	4,6667	5,6667	9,6667	9,0000	5,0000	4,6667	9,3333	4,3333	5,0000	5,3333	9,3333

The normalized fuzzy decision matrix is constructed as Table 4.

**Table 4.** Normalized fuzzy decision matrix

	C1	C2	C3	C4	C5	C6	C7	C8	C9	C10	C11
Alternative 1	0,2759	0,7931	0,6207	0,2759	0,3448	0,7931	0,7143	0,3214	0,2857	0,7857	0,2143
	0,3793	0,8966	0,7241	0,3793	0,4483	0,8966	0,8214	0,4286	0,3929	0,8929	0,3214
	0,3793	0,8966	0,7931	0,3793	0,4828	0,8966	0,8571	0,4286	0,3929	0,8929	0,3571
	0,4828	1,0000	0,8966	0,4828	0,5862	1,0000	0,9643	0,5357	0,5000	1,0000	0,4643
Alternative 2	0,7931	0,6207	0,2759	0,3448	0,7931	0,6897	0,3214	0,2857	0,7857	0,2143	0,3214
	0,8966	0,7241	0,3793	0,4483	0,8966	0,7931	0,4286	0,3929	0,8929	0,3214	0,4286
	0,8966	0,7931	0,3793	0,4828	0,8966	0,8276	0,4286	0,3929	0,8929	0,3571	0,4286

Good	(7,9,10)
Very good	(9,10,10)

As stated in previous part, a supplierselection problem discussed in this study in other words a MCDM problem can be expressed briefly in matrix format as follows [15]:

$$D = A_m \begin{bmatrix} C_1 & C_2 & \dots & C_n \\ A_1 \begin{bmatrix} x_{11} & x_{12} & \dots & x_{1n} \\ x_{21} & x_{22} & \dots & x_{2n} \\ \vdots & \vdots & \vdots & \vdots \\ x_{m1} & x_{m2} & \dots & x_{mn} \end{bmatrix} \end{bmatrix},$$

$$W = [w_1, w_2 \dots w_n],$$

Where  $x_{ij}$  ( $\forall i, j$ ) and  $w_j$  ( $j = 1, 2, \dots, n$ ) are linguistic variables,  $(A_1, A_2, \dots, A_m)$  are possible alternatives,  $(C_1, C_2, \dots, C_n)$  are decision criteria,  $w_j$  is the weight of criterion  $C_j$  and  $x_{ij}$  is the rating of alternative  $A_i$  with respect to criterion  $C_j$ . These linguistic variables can be expressed by triangular fuzzy numbers as  $x_{ij} = (a_{ij}, b_{ij}, c_{ij})$  and  $w_j = (a_{j1}, b_{j2}, c_{j3})$ .  $D$  matrix is called fuzzy decision matrix and  $W$  matrix is called fuzzy weights matrix. As a result of the questionnaire forms answered by decision makers, the fuzzy decision matrix in Table 3 and the fuzzy weight of each criterion in Table 5 have been constructed.

	1,0000	0,8966	0,4828	0,5862	1,0000	0,9310	0,5357	0,5000	1,0000	0,4643	0,5357
<b>Alternative 3</b>	0,6207	0,2759	0,3448	0,7931	0,6897	0,3103	0,2857	0,7857	0,2143	0,3214	0,3214
	0,7241	0,3793	0,4483	0,8966	0,7931	0,4138	0,3929	0,8929	0,3214	0,4286	0,4286
	0,7931	0,3793	0,4828	0,8966	0,8276	0,4138	0,3929	0,8929	0,3571	0,4286	0,4643
	0,8966	0,4828	0,5862	1,0000	0,9310	0,5172	0,5000	1,0000	0,4643	0,5357	0,5714
<b>Alternative 4</b>	0,2759	0,3448	0,7931	0,6897	0,3103	0,2759	0,7857	0,2143	0,3214	0,3214	0,7857
	0,3793	0,4483	0,8966	0,7931	0,4138	0,3793	0,8929	0,3214	0,4286	0,4286	0,8929
	0,3793	0,4828	0,8966	0,8276	0,4138	0,3793	0,8929	0,3571	0,4286	0,4643	0,8929
	0,4828	0,5862	1,0000	0,9310	0,5172	0,4828	1,0000	0,4643	0,5357	0,5714	1,0000

**Table 5.** Fuzzy weights of alternatives

	<b>Alternative 1</b>	<b>Alternative 2</b>	<b>Alternative 3</b>	<b>Alternative 4</b>
<b>C1</b>	0,1000	0,2000	0,2333	0,3333
<b>C2</b>	0,4333	0,5000	0,5667	0,6667
<b>C3</b>	0,4000	0,5000	0,5000	0,6000
<b>C4</b>	0,7333	0,8333	0,8333	0,9333
<b>C5</b>	0,7333	0,8333	0,8333	0,9333
<b>C6</b>	0,5333	0,6333	0,6667	0,7667
<b>C7</b>	0,7333	0,8333	0,8333	0,9333
<b>C8</b>	0,7333	0,8333	0,8333	0,9333
<b>C9</b>	0,7000	0,8000	0,8000	0,9000
<b>C10</b>	0,7333	0,8333	0,8333	0,9333
<b>C11</b>	0,7333	0,8333	0,8333	0,9333

Then, the weighted normalized fuzzy decision matrix is obtained by multiplying the values in the normalized fuzzy decision matrix by the weight of each alternative.

**Table 6.** Weighted normalized fuzzy decision matrix

	<b>C1</b>	<b>C2</b>	<b>C3</b>	<b>C4</b>	<b>C5</b>	<b>C6</b>	<b>C7</b>	<b>C8</b>	<b>C9</b>	<b>C10</b>	<b>C11</b>
<b>Alternative 1</b>	0,0276	0,3437	0,2483	0,2023	0,2529	0,4230	0,5238	0,2357	0,2000	0,5762	0,1571
	0,0759	0,4483	0,3621	0,3161	0,3736	0,5678	0,6845	0,3571	0,3143	0,7440	0,2679
	0,0885	0,5080	0,3966	0,3161	0,4023	0,5977	0,7143	0,3571	0,3143	0,7440	0,2976
	0,1609	0,6667	0,5379	0,4506	0,5471	0,7667	0,9000	0,5000	0,4500	0,9333	0,4333
<b>Alternative 2</b>	0,0793	0,2690	0,1103	0,2529	0,5816	0,3678	0,2357	0,2095	0,5500	0,1571	0,2357
	0,1793	0,3621	0,1897	0,3736	0,7471	0,5023	0,3571	0,3274	0,7143	0,2679	0,3571
	0,2092	0,4494	0,1897	0,4023	0,7471	0,5517	0,3571	0,3274	0,7143	0,2976	0,3571
	0,3333	0,5977	0,2897	0,5471	0,9333	0,7138	0,5000	0,4667	0,9000	0,4333	0,5000
<b>Alternative 3</b>	0,0621	0,1195	0,1379	0,5816	0,5057	0,1655	0,2095	0,5762	0,1500	0,2357	0,2357
	0,1448	0,1897	0,2241	0,7471	0,6609	0,2621	0,3274	0,7440	0,2571	0,3571	0,3571
	0,1851	0,2149	0,2414	0,7471	0,6897	0,2759	0,3274	0,7440	0,2857	0,3571	0,3869
	0,2989	0,3218	0,3517	0,9333	0,8690	0,3966	0,4667	0,9333	0,4179	0,5000	0,5333
<b>Alternative 4</b>	0,0276	0,1494	0,3172	0,5057	0,2276	0,1471	0,5762	0,1571	0,2250	0,2357	0,5762
	0,0759	0,2241	0,4483	0,6609	0,3448	0,2402	0,7440	0,2679	0,3429	0,3571	0,7440
	0,0885	0,2736	0,4483	0,6897	0,3448	0,2529	0,7440	0,2976	0,3429	0,3869	0,7440
	0,1609	0,3908	0,6000	0,8690	0,4828	0,3701	0,9333	0,4333	0,4821	0,5333	0,9333

After constructing the weighted normalized fuzzy decision matrix, the fuzzy positive ideal solution (FPIS) and fuzzy negative ideal solution (FNIS) values are determined as follows;

$$A^* = [(1,1,1), (1,1,1), (1,1,1), (1,1,1), (1,1,1), (1,1,1), (1,1,1), (1,1,1), (1,1,1), (1,1,1), (1,1,1)]$$

$$A^- = [(0,0,0), (0,0,0), (0,0,0), (0,0,0), (0,0,0), (0,0,0), (0,0,0), (0,0,0), (0,0,0), (0,0,0), (0,0,0), (0,0,0)]$$

To determine the distance between FPIS and FNIS, vertex method is used for calculation. After the same procedure is realized for other alternatives and criteria, the distances of the alternatives to FPIS and FNIS according to the criteria are determined as in Table 7 and 8.

**Table 7.** Distance between  $A_i$  ( $i=1, \dots, 4$ ) and  $A^*$  respect to each criterion

	$d(A_1, A^*)$	$d(A_2, A^*)$	$d(A_3, A^*)$	$d(A_4, A^*)$
C1	0,9130	0,8048	0,8317	0,9130
C2	0,5216	0,5929	0,7918	0,7457
C3	0,6224	0,8077	0,7650	0,5556
C4	0,6844	0,6150	0,2772	0,3438
C5	0,6150	0,2772	0,3438	0,6563
C6	0,4290	0,4822	0,7296	0,7516
C7	0,3232	0,6443	0,6734	0,2807
C8	0,6443	0,6734	0,2807	0,7178
C9	0,6861	0,3065	0,7286	0,6581
C10	0,2807	0,7178	0,6443	0,6307
C11	0,7178	0,6443	0,6307	0,2807

**Table 8.** Distance between  $A_i$  ( $i=1, \dots, 4$ ) and  $A^-$  respect to each criterion

	$d(A_1, A^-)$	$d(A_2, A^-)$	$d(A_3, A^-)$	$d(A_4, A^-)$
C1	0,1003	0,2198	0,1926	0,1003
C2	0,5054	0,4367	0,2236	0,2739
C3	0,3998	0,2049	0,2506	0,4644
C4	0,3331	0,4076	0,7625	0,6934
C5	0,4076	0,7625	0,6934	0,3615
C6	0,6013	0,5481	0,2870	0,2647
C7	0,7182	0,3744	0,3450	0,7600
C8	0,3744	0,3450	0,7600	0,3053
C9	0,3317	0,7302	0,2936	0,3599
C10	0,7600	0,3053	0,3744	0,3928
C11	0,3053	0,3744	0,3928	0,7600

After these calculations,  $d_i^*$  and  $d_i^-$  values are attained then closeness values are calculated for each alternative and then supplier performance rankings are obtained by fuzzy TOPSIS method.

**Table 9.** Distance coefficients of alternatives and ranking table

	Alternative 1	Alternative 2	Alternative 3	Alternative 4
$d_i^*$	6,4376	6,5663	6,6969	6,5339
$d_i^-$	4,8371	4,7089	4,5756	4,7362
$d_i^* + d_i^-$	11,2746	11,2753	11,2725	11,2701
$CC_i$	0,4290	0,4176	0,4059	0,4202

When the closeness coefficients of four alternatives are ranked from the largest to the smallest, it is seen that Alternative 1 is 0.4290, Alternative 4 is 0.4202, Alternative 2 is 0.4176 and Alternative 3 is 0.4059. Under these circumstances, the firm must work with the Alternative 1 that has the highest coefficient.

#### 4. CONCLUSION

During recent years, supply chain management is an integral part of business life. It is mostly accepted that a well-organized and managed supply chain is essential to company success and customer satisfaction. Many studies talk about the advantages of it. To construct long term solid relations with their suppliers can decrease purchasing costs, production costs for the firm and also boost customer

services and financial position. In this way, firms strengthen their competitiveness. Therefore, supplier selection becomes significant issue for firms in today's global market conditions.

Supplier selection is a difficult and critical process because it includes many factors to determine the right supplier. If decision makers want to complete this selection process in an effective way, they should consider these factors for example, quality, delivery time, costs, flexibility, etc. In order to consider multiple factors, the system to be established for supplier selection should be a multi-criteria system. Thus, multi-criteria selection and evaluation systems have the opportunity to provide long-term competitive advantage. Generally, decision making process often contains uncertain conditions. Especially, the competition and uncertainty are intense in textile sector. The demand structure, fashion, market conditions are constantly unsteady. Under these conditions, to select the right supplier becomes a necessity in the sector. Assessing of possible suppliers under these circumstances is possible with fuzzy set theory. The use of linguistic variables in selecting supplier is beneficial when performance indicators of firms cannot be expressed by numerical values. Due to the fuzziness in group decision making process, fuzzy TOPSIS method, which is one of the multi-criteria decision-making models is used in the paper to deal with supplier selection problem of a textile manufacturing firm in Denizli.

In the paper, according to cost, payment due, discount, quality, healthy product, having quality certificate, delivery time, flexibility for changing in orders and delivery time, easy contact and problem solving capability criteria, the four firms supplying knitted fabric and sewing yarn to the company are evaluated by fuzzy TOPSIS method. The ratings and weights of the criteria are expressed by linguistic variables. Closeness coefficients are calculated for each supplier and then the supplier rankings are obtained. The supplier placed on the top at ranking list is considered as optimum supplier.

There are many suppliers in the textile sector with similar characteristics. To select a supplier for a order based manufacturing textile company requires precise evaluation. Minor differences in this process affect the company in different aspects, especially cost and quality. Therefore, the fuzzy TOPSIS method provides more accurate measurements in cases where similar scores occurred like in this study.

Previous researches consider fuzzy TOPSIS method as a tool that can be used in supplier selection process. However, literature lacks empirical evidence when the suppliers perform very close to each other as in this study about selection in textile sector. At this point, decision makers can make very sensitive selection by means of fuzzy TOPSIS model. This study therefore fills that gap.

The main target of the study is to provide decision support in terms of firm managers. The method used in the paper assures more effective solution for supplier selection process in a fuzzy environment. Also, the study samples

---

only one firm's supplier selection problem. For further studies, different methods can be used in not only the

supplier selection problem but also other management decision problems for more firms.

## REFERENCES

1. Ghodsypur SH, O'Brien C. 1998. A decision support system for supplier selection using an integrated analytic hierarchy process and linear programming, *International Journal of Production Economics*, 56-57, 199-212.
2. Shin H, Collier DA, Wilson DD. 2000. Supply management orientation and supplier/buyer performance, *Journal of Operations Management*, 18, 317-333.
3. Chen YJ. 2011. Structured Methodology for supplier selection and evaluation in a supply chain, *Information Sciences*, 181 (9), 1651-1670.
4. Ding H, Benyoucef L, Xie X. 2005. A simulation optimization methodology for supplier selection problem, *International Journal of Computer Integrated Manufacturing*, 18 (2-3), 210-224.
5. Monczka R, Trent R, Handfield R. 1998. *Purchasing and supply chain management*, South-Western College Publishing, New York.
6. Sarkis J, Talluri S. 2002. A model for strategic supplier selection, *Journal of Supply Chain Management*, 38 (1), 18-28.
7. Ho W, Xu X, Dey PK. 2010. Multi-criteria decision making approaches for supplier evaluation and selection: a literature review, *European journal of Operational Research*, 202 (1), 16-24.
8. De Boer L, Labro E, Morlacchi P. 2001. A review of methods supporting supplier selection, *European Journal of Purchasing and Supply Management*, 7 (2), 75-89.
9. Chen C-T, Lin C-T, Huang S-F. 2006. A fuzzy approach for supplier evaluation and selection in supply chain management, *International Journal of Production Economics*, 102 (2), 289-301.
10. Chen SJ, Hwang CL. 1992. *Fuzzy Multiple Attribute Decision Making: Methods and Applications* Springer-Verlag, Berlin.
11. Delgado M, Verdegay JL, Vila MA. 1992. Linguistic decision-making models, *International Journal of Intelligent Systems*, 7, 479-492.
12. Hwang CL, Yoon K. 1981. *Multiple attribute decision making, methods and applications: 186 (Lecture Notes in Economics and Mathematical Systems)*, Springer-Verlag, New York.
13. Herrera F, Herrera-Viedma E. 2000. Linguistic decision analysis: Steps for solving decision problems under linguistic information, *Fuzzy Sets and Systems*, 115, 67-82.
14. Herrera F, Herrera-Viedma E, Verdegay JL. 1996. A model of consensus in group decision making under linguistic assessments, *Fuzzy Sets and Systems*, 78, 73-87.
15. Chen CT. 2000. Extensions of the TOPSIS for group decision making under fuzzy environment, *Fuzzy Sets and Systems*, 114, 1-9.
16. Chen CT. 2001. A fuzzy approach to select the location of the distribution center, *Fuzzy Sets and Systems*, 118, 65-73.
17. Zadeh LA. 1975. The concept of a linguistic variable and its application to approximate reasoning, *Information Sciences*, 8, 199-249.
18. Cheng JZ, Chen PT, Yu HCD. 2005. Establishing a man access strategy for future broadband service: A Fuzzy MCDM analysis of SONET/SDH and Gigabit Ethernet, *Technovation*, 25 (5), 557-567.
19. Saghaifan S, Hejazi R. 2005. Multi criteria group decision making using a modified Fuzzy TOPSIS procedure, Proceedings of the 2005 International Conference on Computational Intelligence for Modelling, Control and Automation, and International Conference on Intelligent Agents, Web Technologies and Internet Commerce CIMCA-IAWTIC'05, IEEE.(215-221), Vienna, Austria.
20. Kleyle R, Korvin AD, Karim K. 1997. Investing in new companies in an unstable economic environment: A fuzzy set approach, *Managerial Finance*, 23 (6), 68-80.
21. Bellman RE, Zadeh LA. 1970. Decision-making in a fuzzy environment, *Management Science*, 17 (4), 141-164.
22. Cheng S, Chan CW, Huang GH. 2002. Using multiple criteria decision analysis for supporting decisions of solid waste management, *Journal of Environment Science Health*, 37 (6), 975-990.
23. Zouggari A, Benyoucef L. 2012. Simulation based fuzzy TOPSIS approach for group multi-criteria supplier selection problem, *Engineering Applications of Artificial Intelligence*, 25, 507-519.
24. Singh RK, Benyoucef L. 2012. Fuzzy logic and interval arithmetic-based topsis method for multicriteria reverse auctions, *Service Science*, 4 (2), 101-117.
25. Orji IJ, Wei S. 2014. A decision support tool for sustainable supplier selection in manufacturing firms, *Journal of Industrial Engineering and Management*, 7 (5), 1293-1315.
26. Kannan D, Jabbar ABL de Sousa, Jabbar C JC. 2014. Selecting green suppliers based on GSCM practices: Using fuzzy TOPSIS applied to a Brazilian electronics company, *European Journal of Operational Research*, 233 (2), 432-447.
27. Igoulalene I, Benyoucef L, Tiwari MK. 2015. Novel fuzzy hybrid multi-criteria group decision making approaches for the strategic supplier selection problem, *Expert Systems with Applications*, 42 (7), 3342-3356.
28. Wang JW, Cheng CH, Cheng HK. 2009. Fuzzy Hierarchical TOPSIS for supplier selection, *Applied Soft Computing*, 9, 377-386.
29. Razmi J, Songhori MJ, Khakbaz MH. 2009. An integrated fuzzy group decision making/fuzzy linear programming (FGDMLP) framework for supplier evaluation and order allocation, *International Journal of Advanced Manufacturing Technology*, 43 (5-6), 590-607.
30. Shahanaghi K, Yazdian SA. 2009. Vendor selection using a new fuzzy group TOPSIS approach, *Journal of Uncertain Systems*, 3 (3), 221-231.
31. Liao CN, Kao HP. 2011. An integrated fuzzy TOPSIS and MCGP approach to supplier selection in supply chain management, *Expert Systems with Applications*, 38, 10803-10811.
32. Li L, Zabinsky ZB. 2011. Incorporating uncertainty into a supplier selection problem, *International Journal of Production Economics*, 134 (2), 344-356.
33. Rouyendegh BD, Saputro TE. 2014. Supplier selection using integrated fuzzy TOPSIS and MCGP: A case study, *Procedia - Social and Behavioral Sciences*, 116, 3957-3970.
34. Zavadskas EK, Turskis Z, Tamosaitiene J. 2008. Construction risk assessment of small scale objects by applying the TOPSIS method with attributes values determined at intervals, The 8<sup>th</sup> International Conference Reliability and Statistic in Transportation and Communication, Latvia.
35. Hung CC, Chen LH. 2009. A fuzzy TOPSIS decision making model with entropy weight under intuitionistic fuzzy environment, Proceedings of the International Multi-Conference of Engineers and Computer Scientists IMECS, Hong Kong.
36. Wang YJ, Lee HS. 2007. Generalizing TOPSIS for fuzzy multiple-criteria group decision-making, *Computers and Mathematics with Applications*, 53, 1762-1772.
37. Bottani E, Rizzi A. 2006. A fuzzy TOPSIS methodology to support outsourcing of logistics services, *Supply Chain Management: An International Journal*, 11 (4), 294-308.
38. Zadeh LA. 1987. A fuzzy set theoretic interpretation of linguistic hedge, *Fuzzy Sets and Applications: Selected Papers by Zadeh, L. A.* Ed.: Yager RR, Ovchinnikov S, Tong RM, Nguyen HT. John Wiley&Sons Publishing, Canada, 467-498.

- 
39. Gzeng GH, Huang JJ. 2011. *Multiple Attribute Decision Making Methods and Applications*. CRC Press, New York.
  40. Hanss M. 2005. *Applied fuzzy arithmetic: An introduction with engineering applications*, Springer-Verlag, Berlin.
  41. Sanchez J, Gomez AT. 2003. Applications of fuzzy regression in actuarial analysis, *The Journal of Risk and Insurance*, 70 (4), 665-699.
  42. Kaufmann A, Gupta MM. 1985. *Introduction to Fuzzy Arithmetic: Theory and Applications*, Van Nostrand Reinhold, New York.
  43. Jahanshahloo GR, Lofti FH, Izadikhah M. 2006. Extension of the TOPSIS method for decision-making problems with fuzzy data, *Applied Mathematics and Computation*, 181, 1544-1551.
  44. Monjezi M, Dehghani H, Singh TN, Sayadi AR, Gholinejad A. 2010. Application of TOPSIS method for selecting the most appropriate blast design, *Arabian Journal of Geosciences*, 5 (1), 95-101.